# Innate immune control of virus replication and transmission

A DISSERTATION
SUBMITTED TO THE FACULTY OF THE GRADUATE SCHOOL
OF THE UNIVERSITY OF MINNESOTA
BY

Elizabeth Jean Fay

IN PARTIAL FULFILLMENT OF THE REQUIREMENTS
FOR THE DEGREE OF
DOCTOR OF PHILOSOPHY

Ryan A. Langlois, Ph.D.

May 2020

## ACKNOWLEDGEMENTS

I am extremely grateful for the support and encouragement I have received during my Ph.D.

I thank my thesis committee: Reuben Harris (chair), Lou Mansky, Michael Smanski, and Kris Hogquist, for their guidance and support.

My advisor, Ryan Langlois, has been my greatest advocate during my graduate career. I have been inspired by his dedication to his trainees, creative (crazy) energy, tireless work ethic, and commitment to celebrate every achievement. His belief in my abilities often outweighed my own. I am incredibly grateful for his mentorship.

I have worked alongside some of the kindest, most supportive people during my time graduate school. My MCSB classmates have always been there for a lunch, a coffee, or (most often) a drink when needed. The members of Langlois Lab have made my graduate experience genuinely special. Through both encouragement and example, they have made me a better scientist, mentor, and human. For all the laughter, rants, puzzles, and weird YouTube videos, I thank them for getting me through the worst days and for celebrating my best days. I will miss doing science with them.

None of this work would have been possible without my amazing co-authors, particularly Lucy Sjaastad, Stephanie Aron, and Keir Balla. I would also like to thank Steve Shen and Nels Elde. I am grateful for the skills and support they provided to these studies.

I am truly in awe of the unconditional support I have received from my family during graduate school. They have (often blindly) celebrated my accomplishments and kept me grounded in reality. They are always there when I need to escape the madness of grad school for a completely different kind of madness that only family can offer.

Finally, I thank my husband, Alex. He has simultaneously pushed me to be my best and helped keep me sane. He has listened to my problems, supported me through difficult decisions, and made sure I had plenty of food, water, and fresh air. I would not have made it without his love and support. And, of course, Charlie and Mira.

## ABSTRACT

The activation of innate immune pathways is a critical step in the response to virus infection. The failure of infected cells to control virus replication can lead to massive destruction of tissue, resulting in severe illness or death of the host and spread to new hosts. The ongoing coronavirus pandemic highlights the critical need to understand the mechanisms by which infected cells activate the innate immune response following virus infection, and how failure to activate this response leads to virus spread and cross-species transmission. Here, I describe two model systems used to understand the innate immune response to viruses. First, I use genetically engineered reporter influenza A viruses to identify infected cells and characterize the early response *in vivo*. I have found distinct responses based on the magnitude and round of infection, as well as cell type- and stage-specific antiviral signatures. In the second model system, I aim to understand the dynamics of how viruses transmit between hosts. I leveraged a model whereby pet store mice—which harbor a myriad of mouse pathogens—are co-housed with clean laboratory mice. This ‘dirty’ mouse model offers a platform for studying the acute transmission of viruses between hosts via natural mechanisms—through direct contact, air, and saliva and other fluids. I co-housed pet store mice with wild type laboratory mice and mice deficient in interferon receptors to characterize the role of these important innate immune pathways. Finally, I have co-housed laboratory mice with the bedding of pet store rats to analyze immune and non-immune species barriers to transmission. Overall, the findings of these studies will help elucidate mechanisms of innate immune activation by viruses.

## TABLE OF CONTENTS

## LIST OF TABLES

## LIST OF FIGURES

# CHAPTER 1: Induction and antagonism of the innate immune response by virus infection

## INTRODUCTION

Viruses are obligate intracellular parasites that likely infect all forms of life. The global virome is incredibly diverse, including diversity in genome size/structure, replication cycle, host specificity, and pathogenicity. Advances in metagenomics have led to a global estimate of $10^{31}$ virus particles in existence at any given moment (1). While fewer than 300 viruses are known to infect humans, an estimated 600,000-800,000 viruses in mammals or birds have zoonotic potential, meaning these viruses do not infect humans but could gain the ability to infect humans (2). The most devastating human virus pandemics have occurred following emergence from zoonotic reservoirs, including human immunodeficiency virus (HIV), Ebolavirus, and avian influenza A viruses (IAVs). The 1918 influenza pandemic—which likely emerged from waterfowl (3)—infected over a third of the global population and caused 50-100 million deaths. All IAV endemic and pandemic strains since 1918 (including the 1957, 1968, and 2009 pandemics) have been descendants of the 1918 strain (3), adding millions more deaths resulting from a single emergence. The ongoing coronavirus pandemic—which was first identified in late 2019 and has over 5,000,000 confirmed cases and nearly 350,000 confirmed deaths globally (Johns Hopkins University Coronavirus Research Center, current as of 22-May-2020)—highlights the need to understand mechanisms of emergence**.** The rapid increase in the global human population both increases the occurrence of disease transmission between humans and

increases exposure to animal reservoirs. However, it is difficult to identify viruses with pandemic potential. Such predictions require both intensive screening of animal populations for these viruses and an understanding of the virus and host factors that restrict or allow cross-species transmission.

The innate immune response is a critical line of defense against virus infections. Innate immune receptors are antigen non-specific, allowing the host to respond to a wide range of pathogens without needing prior exposure. This is especially important in the face of emerging viruses for which there is little or no existing immunity. While activation of the innate immune response is necessary to control virus replication, it can also lead to a robust inflammatory response and widespread tissue damage. The failure of infected cells to control virus replication can lead to cell death, spread of the virus to neighboring infected cells, transmission of the virus to additional hosts, and increased severity of disease or death of the host. Understanding the complexities of virus-host interactions at the cellular level is important for predicting emerging viruses, developing antivirals to contain outbreaks when human infection does occur, and generating effective vaccines to prevent pandemics. This introduction will describe the innate immune receptors that detect virus infections, the response that is mounted upon receptor activation, and highlight how this interaction has driven evolution of both viruses and their hosts.

## INNATE IMMUNE RESPONSE TO VIRUSES

### *Detection and response in infected cells*

Detection of viruses by infected cells initiates an immune response to inhibit virus replication and protect the host. In mammals, viruses are detected through pattern recognition receptors (PRRs), which detect specific viral pathogen-associated molecular patterns (PAMPs). Virus infections are sensed by cytoplasmic sensors such as RIG-I-like receptors (RLRs) and cyclic GMP-AMP synthase (cGAS) and membrane-bound toll-like receptors (TLRs). These receptors recognize viral nucleic acids: cytosolic double-stranded or uncapped RNA (RLRs), cytosolic double-stranded DNA (cGAS), or endosomal nucleic acids (TLRs) (4, 5). Upon ligand binding, these receptors signal through their cognate adaptor proteins to activate interferon response factor (IRF) -3 and -7. Activated IRFs translocate to the nucleus to upregulate, among other genes, type I and III interferons (IFNs) (Figure 1-1). The effect of these critical antiviral cytokines will be discussed in a later section.

PRR agonists have been identified using synthetic nucleic acid molecules and validated using virus infection models *in vitro* (6). Aberrant replication products—such as defective interfering genomes—are potent RIG-I agonists for many RNA virus infections, including IAV (7), Sendai virus (8), and some strains of measles virus (9). How and when these agonists are produced is uncharacterized for many viruses.

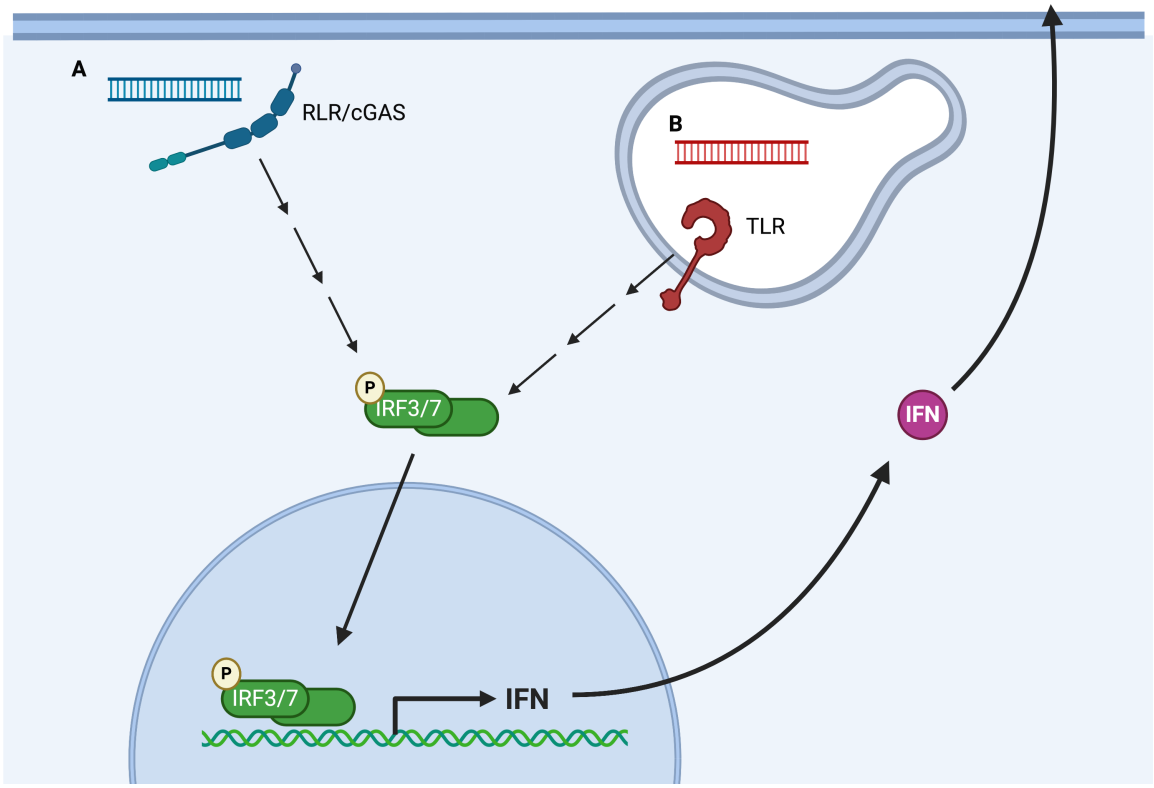


**Figure 1-1.** Detection of viruses upregulates IFN. Viral nucleic acids are detected through cytoplasmic RLRs or cGAS (A) or endosomal TLRs (B). This interaction initiates a cascade that ultimately leads to phosphorylation of IRF 3 and/or 7 (IRF3/7). Activated IRF3/7 translocates to the nucleus to upregulate IFN, which is then released from the cell. Image created using BioRender.

### *The interferon response*

The innate immune response induced in infected cells both controls local virus replication and has global effects mediated by molecules secreted from infected cells, primarily IFN. IFNs act in an autocrine and paracrine manner by signaling through the IFN receptors, ultimately upregulating a set of IFN-stimulated genes (ISGs) which establish the antiviral state in the host. In addition to IFN, other secreted cytokines and chemokines function to induce other aspects of the immune response, including inflammation and activation of the adaptive immune response.

Type I and type III IFNs (IFN-I and IFN-III) are the primary mediators of the antiviral response. These IFNs bind to the IFN-$\alpha$ receptor (IFN$\alpha$R) and IFN-$\lambda$ receptor (IFN$\lambda$R), respectively, and signal through converging pathways to upregulate ISGs (10). Engagement of IFN with its cognate receptor activate Janus kinases (JAKs) and tyrosine kinase 2 (TYK2), which then phosphorylate signal transducer and activator of transcription -1 (STAT1) or -2 (STAT2). Phosphorylated STAT1-STAT2 heterodimers associate with IRF9 to form the heterotrimeric complex IFN-stimulated gene factor 3 (ISGF3). This complex translocates to the nucleus where it acts as a transcription factor by binding to IFN-stimulated response elements (ISRE) to regulate expression of ISGs (Figure 1-2). Semi- or unphosphorylated ISGF3 can activate gene expression, both aberrantly and in the context of infection (11, 12).

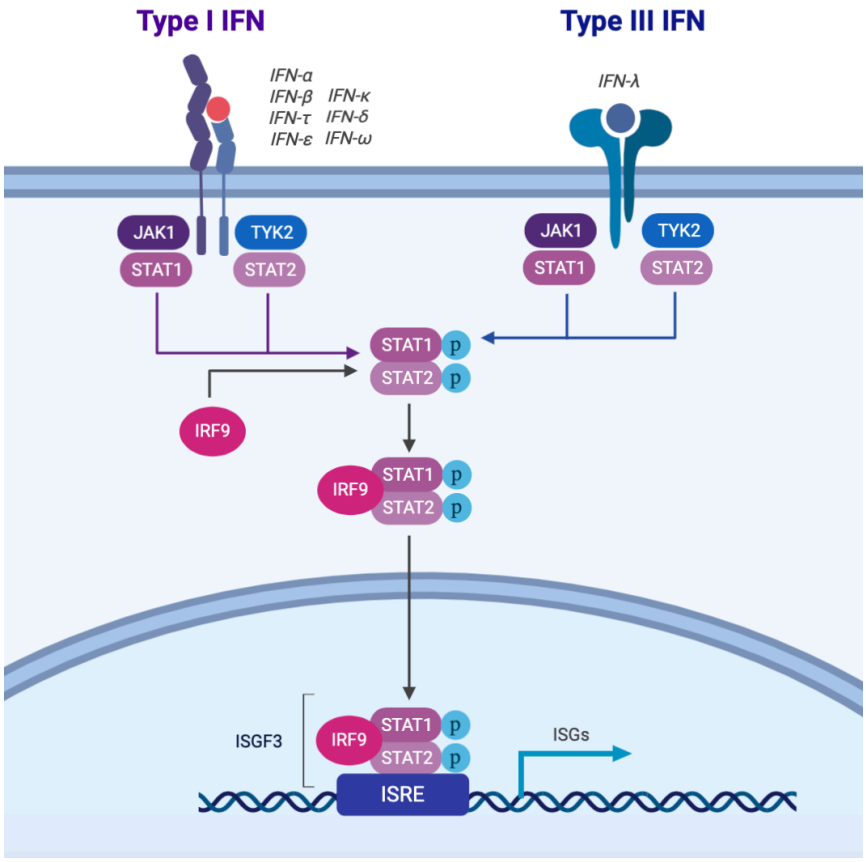


**Figure 1-2.** IFN signaling upregulates ISGs. Binding of IFNs to their congnate receptors activates JAKs and TYK2, which phosphorylate STAT1/2. Phosphorylated STAT1/2 associate with IRF9, and this complex translocates to the nucleus to activate genes downstream of ISREs. Image modified from BioRender template.

While they signal through similar pathways, IFN-I and IFN-III differ in important ways. The IFNαR and IFNλR differ in their expression; while the IFNαR is expressed on all nucleated cells, IFNλR is restricted primarily to epithelial cells (hepatocytes and neutrophils also express IFNλR) (13, 14). Additionally, the response to IFN-III is delayed compared to IFN-I (15, 16). Type I IFN-β expression is primarily regulated by IRF3, which is constitutively expressed and activated upon virus infection. In contrast, type III IFNs require IRF7, an ISG, which may explain

the delayed IFN-III response (13). However, rapid and robust induction of IFN-III has been observed under certain conditions *in vitro* and *in vivo* (17, 18).

IFN-I has long been considered the primary inducer of an effective antiviral response. However, in epithelial tissues such as the lung and gut, IFN-III has a nonredundant role in controlling virus infections. IFN-III signaling has been shown to be sufficient for protecting mice against IAV infection in the absence of IFN-I signaling (18). This is also true in intestinal infections; IFN-III signaling is necessary for norovirus clearance independent of adaptive immunity (19). Additionally, the IFN-III response is less inflammatory than IFN-I due to their differential ability to upregulate IRF1 (16, 20). Mice deficient in IFN-III signaling have higher IAV loads and more lung damage compared to IFN-I deficient mice. Moreover, a lack of IFN-III production resulted in enhanced IFN-I production, more robust innate immune cell infiltration, more extensive tissue damage, and ultimately increased mortality (21), suggesting that IFN-III is more important for host survival during IAV infection.

### *IFN-stimulated genes*

ISGs are broadly defined as genes upregulated following IFN stimulation of cells. In a single cell, hundreds of genes are induced by IFN, and an estimated 10% of the human genome has the potential to be regulated by IFN (22). However, while screens using different species and cell types have identified many ISGs, when compared across animals only 62 genes were found to be commonly upregulated following IFN-I stimulation (22). This suggests that there are a set of conserved ISGs, but also species-specific ISGs. Many ISGs have unknown

antiviral functions and, despite robust protection following IFN treatment, few ISGs display antiviral activity when expressed individually in cells (23, 24). IFN treatment still effectively protects against virus infections *in vitro*, which could suggest that ISGs work cooperatively through unknown mechanisms to inhibit virus replication.

ISGs exert their effects both directly and indirectly. For example, components of the RIG-I pathway—including *Ddx58* (RIG-I), *Mavs*, and *Irf3/7*—are ISGs and promote an antiviral state without directly interfering with the virus life cycle. Directly antiviral ISGs have been found to target many stages of virus infection. ISGs inhibit IAV entry (IFITM3) (25, 26) replication (PKR) (27), and egress (SERPINE1) (28). Some ISGs have been identified to have proviral functions. For example, LY6E promotes entry of a subset of RNA viruses, including Dengue virus and IAV (29). The endosomal cation channel MCOLN2 enhances infection of several viruses by promoting intracellular trafficking of endocytosed virions (30). Other putative proviral ISGs have been identified (including ADAR, FAM46C, and APOBEC3A) (23), but their mechanisms remain undefined.

While they are defined by their IFN responsiveness, some ISGs can be upregulated directly by virus infection independent of IFN signaling. Herpesvirus infection—including human cytomegalovirus and herpes simplex virus-1—can upregulate ISGs through IRF3 and STAT1 activation (31). Similarly, vesicular stomatitis virus and IAV upregulate IRF1 and IRF3, respectively, to upregulate ISGs independent of IFN (32, 33). Activation of IRF3/7—and subsequent upregulation of antiviral genes—has been documented following virus entry independent of PRR signaling and IFN (34, 35). These data suggest direct

induction of ISGs as a mechanism to rapidly establish the antiviral state during infection.

***Inflammation, cell death, and activation of the adaptive immune response***

Activation of PRRs and signaling through IFN receptors also upregulates classes of cytokines and chemokines that initiate and regulate the inflammatory response. While inflammation is critical to clearing infection, it also contributes to tissue destruction and severity of disease. Expression of pro-inflammatory cytokines is primarily mediated by the transcription factor nuclear factor κ-light-chain-enhancer of activated B cells (NFκB), which is activated by PRR signaling along with IRF3/7. Many factors contribute to the balance between IRF and NFκB activation, including age of the host (36) and expression of the scaffold protein CARMA3, which positively regulates MAVS-mediated NFκB activation (37). Additional uncharacterized viral and host factors may contribute to balancing between the antiviral and inflammatory functions of PRR and IFN responses.

Death of infected cells through apoptosis is a mechanism to inhibit virus replication by removing access to necessary host factors. Virus infection can induce cell death through both intrinsic pathways (e.g. through DNA damage or metabolic stress) and extrinsic pathways through the release of cytokines and activation of death receptors (38). Many viruses express proteins that induce or suppress apoptosis, suggesting apoptosis is both a pro- and antiviral process, depending on the biological context. Herpesviruses and poxviruses, among others, express proteins homologous to host antiapoptotic proteins as a way to inhibit

apoptosis and favor virus propagation (38). In contrast, norovirus and other *Calicivirus* species express polyproteins that are cleaved by host caspases at late timepoints (18-24h post-infection), and these cleaved proteins further promote caspase activity and cell death, leading to spread of new viruses to neighboring cells (39, 40), suggesting apoptosis as a proviral mechanism. Whether pro- or anti-viral, widespread apoptosis has a profound impact on the pathogenesis of viral infections. IAV both directly induces apoptosis in infected cells and indirectly through inflammatory and cytotoxic T cell responses (41). In mice, an inability to control IAV infection through IFN-I induction led to a robust inflammatory response and inflammasome-induced lethality (36). However, in some strains of mice, the IFN-I response leads to uncontrolled inflammation, extensive lung damage, and ultimately increased mortality (42). Altogether, apoptosis and inflammation must be tightly regulated to balance between virus clearance and tissue damage.

Both inflammatory signals and cell death-associated signals recruit and activate innate immune cells, including macrophages and dendritic cells (43-45). Innate immune cells serve as the bridge between the innate and adaptive immune response. These cells acquire viral antigens—either through direct infection or phagocytosis—and present these antigens to activate naïve T and B cells to establish long-lasting immunity to specific viral pathogens. RIG-I signaling in dendritic cells and other hematopoietic cells is critical for generating functional memory T cells (46), and IFN-III signaling promotes generation of antibodies (47) during IAV infection, further highlighting the importance of an effective innate response in protecting the host from ongoing and future infections.

***Negative regulation of the innate immune response***

While innate immune control of virus replication promotes survival of the host, the response must also be tightly regulated to prevent widespread tissue damage due to inflammation, cytotoxic immune cells, and virus-induced apoptosis. Key signaling proteins are often only transiently turned on, and many ISGs serve as inhibitors of PRR or IFN signaling. Binding of IFN-I to the cognate receptor leads to endocytosis of the receptor-ligand complex and degradation of the receptor (48-51). IRF and STAT proteins are regulated via post-translational modifications such as phosphorylation, ubiquitination, and acetylation; the addition and removal of these modifications can happen rapidly, allowing for control of signaling without changing expression of these genes (52, 53). PRR and IFN signaling also upregulate negative regulators of the response. Two ISGs are major negative regulators of IFN: USP18 and suppressor of cytokine signaling (SOCS) proteins. SOCS proteins bind to both the IFNAR and JAK proteins to prevent interaction with STATs (54, 55). SOCS1 can also attenuate IFN-III signaling (56). USP18 binds to IFN$\alpha$R to prevent JAK binding and subsequent signaling (57). In contrast to SOCS1, USP18 only regulates IFN-I (56). Negative regulation of RIG-I and MDA5 by an additional RLR, LGP2, has been documented, however LGP2 has also been shown to promote RLR signaling, suggesting its function may be context-specific (58-61).

***Non-canonical innate immunity***

Innate immune receptors and effectors are defined by their consistent response regardless of previous exposure to a given pathogen, which is in contrast to the memory associated with adaptive immunity. The activation of these pathways has been viewed as similarly consistent, with different cell types able to respond to a wide range of pathogens in a similar manner. There are several important exceptions to this rule, and recent findings have also shifted away from the idea that innate immunity is absent of memory.

Many recent studies using single-cell RNA sequencing or other deep sequencing techniques have identified both heterogeneous virus replication between infected cells and heterogeneous responses from infected cells. This has been documented for IAV (62, 63), West Nile virus (64), herpes simplex virus-1 (65), and foot-and-mouth disease virus (66), among others. These studies have identified both virus and host factors that contribute to the observed heterogeneity, and these factors also contribute to a heterogenous innate immune response. For example, cells infected with an IAV virion lacking a polymerase gene contain lower amounts of virus RNA, and cells infected with a virion lacking the immune antagonist nonstructural 1 (NS1) gene produce more IFN (63). The level of foot-and-mouth disease virus replication varies with host cell cycle phase (66). Many of these studies have been completed in *in vitro* systems. Similar heterogeneity in both the virus and response likely exists *in vivo*, and there are likely many unknown contributing factors.

Cell type-specific responses to both infection and IFN have been well described. Hematopoietic cells—particularly monocytes—have higher basal and induced IFN-I responses than non-hematopoietic cells (67). Stem cells display a unique resistance to many viral infections (68-71). For decades, the mechanism of this resistance was unknown. Recently, it was found that pluripotent and multipotent cells basally express canonical ISGs (72). This finding is consistent across different types of stem cells, and the intrinsic expression of ISGs is critical in mediating resistance to infection. Stem cells also do not produce nor respond to IFN-I (73, 74). Induced activation of IRF7 in induced pluripotent stem cells resulted in both short- and long-term transcriptional changes that reduced the differentiation potential of these cells (74). This suggests that the IFN resistance of stem cells preserves their pluripotency, and the intrinsic expression of ISGs is critical for them to survive viral infections. Viruses require many host factors for replication—discussed in a later section—and different cell types may express such factors at different levels. Therefore, additional cell type-specific responses likely exist but have yet to be characterized.

Several recent studies have documented innate immune 'memory,' or the ability of cells to respond more rapidly to stimuli after a prior exposure. Innate immune memory is mediated by epigenetic changes that make cells more responsive to secondary stimuli. Macrophages can be 'trained' by priming with β-glucan, which alters the histone acetylation profile of several promoters to make them more responsive to subsequent infection (75). In both hematopoietic and non-hematopoietic cells, ISGs accumulate the activation-associated histone H3.3

as they are transcribed. This confers ‘transcriptional memory’ that permits faster and more robust upregulation of these ISGs following subsequent stimulation (76-78).

## VIRUS-HOST INTERACTIONS

### *Non-immune host responses to virus infection*

Beyond activating immune pathways, viruses have an extensive impact on the host cell. Viruses require host machinery for replication, transcription, translation, entry/egress, and trafficking through the cells. siRNA screens have identified hundreds of host proteins required for IAV protein localization, genome transcription and replication, and virus packaging and budding (79, 80). In addition to using host proteins directly, viruses need access to host metabolites, including nucleotides and amino acids, and therefore can have a profound impact on host cell metabolism. Many viruses shift the balance between glycolysis and oxidative phosphorylation in infected cells, and this shift can go either direction depending on the requirements for the virus. Certain strains of rubella virus induce oxidative phosphorylation to provide glutamine to promote virus replication (81). In contrast, Dengue virus induces glycolysis (82). The requirement of non-immune proteins for virus replication adds complexity to virus-host interactions, and—along with innate immune proteins—can provide additional species barriers to virus transmission.

***The molecular arms race between virus and host***

The host immune response places enormous evolutionary pressure on viruses. Many viruses encode proteins that antagonize innate immune signaling or directly inhibit antiviral proteins. The primary immune antagonist protein for IAV—NS1—has been found in both the nucleus and cytoplasm of infected cells, where it completes diverse antiviral mechanisms. NS1 proteins of various IAV strains have been found to inhibit RIG-I directly, inhibit IFN-I production, directly inhibit the antiviral proteins PKR and 2'-5' oligoadenylate synthetase (OAS), and interfere with various other host processes to promote virus propagation (83). Both IAV NS1 and the recently identified polymerase acidic-X (PA-X) also regulate host shutoff, or the inhibition of host gene expression as both a mechanism to prevent antiviral gene expression and to promote viral gene expression (84, 85). HIV-1 viral infectivity factor (Vif) is also a multifunctional protein, but the best-characterized function is inhibiting host APOBEC3 proteins, a family of DNA cytosine deaminases that restrict HIV-1 by driving deleterious hypermutation in the viral cDNA (86). Vif coordinates an E3 ubiquitin ligase complex that results in the degradation of several host APOBEC proteins. A recent study also suggests Vif induces cell cycle arrest to promote virus replication through an unknown mechanism (87). Many virus-encoded proteases—including those of hepatitis C and hepatitis A viruses—cleave MAVS to inhibit PRR signaling (88). These are just three well-characterized examples of viral immune antagonists, but the overall prevalence of such proteins in the global virome suggests the innate immune response is a prominent driver of virus evolution.

Viruses also exert an immense amount of selective pressure on hosts. As viruses evolve to evade host defenses, the host must also adapt to continue to combat virus infections. This creates a molecular arms race between virus and host, leading to the adaptation and evolution of both viral and host species. 50,000-100,000 years ago, modern humans and Neanderthals co-existed and interbred. After thousands of years of recombination and purifying selection, remnants of Neanderthal genes still exist in the human genome; approximately 2-3% of the genome in Asian and European humans is of Neanderthal origin. These introgressed gene segments are strongly enriched for virus-interacting proteins (89). Moreover, computational analyses comparing virus interacting proteins to the entire human proteome revealed that viruses drive approximately 30% of all protein adaptations (90). These data implicate viruses as the dominant driver of protein adaptations in humans and other mammals.

Many antiviral mechanisms target and disrupt virus gene expression by inhibiting replication or preventing translation of virus mRNA. This introduces the critical need to distinguish between virus and host; aberrant targeting of host genes can ultimately harm rather than protect the host. The host therefore has to balance evolution of antiviral defenses with maintenance of fitness. For example, antiviral OAS proteins sense double-stranded RNA and activate RNase L to cleave the RNA (91). However, due to the limited binding preference for nucleotide sequences and resulting targeting of host RNAs, OAS1 is lost in many primate species (92, 93). Viruses—due to their restricted genetic space—must also balance antiviral antagonism with fitness. Certain adaptations in IAV nucleoprotein

(NP) confer resistance to the host antiviral factor MxA (94, 95). However, these adaptations also destabilize NP and create a requirement of heat shock-regulated host chaperones for IAV propagation (96). Under restrictive temperatures (i.e. in the absence of heat shock), NP either adapts immune evasion and becomes unstable or retains stability but is susceptible to MxA-mediated restriction.

Many RNA viruses lack proofreading functions and therefore accrue many more mutations during their life cycle compared to hosts. This difference in mutation rates between virus and host—RNA viruses have mutation rates up to a million times higher than their hosts (97)—and the need to defend against many pathogens presents an interesting problem: how can the host possibly keep up? Many—if not all—virus antagonist proteins are under positive selection, meaning they have an accelerated accumulation of coding mutations, particularly in regions that directly interact with viral products (88). Another common mechanism of antiviral evolution is gene duplication. This gives the host genetic space to evolve to escape virus antagonism or gain resistance to new viruses without sacrificing established antiviral functions. This mechanism has been documented for many antiviral gene families, including *IFIT* (98) and *APOBEC3* (86, 99). The antiretroviral TRIM5-cyclophilin A (CypA) fusion protein has evolved independently in two distinct lineages via retrotransposition. This fusion swaps the retrovirus capsid recognition domain of TRIM5 for that of CypA, creating a protein with novel antiretroviral recognition and inhibition (100). As the host continues to evolve, the pressure is placed back on the virus to evade the immune response. Continued research into the ongoing arms race between viruses and host will reveal

additional host adaptation strategies. The identification of novel viruses in mammals and emergence of novel viruses into the human population will also reveal new host immune mechanisms and virus immune antagonists.

## CONCLUSIONS

Emerging viruses remain a significant threat to public health. In this chapter, I have highlighted the role of the innate immune response in controlling virus replication and spread in a host, and how the relationship between virus and host has shaped evolution in both species. Several important questions remain, including virus and host factors that drive effective immune responses *in vivo* and what virus and host factors contribute to cross-species transmission. These questions will be addressed in subsequent chapters of this thesis.

In Chapter 2, I will discuss the heterogeneity in IAV replication during the early days of infection *in vivo*. We hypothesized that this heterogeneity would correlate with differences in the antiviral response in infected cells. We also hypothesized that the immune response initiated by the first infected cells would affect tropism of IAV as it spreads within the lung *in vivo*.

Chapter 3 will characterize an additional reporter IAV that allows dissection of the immune response to primary IAV mRNA transcription and subsequent replication of genomic viral RNA. We hypothesized that there would be distinct responses to these two stages of IAV replication *in vivo*. This study also interrogates the epithelial cell type-specific responses to infection. Lung epithelial cell subsets have distinct functions under homeostatic conditions, and we therefore

hypothesized that different cell types would have distinct antiviral responses *in vivo*.

Chapter 4 will introduce a new model to analyze intra- and inter-species transmission of viruses and other pathogens. In this model, pet store mice harboring myriad pathogens are co-housed with our specific pathogen-free laboratory mice, resulting in transmission of pathogens via natural transmission routes. We use both wild type and IFN receptor knockout mice, allowing us to assess the role of the IFN response in controlling virus transmission to and dissemination within a host. This model uniquely allows access to both the reservoir and host, giving the opportunity to identify virus mutations and adaptations that occur during transmission and dissemination. Using pet store rats, we have also expanded this model to interrogate species barriers to transmission.

The data presented in Chapters 2 and 3 offer new insight into IAV and host factors that affect innate immune activation and regulation of the response. The model in Chapter 4 has significant potential to interrogate the role of the innate immune response in intra- and inter-species transmission. In Chapter 5 will highlight how these recent findings have deepened our understanding of the innate immune response to viruses and how these findings can inform our pandemic preparedness.

**FOOTNOTES**

[1]Abbreviations used this chapter: AMP, adenosine monophosphate; APOBEC, apolipoprotein B mRNA editing enzyme, catalytic polypeptide-like; CARMA3,

caspase recruitment domain and membrane-associated guanylate kinase-like protein 3; cGAS, cyclic GMP-AMP synthase; CypA, cyclophilin A; GMP, guanosine monophosphate; HIV, human immunodeficiency virus; IAV, influenza A virus; IFITM3, IFN-induced transmembrane protein 3; IFN, interferon; IFN$\alpha$R, IFN-$\alpha$ receptor; IFN$\lambda$R, IFN-$\lambda$ receptor; IRF, IFN response factor; ISG, IFN-stimulated gene; ISGF3, IFN-stimulated gene factor 3; ISRE, IFN-stimulated response element; JAK, Janus kinase; LGP2, laboratory of genetics and physiology 2; LY6E, lymphocyte antigen 6 family member E; MAVS, mitochondrial antiviral signaling protein; MCOLN2, mucolipin-2; MDA5, melanoma differentiation-associated protein 5; mRNA, messenger RNA; NF$\kappa$B, nuclear factor $\kappa$-light-chain-enhancer of activated B cells; NP, nucleoprotein; NS1, nonstructural 1; OAS, oligoadenylate synthetase; PA-X, polymerase acidic X; PAMP, pathogen associated molecular pattern; PKR, protein kinase R; PRR, pattern recognition receptor; RIG-I, retinoic acid inducible gene 1; RLR, RIG-I-like receptor; siRNA, small interfering RNA; SOCS, suppressor of cytokine signaling; STAT, signal transducer and activator of transcription; TLR, toll-like receptor; TRIM5, tripartite motif containing 5; TYK2, tyrosine kinase 2; USP18, ubiquitin specific peptidase 18; Vif, viral infectivity factor

## CHAPTER 2: Distinct antiviral signatures revealed by the magnitude and round of influenza virus replication *in vivo*


### SUMMARY

Influenza virus has a broad cellular tropism in the respiratory tract. Infected epithelial cells sense the infection and initiate an antiviral response. To define the antiviral response at the earliest stages of infection we used a series of single cycle reporter viruses. These viral probes demonstrated cells *in vivo* harbor a range in magnitude of virus replication. Transcriptional profiling of cells supporting different levels of replication revealed tiers of interferon-stimulated gene expression. Uninfected cells and cells with blunted replication expressed a distinct and potentially protective antiviral signature, while cells with high replication expressed a unique reserve set of antiviral genes. Finally, we used these single cycle reporter viruses to determine the antiviral landscape during virus spread, which unveiled disparate protection of epithelial cell subsets mediated by interferon *in vivo*. Together these results highlight the complexity of virus-host interactions within the infected lung and suggest that magnitude and round of replication tune the antiviral response.

## INTRODUCTION

Influenza A virus (IAV) drives significant morbidity and mortality worldwide each year. IAV has a broad cellular tropism in the respiratory tract with the ability to infect many epithelial cell types (101). Rig-I-like receptors detect virus in epithelial cells, resulting in the production of type I and III interferons (IFNs) and other proinflammatory cytokines (10). IFNs act through autocrine and paracrine signaling pathways to induce the production of IFN-stimulated genes (ISGs), which promote a general antiviral state. Several individual ISGs have been identified that perturb IAV at multiple stages of the viral life cycle. For example, IFITM3 blocks entry, Mx disrupts the IAV polymerase, and PKR inhibits viral protein synthesis (27, 102-105). The induction of an antiviral state can also be driven directly by virus replication, independent of IFN signaling (32, 106, 107). It is unknown how the level of virus replication within a single cell affects the induction of global cellular responses. Even in the presence of a robust antiviral response, some infected cells continue manufacturing new viruses and naïve cells still become infected. How the antiviral response alters tropism during virus spread has not been determined.

Studies aimed at determining the cellular response to IAV infection have been performed by exploiting powerful genetic systems (CRISPR, RNAi, yeast two-hybrid, etc.) *in vitro* or by assessing bulk infected tissue *in vivo* (105, 108-110). While these analyses have been critical for evaluating host factors that support or inhibit IAV, the understanding of the complex interplay between different cell types, anatomical locations, and immune responses in the context of virus infection *in vivo* is still incomplete. Single cell analyses can help bridge this gap and have

demonstrated the heterogeneity in IAV replication and the antiviral response *in vitro* (62, 111, 112). Unfortunately, current single cell mRNA-seq strategies using wt virus cannot distinguish between newly infected cells and cells in which replication has been controlled *in vivo*.

To overcome these limitations, we engineered a reporter virus to specifically label cells in the first round of replication. This virus cannot spread; therefore, any differences in viral abundance will be a direct result of replication intensity. Infection of mice revealed uninfected cells and cells with both low and high levels of virus replication. These populations exhibited unique ISG signatures, and this finding was corroborated through the use of a reporter virus capable of specifically detecting active replication. This suggests that the antiviral response is tuned to the level of virus replication to generate a response appropriate to the level of threat. To understand how the antiviral response and tropism change from the first to second wave of replication we sequentially infected mice with viruses incapable of spreading. This strategy uncovered differential protection of ciliated epithelial cells mediated by IFN. These data demonstrate that epithelial cells supporting high or low levels of replication *in vivo* display tailored antiviral responses and that protection afforded by IFN is not equal amongst all cell types during virus spread. Together these findings demonstrate the complexity of virus-host interactions *in vivo* and illustrate how the cellular response is tuned to the level and round of replication.

## MATERIALS AND METHODS

### *Mice and virus infection*

C57BL/6J mice were purchased from The Jackson Laboratory. Mice were infected intranasally (i.n.) with the indicated doses of sclAV. Inactivated virus was generated through 20 minutes of UV exposure at room temperature. Carrier-free IFNβ1 (1.5-3 μg/mouse) and λ3 (2.5-3 μg/mouse) (R&D Systems) were administered i.n.. BrdU was administered i.p. at 1 mg/mL prior to infection and supplemented in the water at 0.8 mg/mL. Experiments involving mice were performed as dictated by the University of Minnesota Institutional Animal Care and Use Committee.

### *Tissue culture*

Madin-Darby Canine Kidney (MDCK) cells expressing WSN HA (MDCK WSN HA, kind gift from Dr. Adolfo García-Sastre, Mount Sinai), MDCK expressing PR8 HA (MDCK PR8 HA, kind gift from Dr. Luis Martinez-Sobrido, University of Rochester), and HEK293T cells (293T, ATCC) were maintained in DMEM with 10% FBS and 1% penicillin/streptomycin. MDCK PR8 HA cells were supplemented with 0.25 mg/mL hygromycin B.

### *Virus Rescue*

Viruses were rescued in 293T cells by plasmid-based transfection with IAV PR8 in the pDZ vector using methods previously described (113, 114). The 5' (106 bp) and 3' (156 bp) packaging signals were preserved, except AUG codons in the

5’ packaging signal were mutated. The designed gene of interest (mCherry, GFP, destGFP (pCAG-GFPd2 was a gift from Connie Cepko, Addgene plasmid #14760 (115)), or Cre recombinase) was cloned in between the HA packaging signals. pCAGGs WSN HA plasmid was supplemented into the transfection. 24 h following transfection, 750,000 MDCK WSN HA cells were added to the culture in Opti-MEM containing TPCK trypsin (0.5µg/mL). The following day, 500 µL Opti-MEM containing TPCK trypsin (1 µg/mL) was added. The next day, 500 µL Opti-MEM containing TPCK trypsin (2 µg/mL) was added to the culture. One day later, the supernatant was harvested, centrifuged to remove cellular debris, and stored at -80°C. Viruses were then grown on MDCK PR8 HA cells to exchange the HA from WSN to PR8. Plaque assays were carried out in MDCK WSN HA cells. Infections were carried out in infection media (PBS with 10% Ca/Mg, 1% pen/strep, 5% BSA) at 37°C for 1 h. Infection media was then replaced with an agar overlay (MEM, 1mg/mL TPCK trypsin, 1% DEAE-dextran, 5% $NaCO_3$, 2% agar) and cells cultured at 37°C for 40 h and then fixed with 4% formaldehyde. Blocking and immunostaining were done for 1 h at 25°C in 5% milk using the following antibodies: polyclonal anti-IAV PR8/34, 1:5000 (V301-511-552), Peroxidase Rabbit Anti-Chicken IgG, 1:5000 (303-035-003, Jackson Immuno Research). TrueBlue Peroxidase Substrate (50-647-28, Kirkegard & Perry Laboratories) was used as directed for detection of virus plaques.

***Flow cytometry***

Mice were euthanized and lungs were inflated with 2 mL dispase (Corning) and 0.5 mL 1% low melt agarose (Lonza) and allowed to sit covered with an ice pack for two minutes. Lungs were then removed from mouse and transferred to 1 mL dispase and incubated at room temperature for 45 minutes. Next, lungs were cut into pieces and transferred to DMEM with DNase I (Sigma-Aldrich) 95 U/mL and shaken for 10 minutes at room temperature. Solution was filtered off and lungs were homogenized in GentleMACS dissociator in harvest buffer (RPMI1640 with 4% bovine serum, 1% HEPES, and 1% L-glutamine). Red blood cells were lysed with ACK buffer and cells were filtered through 70 μm filter mesh to obtain a single cell suspension prior to staining. Cells were stained with Ghost Dye Red 780 (Tonbo), followed by the following antibodies against surface markers: CD45 (30-F11), Podoplanin (clone 8.1.1), CD24 (M1/69) (Biolegend), CD31 (clone 390, BD Bioscience). Prior to intracellular BrdU staining, cells were fixed overnight using the BD CytoFix/Cytoperm kit (BD Biosciences) and treated with DNAse I (2.5 mg/mL, Sigma-Aldrich). Fixed cells were stained for intracellular BrdU (clone MoBU-1, Life Technologies). Cell counts were obtained using AccuCheck counting beads (Thermofisher Scientific). Data was acquired on a BD LSRFortessa (Becton Dickinson, San Jose, CA).

***Next-generation mRNA sequencing analysis***

Mice were infected and lung epithelial cells were FACS sorted as stated previously. Cells were sorted into 1.5 mL microcentrifuge tube and RNA was isolated using RNeasy Micro or Micro Plus kit (Qiagen) The cDNA library was prepared using the SMARTer Universal Low Input RNA Kit (Takara Bio). Samples were sequenced as 50 base pair single-end reads using the HiSeq2500. We obtained an average of 12 million reads per sample. Sequencing reads were mapped to the mouse (mm10) and influenza A/PR/8/34(H1N1) genomes using Bowtie aligner (bowtie2 version 2.2.4) with local mode, 22 nt seed sequence, and ≤1 nt mismatch (-L 22 and -N 1 parameters) (116). Reads were subsequently sorted and filtered by removing the PCR duplicates with Samtools (version 1.16) (117) and were assigned to Ensembl gene model (Mus_musculus.GRCm38.87.gtf) with featureCounts of the Subread software package (version 1.5) (118). For the IAV read assignment, reads were mapped to the combined mm10 and IAV mRNA (Influenza Research Database). Both reads assignment tables were merged to create raw reads count matrix for subsequent statistical analysis. To determine if IAV transcripts were truncated in some samples, sample raw reads that were mapped to the customized reference (mouse genome and IAV mRNA) were visualized in the Integrated Genome Viewer (IGV) (119). Scales were adjusted to make coverage profiles more easily comparable across samples. The 221 differentially expressed ISGs in either mCherry low or high group were selected for further cluster analysis (FDR < 0.05). The default scaling and hclust method in complex heatmap package was used for clustering

and generating heatmap (120). The same cutoff was applied to destabilized GFP experimental groups and 197 ISGs were selected for cluster analysis as described above. To obtain significant differentially expressed genes, the experimental groups by design were compared to control group (naïve or negative) and the edgeR bioconductor package was used for statistical analysis (121, 122). Sequencing data deposited under GEO series accession number GSE112794.

***Microscopy and histo-cytometry***

Lungs were fixed for 2h in 2% paraformaldehyde and inflated before being flash frozen in optimum cutting temperature compound. Sections were cut with a Leica CM1860 cryostat and stained before imaging with a Leica DM6000B EPI fluorescent microscope (violet LED). The following antibodies were used: primary antibodies: α-CC10 (polyclonal, Abcam) and α-proSP-C (polyclonal, Millipore Sigma); secondary antibody: goat α-rabbit (polyclonal, ThermoFisher). Histo-cytometry analysis was performed with Imaris (Bitplane) by gating the low and high mCherry cells according to mean fluorescence intensity (MFI) using scIAV-ctrl to determine background levels of mCherry fluorescence. An additional gate was created to determine the distance each mCherry cell was from SPC or CC10 markers.

### *Statistical analysis*

Statistical analysis was executed using GraphPad Prism 7 software. Comparisons between two groups were performed using a two-tailed Student *t* test, and $p<0.05$ was considered statistically significant. Error bars are calculated using standard error of the mean.

## RESULTS

### *Single-cycle infection reveals IAV replication heterogeneity in vivo*

To determine the infected cell landscape during the first round of IAV replication *in vivo* we engineered a reporter virus incapable of disseminating. The Hemagglutinin (HA) open reading frame of IAV was replaced by mCherry while preserving complete HA vRNA 3' and 5' packaging signals and virus grown in an HA complementing cell line (123, 124). The virus cannot produce *de novo* HA protein and assemble new virions that can infect other cells (thus termed single-cycle IAV (scIAV)). Infection of mice revealed three distinct populations of lung epithelial cells: those with no, low, or high mCherry fluorescence (Figure 2-1A). The heterogeneity in mCherry expression suggests that virus polymerase activity during the early stages of scIAV infection varies from cell to cell. Both low and high mCherry populations were observed at similar ratios at both 12 and 24 hpi (Figure 2-1A) and required *de novo* virus polymerase activity (Figure 2-2A and B). Both mCherry low and high $CD24^{high}$ and $podoplanin^{+}$ (pdpn) (ciliated epithelial cells and type I alveolar (ATI) cells, respectively) were identified, suggesting cell type does not drive replication heterogeneity (Figure 2-2C).

Replication disparity could be driven by anatomical location and/or proximity to other infected cells. To address this, mice were infected with scIAV-mCherry and lungs were analyzed by fluorescence microscopy. We detected mCherry low and high cells in both large and small airways and did not observe any restriction based on proximity to other infected cells (Figure 2-1B and 2-2D). To further define tropism during the first round of infection, we determined the number of mCherry low and high club cells (CC10) and type II alveolar cells (SPC). We found similar ratios of mCherry low to high cells in both cell types (Figure 2-2E-H), suggesting that heterogeneity in early virus replication levels is not driven by cell type.

Multiple IAV particles can infect a single cell, which could drive differences in fluorescence intensity between cells. To address this, mice were infected with a mixture of scIAV-mCherry and scIAV-GFP. At 24 hpi there was only a small percentage of mCherry-GFP double positive cells. (Figure 2-1C). The difference in fluorescence intensity between the low and high populations is approximately 25-fold (Figure 2-2I), further suggesting that infection with multiple particles is not driving the disparity. To determine if the range of replication is dependent on virus dose, mice were infected with a 10-fold lower inoculum of scIAV-mCherry and cells supporting low and high replication were still observed (Figure 2-2J).

Prolonged presence of infectious particles in the lungs could result in varied time of infection and lead to replication disparity. This is unlikely given the speed of IAV entry *in vitro* and that virus dose and duration of infection did not impact heterogeneity in single cell analyses (62, 125, 126). However, the half-life of an infectious particle *in vivo* has never been experimentally determined. We exploited

the scIAV system to address this question. Because scIAVs cannot spread, only viruses that have not yet entered a cell can be detected by plaque assay. Mice were infected with scIAV-mCherry and virus titer from the lungs determined at 6, 12, and 24 hpi. By 6 hpi, only ~6% of the virions delivered in the initial dose were detectable in the extracellular lung environment with a half-life of ~1.7 h (Figure 2-1D). This is consistent with mathematical modeling experiments, which predicted a half-life between 0.6 and 3 h (127, 128). Therefore, the vast majority of virions will have entered cells prior to the induction of the early innate immune responses.

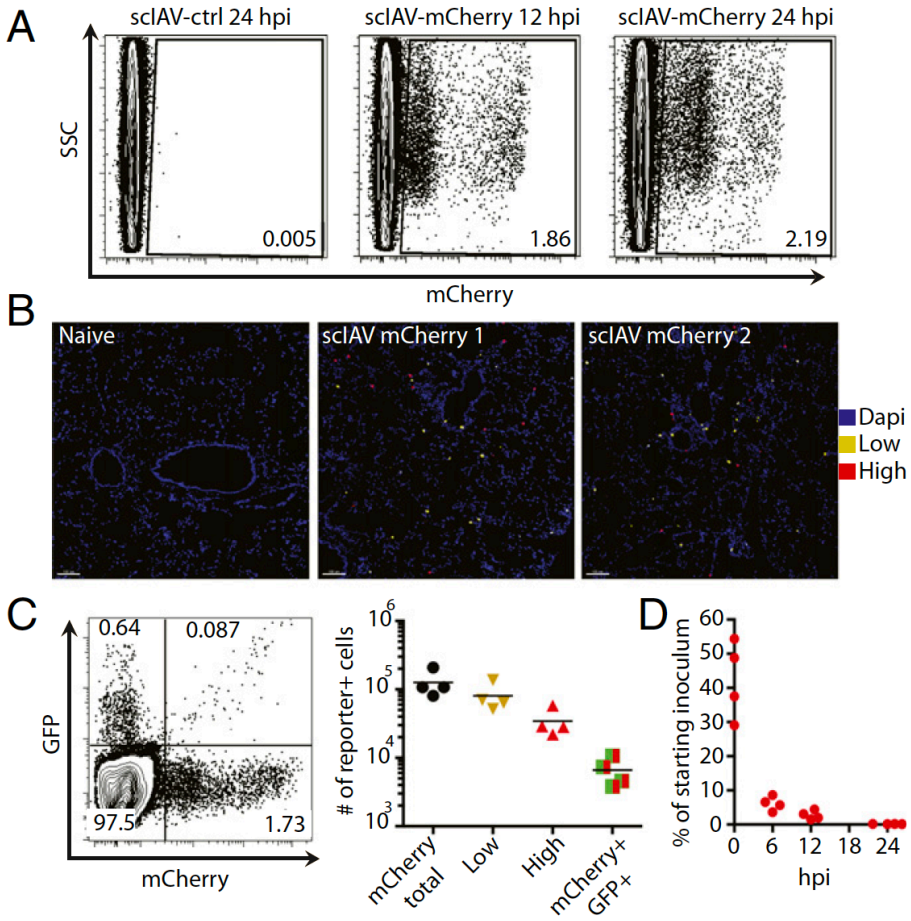


**Figure 2-1.** Heterogeneity in replication levels of IAV in epithelial cells *in vivo*. (A) Mice were infected with $10^5$ pfu of scIAV-ctrl (left) or scIAV-mCherry and live, $CD45^-CD31^-$ cells analyzed for mCherry expression at 12 (middle) or 24 (right) hpi. Data are representative of 2 (12 hpi) or 10 (24 hpi) experiments with 3-4 mice per group. (B) Naïve mice (left) or mice infected with scIAV-mCherry (middle, right) and analyzed for mCherry low and high cells by histo-cytometry. Images are representative of 2-3 experiments with three mice per group and 2 sections per lung. (C) Mice were co-infected with $10^5$ pfu of scIAV-mCherry and $10^5$ pfu of scIAV-GFP. Live, $CD45^-CD31^-$ cells analyzed for GFP and mCherry expression 24 hpi (left). Total $mCherry^+$, mCherry-high, mCherry-low, and $GFP^+mCherry^+$ cells were quantified (right). Data representative of 3 experiments with n=3-4 mice per group. (D) Mice were infected with $10^5$ pfu of scIAV-mCherry and virus from lungs titered on MDCK-HA cells at the indicated hpi.

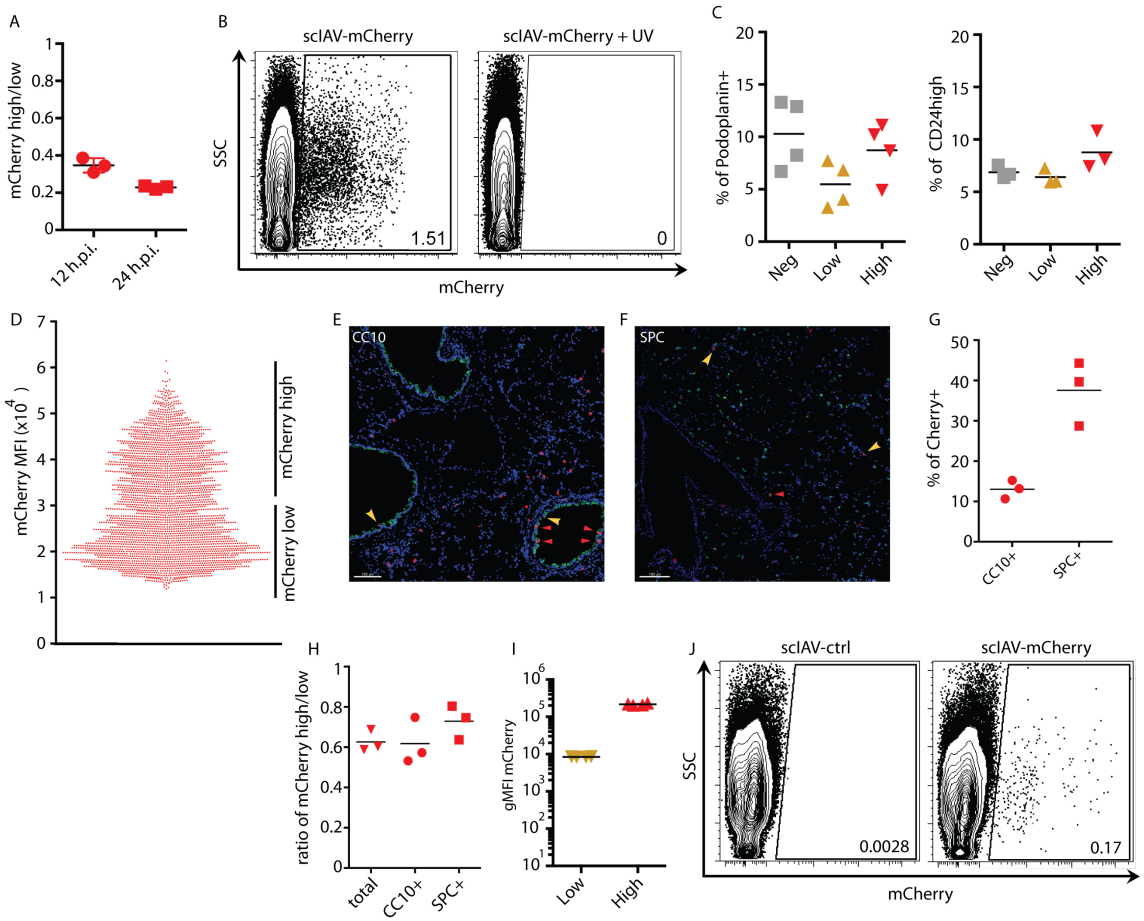


**Figure 2-2.** Heterogeneity in replication levels of IAV in epithelial cells *in vivo*. (A) Ratio of mCherry high to low cells determined by flow cytometry. (B) Mice infected with scIAV-mCherry or UV killed scIAV-mCherry and $CD45^{-}CD31^{-}$cells analyzed at 24 hpi Y-axis side scatter (SSC). (C) Frequency of podoplanin$^{+}$ (left) or $CD24^{high}$ (right) cells among the $CD45^{-}CD31^{-}$ mCherry negative, low, and high populations. Data representative of 5 independent experiments with 3-4 mice per group. (D) Mice infected with scIAV-mCherry and MFI of mCherry$^{+}$ lungs cells analyzed by histo-cytometry. (E and F) Mice infected with scIAV-mCherry and lungs analyzed for CC10 (E) and SPC (F). Arrows indicate cells double positive for mCherry and either CC10 or SPC. Red arrows-mCherry high cells. Yellow arrows-mCherry low cells. Scale bar = 100μ□. Images are representative of 1-2 independent experiments with 3 mice per group and 2 sections per lung. (G) Frequency of CC10$^{+}$ or SPC$^{+}$ cells among the mCherry$^{+}$ population. (H) Ratio of mCherry high and low cells in total, CC10$^{+}$ and SPC$^{+}$ cells. (I) gMFI of mCherry of $mCherry^{+}CD45^{-}CD31^{-}$ cells by flow cytometry. (J) Mice were infected with $10^{4}$ pfu of scIAV-mCherry and $CD45^{-}$ $CD31^{-}$ cells analyzed for mCherry expression at 24 hpi Y-axis side scatter (SSC).

***High levels of replication reveal a distinct antiviral gene signature***

To investigate the intracellular responses to variable levels of IAV replication we profiled the transcriptomes of $CD45^{-}CD31^{-}$ mCherry negative, low, and high cells by mRNA-seq. Reads that mapped to the IAV genome were markedly higher in the mCherry high population compared to low or negative (Figure 2-3A), validating the use of mCherry expression level as a surrogate for virus replication. Failure to package or express all eight segments or internal truncations of segments can result in attenuated replication (129-131). Normalized read counts between segments were similar between mCherry low and high cells and read abundances across segments did not reveal differences in internal truncations between infected cell populations (Figure 2-4A and B) suggesting that we are detecting *bona fide* infected cells. Multidimensional scaling (MDS) of mouse transcripts demonstrated significant differences between mCherry low and high cells across the first two dimensions (Figure 2-3B). Importantly, the negative population was derived from the same lung as $mCherry^{+}$ cells and was subjected to the same inflammatory environment, making it an effective control for determining virus replication-specific gene signatures. Global changes in the transcriptional response of mCherry low and high compared to mCherry negative were analyzed by gene ontology (GO) enrichment. mCherry low and high cells downregulated many of the same pathways, primarily those involved in cell adhesion, extracellular matrix, and development (Figure 2-4C). Cell death pathways were increased in mCherry high cells while DNA replication and cell cycle pathways were upregulated in mCherry low cells (Figure 2-4C). To determine

if cell cycle was associated with lower amounts of replication, we pulsed mice with BrdU, infected with scIAV-mCherry, and analyzed at 24 hpi. There was no increase in $BrdU^+$ cells in the infected cell population, and $BrdU^+$ cells made up only 0.6% of the mCherry low population (Figure 2-4D), suggesting that entry into the cell cycle is not driving restriction of viral replication.

Cells with low or high levels of virus replication may differentially activate antiviral pathways. To determine the antiviral response we analyzed the 221 differentially expressed ISGs and revealed several distinct groups of ISGs that varied with the level of virus replication (Figure 2-3C). Cluster 2 ISGs were highly induced in mCherry negative and low cells but not in mCherry high cells. This cluster included several genes with known antiviral activity against IAV including *Eif2ak2* (PKR), *TRIM56*, and *Pml* (27, 132, 133). Cluster 4 was only induced in mCherry high cells (Figure 2-3C), suggesting that high levels of virus replication may produce a distinct antiviral response. Levels of *Ifnar1* were similar in mCherry low and high cells (Figure 2-4E). Additionally, *Mx1*, which is IFN signaling-dependent (32), was induced to a similar degree in mCherry low and high cells (Figure 2-4E), suggesting that differential extracellular IFN signaling alone may not drive the disparity in ISG expression. Expression of *Irf7* was similar in all infected cells while *Irf3* was decreased in mCherry high cells, suggesting that induction of these critical sensors is not driving the ISG disparity (Figure 2-4E). However, *Ifnb1* was higher in the mCherry high cells than other cell populations (Figure 2-4E). Overall, our data show distinct ISG signatures within cells with low or high virus replication.

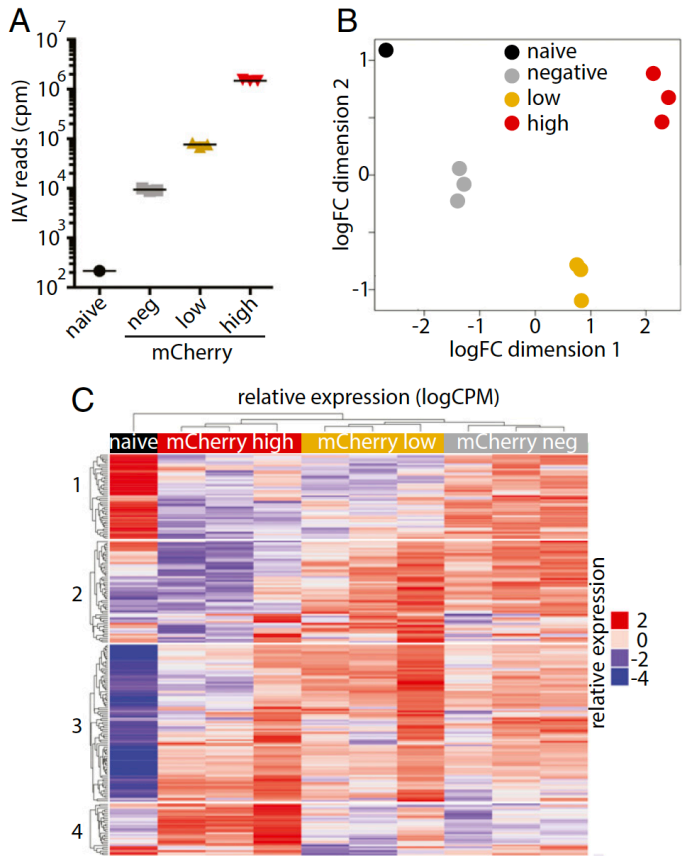


**Figure 2-3.** Unique antiviral signatures in cells supporting low and high levels of replication. Mice were infected with $10^5$ pfu of scIAV-mCherry and live CD45$^-$ CD31$^-$ mCherry negative, low, and high cells were profiled by mRNA-seq. (A) IAV cpm. (B) MDS of naïve and mCherry negative, low, and high cells based on host mRNA reads (C) Heatmap of 221 ISGs differentially expressed in the indicated populations. Cutoff of FDR < 0.05.

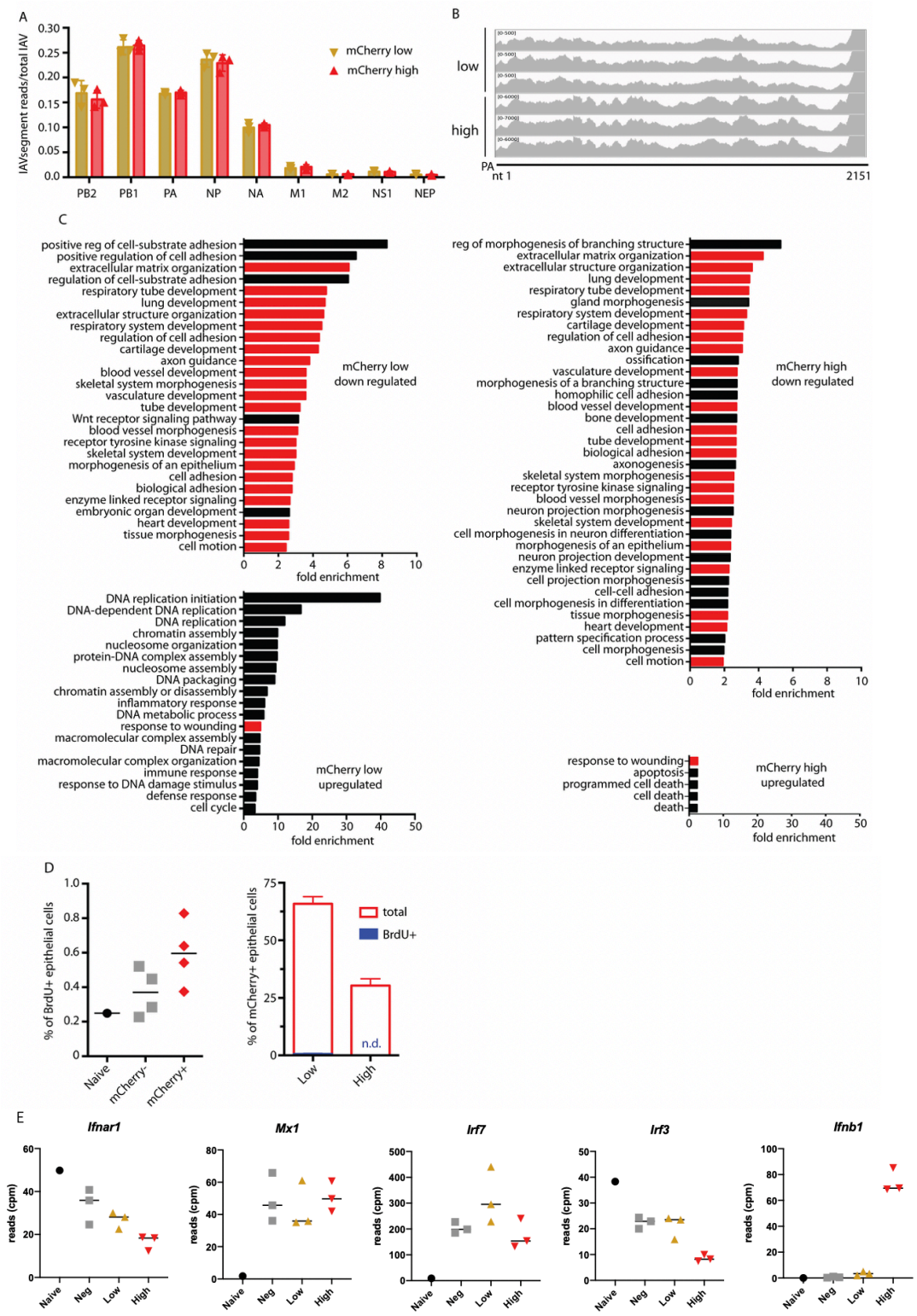


**Figure 2-4.** Unique transcriptional signatures in cells supporting low and high levels of replication. (A) IAV reads in mCherry high and low cells from each segment analyzed as ratio of total IAV reads. (B) IAV-PA reads were mapped in mCherry low or high cells. (C)

Gene ontology enrichment analysis (DAVID, biological process) of genes with >2- or <-2-fold change and FDR <0.05 over mCherry negative. Fold enrichment cutoff of FDR< 0.01. Red bars represent pathways that are shared between mCherry low and high cells. Black bars are unique pathways. (D) Mice were pulsed with BrdU and infected with scIAV-mCherry. The percentage of $BrdU^+$ in the $mCherry^-$ and $mCherry^+$ populations (left) and the percentage of $BrdU^+$ mCherry low or high cells (right) were determined at 24 hpi Data representative of 2 independent experiments with 3-4 mice per group. (E) Read cpm of (L to R**)** *Ifnar1*, *Mx1*, *Irf7*, *Irf3*, and *Ifnb1* in the indicated cell populations. IFN$\alpha$s and IFN$\lambda$2 and 3 were not detected above 3 cpm in any cell population analyzed.

### *Active virus replication imparts specific antiviral responses*

We hypothesized that the ISGs uniquely expressed in mCherry high cells are specific to conditions of unchecked viral replication and may represent a 'last resort' antiviral effort by the host. To identify cells harboring actively replicating virus, we developed a scIAV encoding destabilized GFP (destGFP) in place of HA. The half-life of this protein is only 2 h compared to over 24 h for the standard enhanced GFP (134). Due to this rapid degradation, any $GFP^+$ cells detected *in vivo* must be the result of active virus replication (Figure 2-5A). Mice were infected with scIAV-GFP or scIAV-destGFP and $CD45^-CD31^-$ lung epithelial cells were analyzed for GFP expression at 24 hpi. Less than 15% of the total scIAV-GFP-infected epithelial cells were detected by scIAV-destGFP, suggesting that many wt $GFP^+$ cells are no longer supporting active replication at this timepoint (Figure 2-5B and 2-6A). $GFP^+$ lung epithelial cells from mice infected with wt GFP- or destGFP-expressing viruses were isolated and their transcriptomes profiled by mRNA-seq. As expected, $destGFP^+$ cells contained more IAV mRNA than wt $GFP^+$ cells (Figure 2-5C). Cellular transcripts were analyzed by MDS and revealed significant differences in $destGFP^+$ compared to wt $GFP^+$ cells, primarily across the

second dimension (Figure 2-5D). GO analysis of downregulated pathways in the destGFP$^+$ and wt GFP$^+$ populations revealed the same cell adhesion, extracellular matrix and development pathways that were downregulated in mCherry low and high cells (Figure 2-6B). This concordance suggests that cells specifically decrease certain sets of genes in response to IAV infection.

To assess the antiviral response generated in cells supporting active replication we analyzed ISG expression in sorted destGFP$^+$, destGFP$^-$, wt GFP$^-$, and naïve cells (Figure 2-5E). Cluster 1 ISGs were specifically induced in wt GFP$^-$ and destGFP$^-$ cells. This expression pattern was similar to cluster 2 in the mCherry expression analyses (Figure 2-3). We compared these two clusters and found several overlapping genes (Figure 2-5F), many of which have been demonstrated to have direct antiviral activity against IAV (27, 132, 133, 135). There was also a cluster of ISGs that were only expressed in actively replicating cells (Figure 2-5E, cluster 4b), analogous to cluster 4 in Figure 2-3. We compared cluster 4b to the unique ISGs expressed in mCherry high cells and found a high level of concordance (Figure 2-5G). These data demonstrate that cells supporting high levels of active virus replication express a distinct set of ISGs that is not expressed in other infected cells. Overall, our analyses using scIAV-destGFP recapitulated results obtained using scIAV-mCherry revealing distinct antiviral signatures in cells supporting active virus replication.

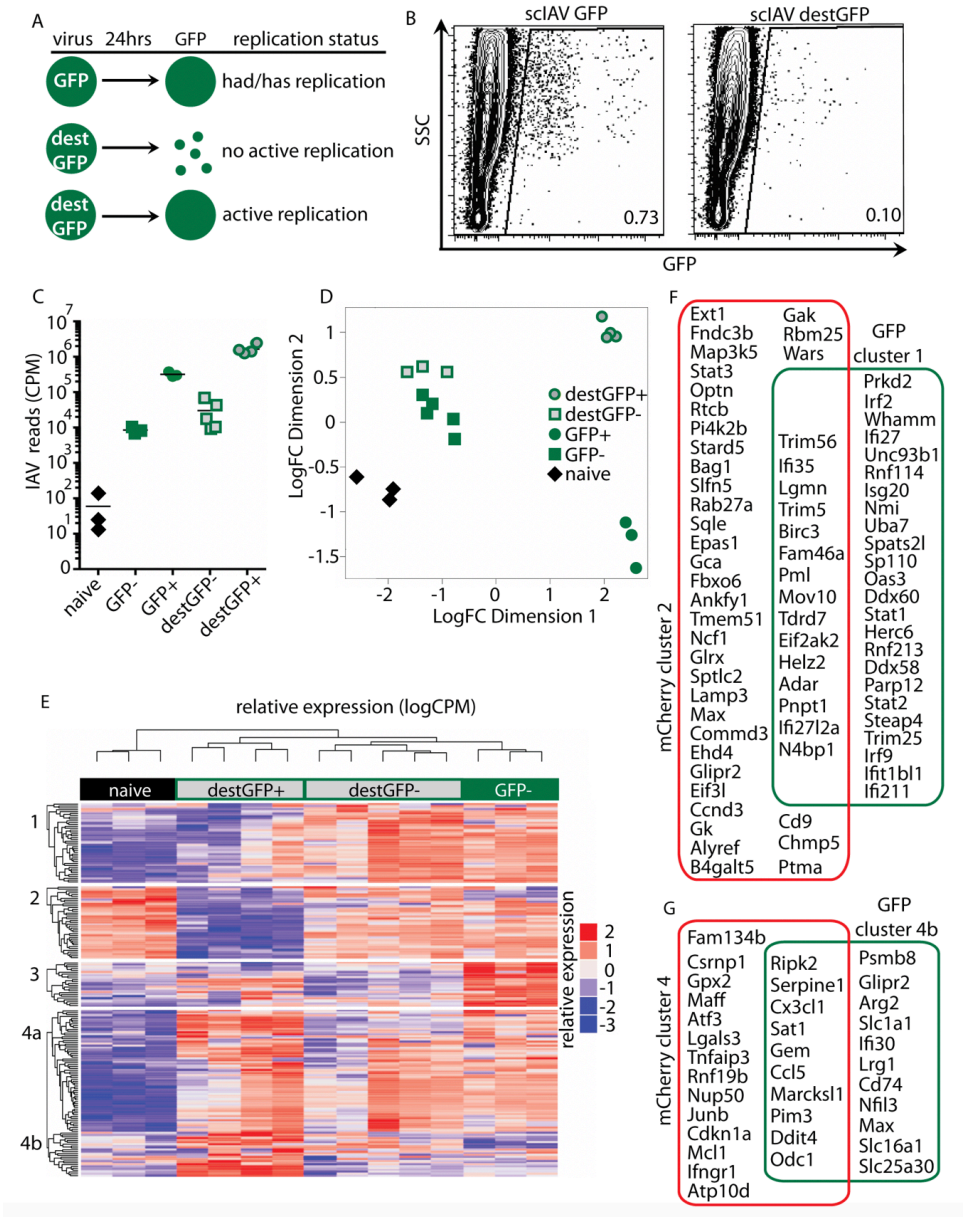


**Figure 2-5.** Virus expressing destabilized GFP labels actively infected cells revealing distinct antiviral responses. (A) Model for the use of scIAV-destGFP to identify cells with actively replicating virus. (B) Mice infected with $10^5$ pfu of scIAV-ctrl, -GFP, or destGFP and live, $CD45^-CD31^-$ cells analyzed for GFP expression 24 hpi. Data representative of 3 experiments with n=3-4 mice per group. (C and D) Live, $CD45^-CD31^-$ $GFP^+$ and $GFP^-$ cells were sorted and mRNA mapped to the mouse and IAV genome. (C) Normalized IAV reads in each of the sorted cell populations. (D) MDS plot of the indicated populations based on mRNA reads. (E) Heatmap of the 197 differentially expressed ISGs in the indicated populations. FDR < 0.05 used as a cutoff. (F) Venn diagram of genes from mCherry cluster 2 in figure 2 and GFP cluster 1 in figure 3. (G) Venn diagram of genes from mCherry cluster 4 in figure 2 and GFP cluster 4b in figure 3. Only genes induced to >10cpm in at least one condition are shown.

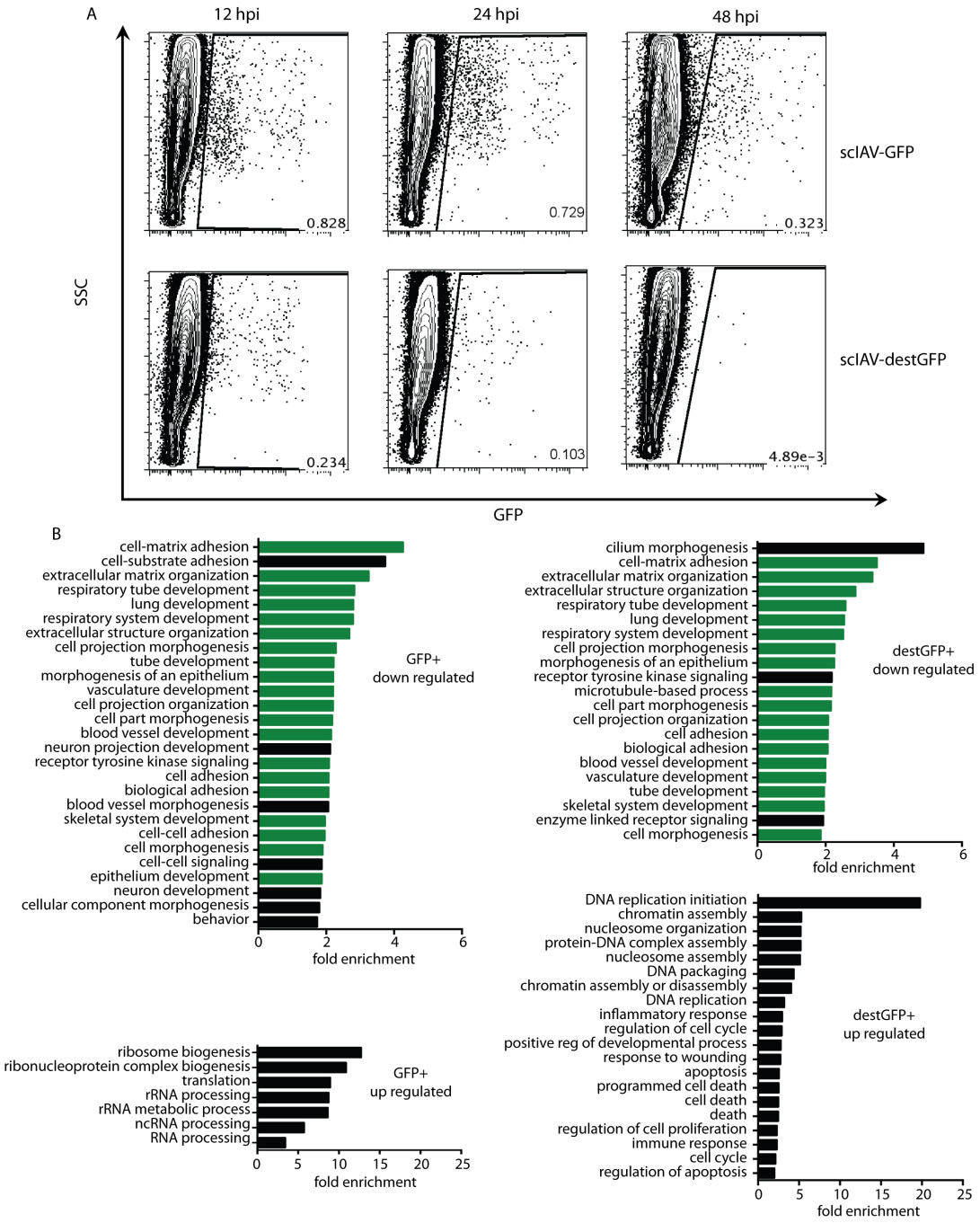


**Figure 2-6.** Virus expressing destabilized GFP labels actively infected cells revealing distinct transcriptional responses. (A) Mice infected with either scIAV-GFP (top) or scIAV-destGFP bottom and $CD45^{-}CD31^{-}$ cells analyzed for GFP expression at 12, 24, and 48 hpi. 24 hpi time point is from figure 3B. Y-axis side scatter (SSC). (B) Gene ontology enrichment analysis (DAVID, biological process) of genes with >2- or <-2-fold change and FDR <0.05 over the corresponding $GFP^{-}$. Pathways with FDR<0.01 by are shown. Green indicates overlapping pathways between $GFP^{+}$ and $destGFP^{+}$. Black bars are unique pathways.

***Tropism is altered by IFN during virus spread***

During an infection, IAV spreads and new cells are infected despite a local antiviral and proinflammatory response. To label cells infected after the initiation of inflammation, we employed a sequential infection strategy using scIAVs with distinct fluorophores to model virus spread *in vivo* (Figure 2-7A). Lung epithelial cells were analyzed for mCherry expression 24 h after the second infection. There was a significant decrease in the overall number of $mCherry^+$ cells in the sequential infection, indicating that the first infection induced an immune response that conferred some protection (Figure 2-7B and C). Interestingly, mCherry low and high cells were observed at similar proportions in single and sequential infection. To determine if there is a change in tropism during the second round of replication, $mCherry^+$ cells were analyzed for markers of ciliated epithelial cells and type I alveolar (ATI) cells ($CD24^{high}$ and $pdpn^+$, respectively). The frequency of $mCherry^+pdpn^+$ cells was similar in single and sequential infection. However, there was a significant decrease in the frequency of $mCherry^+CD24^{high}$ cells in the sequentially infected animals compared to mice infected with scIAV-mCherry alone (Figure 2-7D). To elucidate the mechanisms of protection during the second round of infection, we sorted $CD54^-CD31^-$ mCherry negative, low, and high cells from sequentially infected mice for mRNA-seq analysis. These data were compared to the single infection data shown in figure 2. MDS analysis of the host transcripts demonstrated significant differences between single and sequential infected cells along the second dimension (Figure 2-7E). GO analysis of the genes significantly downregulated in both mCherry low and high sequential infected cells

demonstrated enrichment in several pathways involved in ciliated epithelial cell maintenance and development (Figure 2-7F), further supporting the data in Figure 2-7D. No pathways were significantly upregulated between single and sequentially infected cells. We hypothesized that the first round of replication drives an IFN response that enhances the protection of ciliated epithelial cells, but not ATI cells. To test this, mice were treated intranasally with IFNβ or IFNλ and 16 h later challenged with scIAV-mCherry. ATI cells and ciliated epithelial cells were analyzed for mCherry expression. Both IFNβ and IFNλ treatment led to a significant decrease in the frequency of infected ciliated epithelial cells but did not protect ATI cells (Figure 2-7G and Figure 2-8). These data suggest that tropism is altered during virus spread through differential IFN-mediated protection *in vivo*.

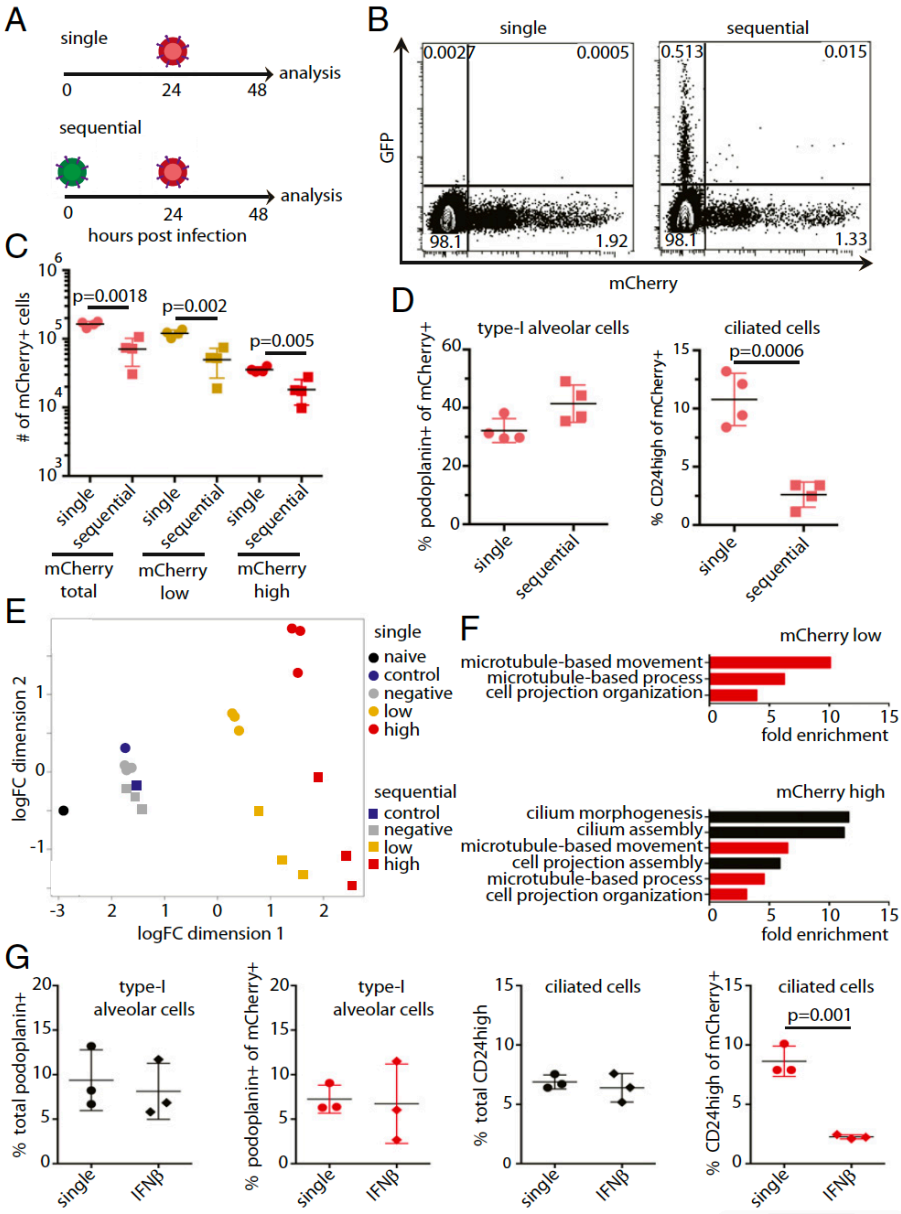


**Figure 2-7.** Tropism is altered by IFNβ during virus spread. (A) Model demonstrating sequential infection strategy. (B) Representative flow plot of (A). (C) Numbers of total mCherry$^{+}$, mCherry low, and mCherry high cells in single and sequential infection. (D) Frequency of total and mCherry$^{+}$ CD24$^{high}$ ciliated cells and pdpn$^{+}$ ATI cells. (E) MDS plot of single infected mCherry negative, low, and high cells from figure 3 and mCherry negative, low, and high cells from sequential infection. (F) Gene ontology enrichment analysis (DAVID, biological process) of the downregulated mCherry low and high genes that were significantly different (FDR < 0.05) from single to sequential infection. (G) CD45$^{-}$ CD31$^{-}$ cells from mice treated with IFNβ and infected with scIAV-mCherry analyzed for total (black) or infected (red) pdpn$^{+}$ and CD24$^{high}$ cells. B-D representative of 5 experiments with n=3-4 mice per group. G representative of 3 experiments with n=3-4 mice per group.

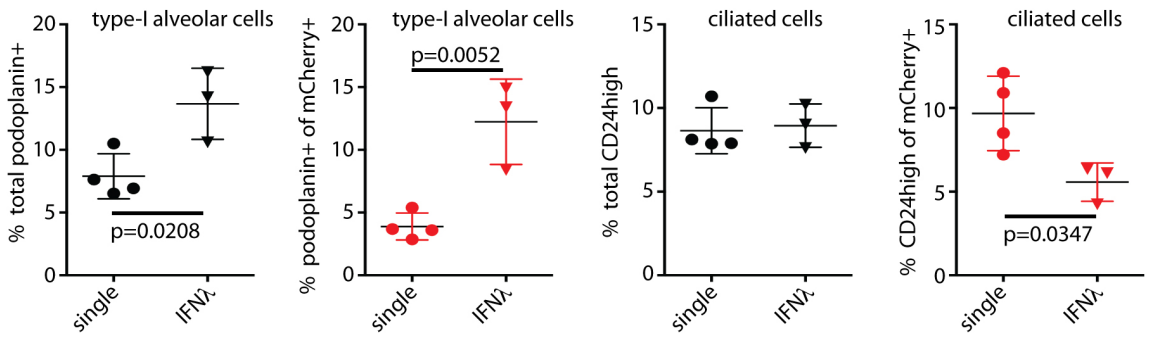


**Figure 2-8.** Tropism is altered by IFNλ during virus spread. CD45$^-$CD31$^-$ cells from mice treated with IFNλ and infected with scIAV-mCherry analyzed for total (black) or infected (red) pdpn$^+$ and CD24$^{high}$ cells. Data representative of 3 experiments with n=3-4 mice per group.

## DISCUSSION

Multiple studies using single-cell sequencing have revealed heterogeneity in IAV replication and the antiviral response *in vitro* (62, 111). These data are consistent with previous reports demonstrating stochasticity in single cell responses to infection (112, 136-138). Importantly, single cell-sequencing following synchronized and unsynchronized IAV infection revealed that duration and infectious dose are not responsible for the heterogeneity (62). Single cell *in vivo* analysis also demonstrated heterogeneity in virus replication and antiviral responses, although the number of epithelial cells analyzed was low (139). Consistent with previous findings, our data reveal heterogeneity in virus replication levels and the cellular response to IAV during the early stages of infection *in vivo.* While we cannot determine if these cellular changes are a cause or a consequence of replication disparity, they reveal that the antiviral signatures are not equal in all infected cells.

IFN-I and –III drive the expression of hundreds of ISGs, which can vary by cell type (140). A landmark series of studies demonstrated a paucity of individual ISGs that inhibit a diverse array of viruses (23, 24). IRF-1, Mx, and IFITM2/3 were among the few ISGs that were able to significantly blunt IAV infection and replication (24). Additionally, IAV grown in absence of ISGs tolerates more mutations, suggesting that multiple ISGs normally constrain the virus (141). We found a constellation of known anti-IAV ISGs expressed in mCherry low and negative cells that were absent in cells supporting active or high levels of replication. While only correlative, it is interesting to speculate that these may be protective combinations of ISGs and failure to induce these genes permits high levels of replication. In addition to host factors, replication disparity could be in part due to mutations in the viral genome that enhance resistance or susceptibility to IFN. As such, Du *et al.* recently identified several IAV mutations that lead to IFN sensitivity (142). Moreover, the basal expression of one or more ISG alone, or in combination with induced ISGs, could be driving the disparate levels of virus replication. mCherry high cells also have increased levels of IFNβ expression compared to other populations of cells in the infected lung (Figure 2-4E). An alternative hypothesis is that autocrine IFN signaling alone, in combination with high levels of replication, or basal ISG levels could drive the distinct ISG responses.

Our data reveal a distinct set of ISGs expressed in cells with high or active virus replication. These ISGs may represent a reserve set of genes that are only turned on in cells that fail to blunt replication. Interestingly, some of these genes

are chemokines and other inflammatory mediators, which may help to orchestrate an inflammatory response to control virus spread from these cells. It may be important to only express these genes when control of replication has failed to prevent immunopathology. In addition, pattern recognition receptor usage may be an underlying mechanism of this ISG signature. While RIG-I is thought to be the primary sensor for IAV in epithelial cells recent evidence demonstrates that MDA5 is important for the cellular response (143). High levels of replication might be needed to activate both RIG-I and MDA5 and could act as an additional level of regulation to prevent aberrant activation of proinflammatory ISGs.

Both immune and epithelial cells sense IAV *in vivo* (144), and responses can be dependent on the cell type. We have previously demonstrated that club cells, which survive virus replication, exhibit prolonged ISG signatures (145, 146). Our data demonstrate that IAV tropism changes over the course of infection. Ciliated cells were afforded greater protection from secondary infection compared to ATI cells. Importantly, this could only be discovered through an *in viv*o scIAV sequential infection strategy. While IFNβ and IFNλ can drive this selective protection, it is unknown if IFN-mediated protection is direct or indirect through other epithelial or innate immune cells.

Here we demonstrate heterogeneity in the levels of virus replication *in vivo*. Using two different virus reporters we reveal that distinct sets of antiviral genes are expressed in cells harboring low and high levels of virus replication. Through a sequential infection strategy, we demonstrate that virus tropism is altered during virus spread where ciliated epithelial cells have augmented protection from

infection. These results demonstrate a dynamic environment within tissues that is driven by both virus replication levels and the cell type infected.

**FOOTNOTES**

[1]This work is published: Sjaastad LE*, Fay EJ*, Fiege JK, Macchietto MG, Stone IA, Markman MW, Shen S, and Langlois RA. 2018. Distinct antiviral signatures revealed by the magnitude and round of influenza virus replication in vivo. Proc Natl Acad Sci U S A. PMID: 30181264. *Authors contributed equally.

[2]Additional contributions: flow cytometry experiments were completed and analyzed by E.J. Fay, L.E. Sjaastad, and J.K. Fiege; microscopy experiments were completed by E.J. Fay and I.A. Stone and analyzed by I.A. Stone; RNA-seq experiments were completed by L.E. Sjaastad and analyzed by E.J. Fay, M.G. Macchietto, M.W. Markman, S. Shen, and R.A. Langlois. Manuscript was written and finalized by E.J. Fay and R.A. Langlois.

[3]Abbreviations used this chapter: ATI, type I alveolar cells; BrdU, bromodeoxyuridine; CC10, club cell 10-kiloDalton protein; CPM, counts per million; CRISPR, clustered regularly interspaced short palindromic repeats; destGFP, destabilized GFP; FACS, fluorescence-activated cell sorting; FDR, false discovery rate; GFP, green fluorescent protein; gMFI, geometric mean fluorescence intensity; GO, gene ontology; HA, hemagglutinin; i.p., intraperitoneal; IAV, influenza A virus; IFITM3, IFN-induced transmembrane protein 3; IFN,

interferon; ISG, IFN-stimulated gene; logFC, logarithmic fold change; MDA5, melanoma differentiation associated protein 5; MDCK, Madin-Darby canine kidney; MDS, multidimensional scaling; MFI, mean fluorescence intensity; pdpn, podoplanin; PFU, plaque forming unit; PKR, protein kinase R; RIG-I, retinoic acid-inducible gene 1; RNAi, RNA interference; scIAV, single-cycle IAV; SPC, surfactant protein C; vRNA, viral RNA; wt, wild type

## CHAPTER 3: Cell type- and replication stage-specific influenza virus responses in vivo


### SUMMARY

Influenza A viruses (IAVs) remain a significant global health burden. Activation of the innate immune response is important for controlling early virus replication and spread. It is unclear how early IAV replication events contribute to immune detection. Additionally, while many cell types in the lung can be infected, it is not known if all cell types contribute equally to establish the antiviral state in the host. Here, we use single-cycle IAVs (scIAVs) to characterize the early immune response to IAV *in vitro* and *in vivo*. We found that the magnitude of virus replication contributes to antiviral gene expression within a cell prior to the induction of a global response. We also developed a scIAV that is only capable of undergoing primary transcription, the earliest stage of virus replication. Using this tool, we uncovered replication stage-specific responses *in vitro* and *in vivo*. Using innate immune receptor knockout cells, we identify RIG-I as the predominant antiviral detector of primary virus transcription and amplified replication *in vitro*. Using a Cre-inducible reporter mouse, we used scIAVs expressing Cre-recombinase to characterize cell type-specific responses *in vivo*. Individual cell types upregulate unique sets of antiviral genes in response to both primary virus transcription and amplified replication. We also identified antiviral genes that are only upregulated in response to direct infection. Altogether, these data offer insight into the early mechanisms of antiviral gene activation during IAV infection.

## INTRODUCTION

Influenza A virus (IAV) is a seasonal pathogen that causes significant global morbidity and mortality annually. Respiratory epithelial cells are the primary targets of IAV. Infected epithelial cells play a critical role in detecting IAV and activating the interferon (IFN) response. Failure of infected cells to control IAV replication can lead to cell death and spread of the virus to neighboring cells, resulting in significant damage to the lung epithelium and severe disease symptoms. The primary innate immune receptor responsible for detection of IAV infection in epithelial cells is retinoic acid inducible gene-I (RIG-I). Detection through another RIG-I-like receptor (RLR), melanoma differentiation-associated protein 5 (MDA5), has also been shown to contribute *in vivo* but not in *ex vivo* studies (143, 147). While many epithelial cell types can be infected throughout the course of infection, it is unknown if all infected cell types contribute equally to establish the antiviral state in the host.

IAV has a segmented, negative-sense RNA genome. Each of the eight gene segments are packaged into virions in complex with the heterotrimeric viral RNA-dependent RNA polymerase (RdRp). Upon infection, these viral ribonucleoprotein (vRNP) complexes traffic to the nucleus where the RdRp both transcribes the viral RNA (vRNA) to generate messenger RNA (mRNA) and replicates the vRNA through a positive sense complementary RNA (cRNA) intermediate (148). While the exact mechanism for how the virus balances between transcription and replication for each gene segment is unknown, replication requires *de novo* polymerase complexes to stabilize the cRNA intermediate (149-152), suggesting

that transcription occurs prior to replication. Additionally, amplification of vRNA has been shown to be required for induction of type I IFN, suggesting early IAV infection is poorly detected by the innate immune system (150, 153). Several groups have described aberrant vRNA products, including defective interfering genomes and mini viral RNAs, as the predominant inducers of innate immune activation through RIG-I (8, 154, 155). When these RNAs are produced during the course of an infection has not been well defined.

Previous methods to assess distinct stages of early virus replication within a cell have used drugs such as actinomycin D or cycloheximide to inhibit transcription or translation (155-157). These drugs also inhibit host cell processes, limiting the ability to analyze the host response. We therefore used a series of viruses genetically restricted in progressing through different stages of replication. Single-cycle IAVs (scIAVs) lacking hemagglutinin protein and unable to spread were used to elucidate mechanisms of innate immune activation during the early stages of IAV infection in mice. We identified unique responses to the magnitude of replication during direct infection *in vivo*. Additionally, we generated a genetically restricted a scIAV such that only primary transcription can occur. Entry and primary transcription alone are detected by RIG-I and drive an antiviral response *in vitro.* Using this tool, we uncovered epithelial cell type-specific responses to primary virus transcription and amplified virus replication *in vivo*. Altogether, these data demonstrate that the antiviral response to IAV is sensitive to the stage of replication and varies across cell types.

## MATERIALS AND METHODS

### *Tissue culture*

Human embryonic kidney 293T (293T, ATCC) cells, human lung adenocarcinoma A549 cells, Madin-Darby canine kidney (MDCK) cells, and MDCK cells expressing IAV-WSN HA (WSN-HA MDCK, kind gift from Dr. Adolfo García-Sastre, Mount Sinai) were maintained in Dulbecco's modified Eagle's medium (DMEM) with 1% fetal bovine serum (FBS) and 1% penicillin-streptomycin. MDCK cells expressing IAV-PR8 HA (PR8-HA MDCK, kind gift from Dr. Luis Martinez-Sobrido, University of Rochester) were supplemented with 125 μg/mL of hygromycin B.

### *Generation of PR8-PB1 MDCK cells*

The PR8-PB1 coding sequence was cloned into the NotI-digested pLEX-MCS lentivirus packaging vector (kind gift from Dr. Wade Bresnahan, University of Minnesota) using In-Fusion cloning (Takara). The lentivirus packaging vector and the pMDG and pΔNRF helper plasmids were transfected into 293T cells using the Lipofectamine 3000 transfection reagents (Invitrogen). At 24 and 48 hours post-transfection, supernatant was harvested and filtered through a 0.45 μm PES filter. A GFP lentivirus (GFP-lenti) was generated as a control to determine the approximate titer of the PB1-lenti stock. MDCK cells were transduced with 10-fold serial dilutions of GFP-lenti to determine titer. MDCK cells were transduced with PB1-lenti at an MOI=0.5. After 48 hours, the cells were diluted to obtain single-cell clones. Positive clones were selected for and maintained in Dulbecco's modified

Eagle's medium (DMEM) with 1% fetal bovine serum (FBS), 1% penicillin-streptomycin, and 5 μg/mL puromcyin. Integration of the lentivirus transgene was verified by western blot (rabbit anti-PB1, PA5-34914, ThermoFisher Scientific) and PCR using genomic DNA and the following primers for PB1: 5'-ACCCATAACGATAGAAAAAACTTGTG-3' and 5'-CCAGTTGGAGGCAATGAGAAGAAAGC-3'.

***Virus rescue***

Viruses were rescued in 293T cells using the IAV-PR8 plasmid-based transfection system in the pDZ vector. scIAV-ΔHA viruses were generated as previously described (158). To generate scIAV-ΔPB1 viruses, mCherry or Cre recombinase (Cre) was inserted between the 5' and 3' packaging signals of PR8 PB1 (100 and 200 bp, respectively). Plasmids were transfected at 500ng/reaction onto 293T cells in Opti-MEM using Lipofectamine 2000 (Invitrogen) and incubated at 37ºC. pCAGGs-WSN-PB1 or -WSN-HA were supplemented into each reaction. After 24 hours, PR8-PB1 MDCK or WSN-HA MDCK cells were added to transfected wells in Opti-MEM containing 0.5μg/mL TPCK-trypsin. Reactions were supplemented at 24 and 48 hours after cell overlay with 500μL of Opti-MEM containing 1-2μg/mL TPCK trypsin. Seventy-two hours after cell overlay, the supernatant was harvested, centrifuged to remove cellular debris, and stored at -80ºC. Viruses were plaque purified and amplified on either PR8-PB1 or PR8-HA MDCK cells. Viral sequences were confirmed using Sanger sequencing. Virus stocks were tittered via plaque assay. Infections were performed in infection media

(PBS with 10% Ca/Mg, 1% pen/strep, 5% BSA) at 37ºC on either PR8-PB1 or WSN-HA MDCK cells. After 1hr, infection media was replaced with an agar overlay (2xMEM, 1µg/mL TPCK-trypsin, 1% DEAE-dextran, 5% $NaCO_3$, 2% oxoid agar) and cultured for 40-42hrs at 37ºC. Plaques were fixed with 4% formaldehyde for 30 minutes prior to removal of the overlay. Blocking and immunostaining were performed at room temperature for 1 hour in 5% milk in PBS. The following antibodies were used in staining: polyclonal anti-IAV PR8/34, 1:5000 (V301-511-552), Peroxidase Rabbit Anti-Chicken IgG, 1:5000 (303-035-003, Jackson Immuno Research). Virus plaques were detected using TruBlue Peroxidase Substrate (50-547-28, Kirkegard & Perry Laboratories).

***Stranded next-generation sequencing of A549 cells***

Infections were performed in A549 cells in infection media at an MOI of 1. Infections were synchronized at 4ºC for 30 minutes then transferred and incubated at 37ºC. The zero hour time point was harvested after 30 minutes at 37ºC and additional time points were harvested at 3, 6, 9, 12 hours post infection. RNA was extracted using TRIzol. The cDNA libraries were prepared using the Stranded Total RNA v2 Pico Mammalian kit (Takara). Samples were sequenced as 150 base pair paired-end reads using NovaSeq (Illumina). The customized influenza A/PR/8/34/(H1N1) mRNA sequence and annotation were used for mapping (available upon request). The forward and reverse virus reads counts were obtained by using FeatureCounts -s parameter (118). The strand specific reads of individual viral genes were summed as either negative or positive strand reads

sample by sample, respectively. To normalize the strand specific viral reads, we first generated the forward or reverse strand reads ratio by using total viral reads as denominator. The ratio of forward or reverse strand reads were then normalized against total mapped reads (relative library size), which were subsequently transformed into counts per million. All RNA sequencing files are available from the NCBI GEO database (accession number GSE147832 ).

***Western blot analysis***

Viral stocks were lysed and separated by SDS-PAGE (2-15% gel). Protein was transferred to a nitrocellulose membrane at 4ºC for 2 hours and blocked with 5% milk in PBS. The membrane was incubated with primary antibodies rabbit anti-PB1 (1:1000, PA5-34914, ThermoFisher Scientific) followed by goat anti-rabbit IgG horseradish peroxidase-conjugated secondary antibody (1:1000, ThermoFisher Scientific). Images were obtained using a Li-Cor Odyssey Fc imaging system.

***Detection of defective interfering particles in scIAV stocks***

RNA was extracted from viral stocks, including an A/Puerto Rico/8/34 stock grown in MDCK cells. RNA was extracted using the NucleoSpin Virus Kit (Macheray-Nagel). RNA was reverse transcribed to cDNA using the SuperScript III One-Step RT-PCR with Platinum Taq (Invitrogen). PB2 and NA gene segments were amplified from each sample as well from a pDZ-PR8-PB2 or NA plasmid control using previously described primers (159): PB2 5’-

GTAGATGCAGCGAAAGCAGGTCAATTAT-3’ and 5’-GTAGCAGCAGTAGAAACAAGGTCGTTTT-3’, NA 5’-GTAGATGCAGCGAAAGCAGGGGTTTAAA-3’ and 5’-GTAGCAGCAGTAGAAACAAGGAGTTTTT-3’. The samples were loaded and run on a 1% agarose gel with 0.012% ethidium bromide in Tris-acetate-EDTA buffer. Images were obtained using a GelDoc EZ Imager (BioRad).

***Next-generation mRNA sequencing of A549 knockout cells***

NTC and knockout A549 cells (kind gift from Michael Gale, Jr., University of Washington) were infected with ΔHA-mCherry or ΔPB1-mCherry at MOI=1. Cells were harvested at 12 hpi and RNA extracted using the RNeasy PLUS Micro kit (Qiagen). cDNA libraries were prepared using the TakaraBio PicoMammalian kit and sequenced as 150 base pair paired-end reads using NovaSeq (Illumina). The raw sequencing reads were mapped to human genome (GRCh38) using Bowtie aligner (bowtie2 version 2.3.4.1) with local mode, 22 nt seed sequence, and ≤1 nt mismatch (-L 22 and -N 1 parameters) (116). The mapped reads were then assigned to Ensembl gene model (Homo_sapiens.GRCh38.87.gtf) with featureCounts of the Subread software package (version 1.5.1) (118). The raw reads count tables were merged to generate data matrix and used for subsequent statistical analysis. To obtain significant differentially expressed genes, the experimental groups by design were compared to control group (naïve) and the edgeR (version 3.24.3) of bioconductor package was used for statistical analysis

(121, 122). Raw reads were normalized by using default method in the package prior to generating stats.

### *Mice and virus infection*

Wild-type C57BL/6J and B6.Cg-*Gt(ROSA)26Sor*$^{tm14(CAG-tdTomato)Hze}$/J mice were purchased from The Jackson Laboratory. Mice were infected intranasally (i.n.) with $10^5$ pfu of sclAV unless otherwise indicated. All experiments involving mice were performed as dictated by the University of Minnesota Institutional Animal Care and Use Committee.

### *Flow cytometry*

Mice were euthanized and lungs were inflated with 2 mL dispase (Corning) and 0.5 mL 1% low melt agarose (Lonza) and allowed to sit covered with an ice pack for two minutes. Lungs were then removed from mouse and transferred to 1 mL dispase and incubated at room temperature for 45 minutes. Next, lungs were incubated in DMEM with DNase I (Sigma-Aldrich) at 95 U/mL and shaken for 10 minutes at room temperature. Lungs were homogenized in GentleMACS dissociator and red blood cells were lysed with ACK buffer. Cells were filtered to obtain a single cell suspension prior to staining. Cells were stained with Ghost Dye Red 780 (Tonbo), followed by the following antibodies against surface markers: CD45 (30-F11), podoplanin (clone 8.1.1), CD24 (M1/69), EpCAM (CD324, clone G8.8), MHCII (I-A/I-E, clone M5/114.15.2) (Biolegend), and CD31 (clone 390, BD Bioscience). Cell counts were obtained using AccuCheck counting beads

(Thermofisher Scientific). Data were acquired on a BD LSRFortessa (Becton Dickinson, San Jose, CA).

***Next-generation mRNA sequencing of sorted mouse lung epithelial cells***

C57Bl/6 mice were infected and mCherry negative, low, and high CD45$^-$ CD31$^-$ cells were FACS sorted. B6.Cg-*Gt(ROSA)26Sor*$^{tm14(CAG-tdTomato)Hze}$/J mice were infected and the following samples were FACS sorted: tdTomato$^+$ ciliated cells (CD24$^{hi}$ podoplanin$^-$), type I alveolar cells (CD24$^-$ podoplanin$^+$), and type II alveolar cells (CD24$^-$ podoplanin$^-$ MHCII$^+$ EpCAM$^+$), and tdTomato$^-$ ciliated cells and type I and II alveolar cells. RNA was isolated from samples using the RNeasy Plus Micro kit (Qiagen). cDNA libraries were prepared using the TakaraBio PicoMammalian kit and were sequenced as 50 base pair paired-end reads using NovaSeq (Illumina). The raw sequencing reads were mapped to mouse genome (GRCm38) using Bowtie aligner (bowtie2 version 2.3.4.1) with local mode, 22 nt seed sequence, and ≤1 nt mismatch (-L 22 and -N 1 parameters) (116). The mapped reads were then assigned to Ensembl gene model (Mus_musculus.GRCm38.87.gtf) accordingly with featureCounts of the Subread software package (version 1.5.1) (118). For flu reads mapping and assignment, the customized influenza A/PR/8/34/(H1N1) mRNA sequence and annotation were used. The raw reads count tables were merged to generate data matrix and used for subsequent statistical analysis. To obtain significant differentially expressed genes, the experimental groups by design were compared to control group (naïve) and the edgeR (version 3.24.3) of bioconductor package was used for statistical

analysis (121, 122). Raw reads were normalized by using default method in the package prior to generating stats.

### *Statistical analysis*

Statistical analyses were completed using GraphPad Prism 7 software. Comparisons between two groups were executed using a two-tailed Student t test. Comparisons between more than two groups were completed using a one-way ANOVA. Additional tests were performed where indicated. Error bars were calculated using SEM.

### *Ethics statement*

Care and use of the animals was in accordance with the Guide for the Care and Use of Laboratory Animals from the National Research Council and the USDA Animal Care Resource Guide. All experimental protocols involving the use of mice were approved by the Institutional Animal Care and Use Committee at the University of Minnesota (protocol: 1708-35040A. approved 09/14/2017; expires 09/13/2020).

## RESULTS

### *Heterogeneous antiviral response to early IAV infection in vivo*

We have previously used a single-cycle influenza virus (scIAV) expressing mCherry in place of the coding sequence for the hemagglutinin (HA) segment (ΔHA-mCherry) to uncover replication heterogeneity during the early stages of IAV

infection in mice (158). Other groups have found similar heterogeneity at early timepoints *in vitro* (62, 63, 160, 161), as well as heterogeneity in the ability to induce IFN production in infected cells (63, 112, 162, 163). Our previous analyses were unable to distinguish genes induced directly by virus infection from those driven by IFN and inflammation. To address this, we assessed an earlier time point, 12 hours post-infection (hpi), where distinct populations of mCherry high and low epithelial cells were still observed *in vivo* (Figure 3-1A). To determine if mCherry high and low cells display distinct antiviral signatures, we infected mice with ΔHA-mCherry and sorted mCherry high, low, and negative epithelial cells at 12 hpi for mRNA-seq analysis. Similar to 24 hpi, at 12 hpi reads mapping to the IAV genome were higher in the mCherry high cells than in mCherry low cells, validating the use of mCherry fluorescence as an indicator of scIAV replication at 12 hpi (Figure 3-1B). Multidimensional scaling (MDS) of host mRNAs revealed significant differences between the mCherry high and low populations (Figure 3-1C). However, there is no difference between the mCherry negative and naïve populations, suggesting that alterations in host gene expression in mCherry$^+$ cells at 12 hpi are driven directly by virus replication, rather than a global inflammatory response. Moreover, mCherry high and low cells display distinct antiviral gene signatures (Figure 3-1D). While the genes analyzed in this study are designated as IFN-simulated genes (ISGs), IFN-independent upregulation by virus replication of some of these genes has been described (31-33) and we do not distinguish between virus-induced and IFN-induced. The putative protective ISGs found in the mCherry low cells at 12 hpi overlap with the genes identified using both ΔHA-

mCherry and ΔHA-destabilized GFP at 24 hpi identified previously (158) (Figure 3-1E, top, S1Table). Among these are genes such as *Eif2ak2* (PKR) which has well-described antiviral activity during IAV infection (27), as well as genes that have not been described to have anti-IAV activity, such as *Helz2*. We also found overlap in the genes upregulated in cells with high levels of virus replication (Figure 3-1E, bottom, Table 3-2), including the chemokines *Cx3cl1*, *Cxcl11*, and *Ccl5*. Gene ontology (GO) analysis of genes significantly upregulated over naïve in mCherry high and low cells revealed that only high levels of virus replication induce apoptosis pathways at 12 hpi (Figure 3-1F). Induction of these ISGs may require high levels of replication as a way to tightly regulate a pro-inflammatory and pro-apoptotic response, making these ISGs a "reserve" set of genes that are only upregulated when other mechanisms of control have failed. These data further suggest that pathologic responses may be driven from only a small subset of infected cells. Altogether, these data suggest that the replication and response heterogeneity observed early during IAV infection is established prior to the induction of a global immune response.

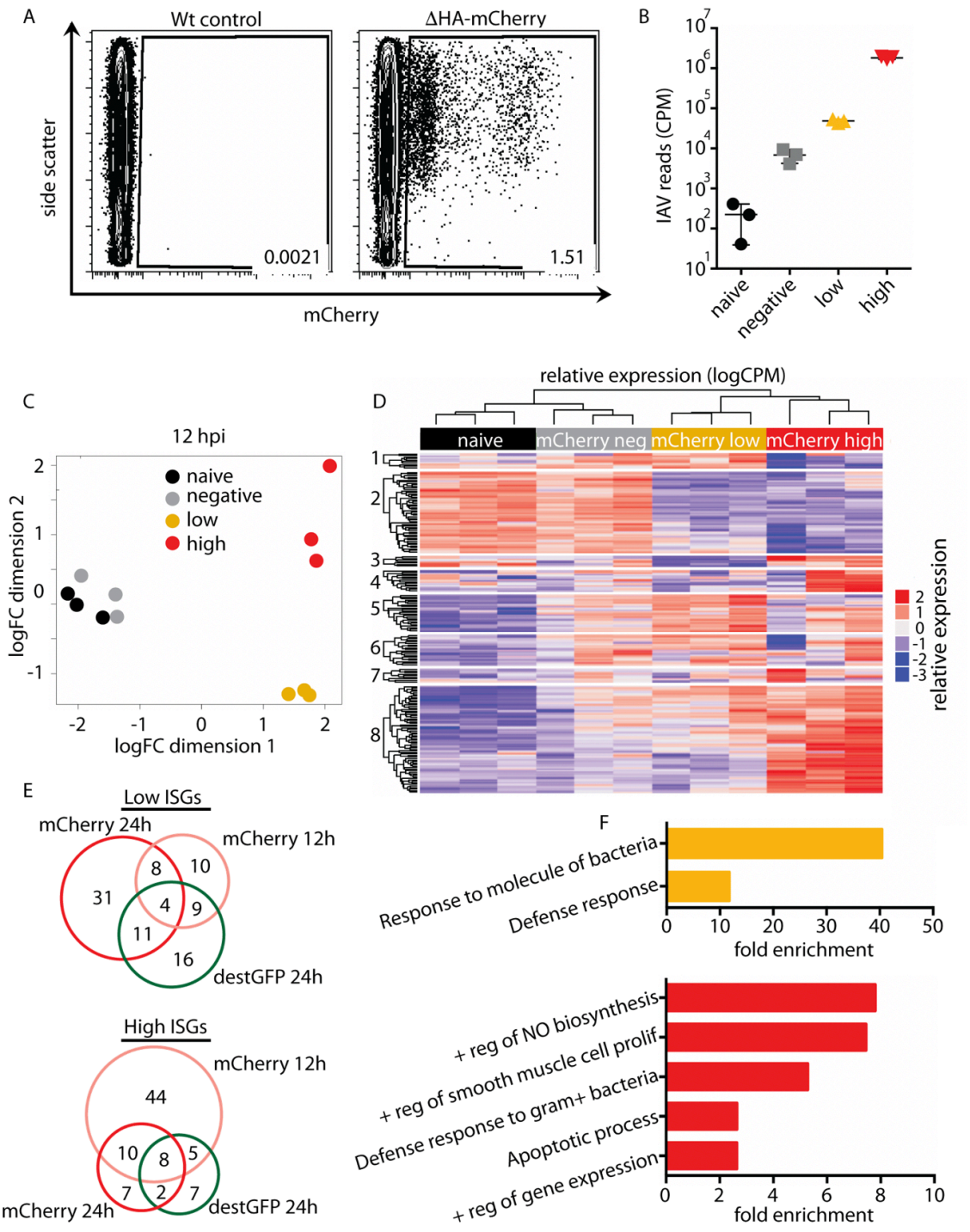


**Figure 3-1.** Heterogeneous antiviral response to scIAV infection at 12 hpi. B6 mice were infected with $10^5$ PFU of scIAV-HA-mCherry or $10^3$ PFU PR8. (A) $CD45^-CD31^-$ cells were analyzed for mCherry expression at 12 hpi. Data representative of six independent experiments with n=3-4 mice per group. mCherry negative, low, and high $CD45^-CD31^-$ cells were sorted at 12 hpi for mRNA-seq analysis. (B) IAV CPM (C) MDS of naïve and

mCherry negative, low, and high cells. (D) Heatmap of 207 ISGs differentially expressed in the indicated populations. Cutoff of false discovery rate (FDR) is ≤ 0.05. (E) Overlapping low ISGs (mCherry 24h cluster 2, GFP cluster 1, and mCherry 12h clusters 1 and 5) and high ISGs (mCherry 24h cluster 4, GFP cluster 4b, and mCherry 12h cluster 8). Only genes induced to ≥10 CPM in at least one sample are shown. (F) Gene ontology analysis (DAVID, biological processes) was performed for genes upregulated in mCherry high, low, and negative cells over naïve (logFC ≥ 1.5, FDR ≤ 0.05). Unique pathways identified in mCherry low (top) mCherry high (bottom) are shown (FDR ≤ 0.05). (B-F) representative of one experiment with n=3 mice per group.

**Table 3-1.** Putative protective ISGs.

| ΔHA-mCherry 12 hpi clusters 1 and 5 | | ΔHA-mCherry 24 hpi cluster 2 | | ΔHA-destGFP cluster1 | |
|---|---|---|---|---|---|
| Unc93b1 | Lap3 | Adar | Lamp3 | Adar | Oas3 |
| Adar | Lrg1 | Alyref | Lgmn | Birc3 | Parp12 |
| Bag1 | Ncf1 | Ankfy1 | Map3k5 | Ddx58 | Pml |
| Casp7 | Nmi | B4galt5 | Max | Ddx60 | Pnpt1 |
| Ccnd3 | Pml | Bag1 | Mov10 | Eif2ak2 | Prkd2 |
| Cd74 | Psmb9 | Birc3 | N4bp1 | Fam46a | Rnf114 |
| Ddx58 | Pxk | Ccl2 | Ncf1 | Helz2 | Rnf213 |
| Eif2ak2 | Rab27a | Ccnd3 | Optn | Herc6 | Sp110 |
| Fbxo6 | Rnf213 | Cd9 | Pi4k2b | Ifi27 | Spats2l |
| Glipr2 | Serpinb9 | Chmp5 | Pml | Ifi27l2a | Stat1 |
| Glrx | Stat1 | Commd3 | Pnpt1 | Ifi35 | Stat2 |
| Helz2 | Stat2 | Ehd4 | Ptma | Ifit1bl1 | Steap4 |
| Ifi27 | Tap1 | Eif2ak2 | Rab27a | Irf2 | Tdrd7 |
| Ifi44 | Tnfsf10 | Eif3l | Rbm25 | Irf9 | Trim14 |
| Irf9 | Uba7 | Epas1 | Rpl22 | Isg20 | Trim25 |
| Lamp3 | | Ext1 | Rtcb | Lgmn | Trim5 |
| | | Fam46a | Slfn5 | Mov10 | Trim56 |
| | | Fbxo6 | Sptlc2 | N4bp1 | Uba7 |
| | | Fndc3b | Sqle | Nmi | Unc93b1 |
| | | Gak | Stard5 | Oas2 | Whamm |
| | | Gca | Stat3 | | |
| | | Gk | Tdrd7 | | |
| | | Glipr2 | Timp1 | | |
| | | Glrx | Tmem51 | | |
| | | Helz2 | Trim5 | | |
| | | Ifi27l2a | Trim56 | | |
| | | Ifi35 | Wars | | |

**Table 3-2.** Putative reserve ISGs.

| ΔHA-mCherry 12 hpi cluster 8 | | ΔHA-mCherry 24 hpi cluster 4 | | ΔHA-destGFP cluster 4b | |
|---|---|---|---|---|---|
| Abtb2 | Junb | Abtb2 | Lgals3 | Arg2 | Nfil3 |
| Alyref | Lgals9 | Atf3 | Mafb | Ccl5 | Odc1 |
| Arg2 | Ly6e | Atp10d | Maff | Cd74 | Pim3 |
| Atf3 | Mafb | Ccl5 | Marcksl1 | Cx3cl1 | Psmb8 |
| B2m | Maff | Cdkn1a | Mcl1 | Ddit4 | Ripk2 |
| Bst2 | Map3k14 | Csrnp1 | Nup50 | Gem | Rnf24 |
| Ccl5 | Marcksl1 | Cx3cl1 | Odc1 | Glipr2 | Sat1 |
| Cd274 | Max | Ddit4 | Pim3 | Ifi30 | Serpine1 |
| Cdkn1a | Mx1 | Fam134b | Ripk2 | Lrg1 | Slc16a1 |
| Ceacam1 | Mx2 | Fam46c | Rnf19b | Marcksl1 | Slc1a1 |
| Csrnp1 | Myd88 | Gem | Sat1 | Max | Tmem140 |
| Cx3cl1 | Nampt | Gpx2 | Serpine1 | | |
| Cxcl10 | Neurl3 | Ifngr1 | Tnfaip3 | | |
| Ddx3x | Nfil3 | Junb | | | |
| Dtx3l | Nt5c3 | | | | |
| Ehd4 | Nup50 | | | | |
| Fkbp5 | Odc1 | | | | |
| Gbp2 | Pim3 | | | | |
| Gbp3 | Psmb8 | | | | |
| Gbp5 | Ripk2 | | | | |
| Gch1 | Rnf19b | | | | |
| Gem | Rsad2 | | | | |
| Gk | Rtp4 | | | | |
| Herc6 | Samhd1 | | | | |
| Hk2 | Serpine1 | | | | |
| Ifih1 | Slc16a1 | | | | |
| Ifit1 | Steap4 | | | | |
| Ifit1bl1 | Tnfaip3 | | | | |
| Ifit2 | Trim21 | | | | |
| Ifit3 | Ube2l6 | | | | |
| Irf1 | Usp18 | | | | |
| Irf7 | Xaf1 | | | | |
| Isg15 | Zbp1 | | | | |

### *Genetic restriction of IAV to primary transcription*

We hypothesized that the heterogeneous scIAV replication is due to differential ability of cells to detect and respond to the very early stages of virus replication. We therefore developed a scIAV that is unable to progress from primary transcription to replication. We replaced the coding sequence for polymerase basic 1 (PB1) with the coding sequence for mCherry (ΔPB1-mCherry). This virus is grown in a cell line that expresses PB1 protein. The resulting viruses package complete RdRps but cannot generate new polymerase complexes in

infected cells. Therefore, any *de novo* RNA generated in infected cells is being produced only by incoming virus RdRps. We first quantified levels (+)-sense (m/cRNA) and (-)-sense (vRNA) generated by ΔHA-mCherry and ΔPB1-mCherry at 0, 3, 6, 9, and 12 hpi in A549 cells. We found that while both viruses can produce (+)-sense RNA, scIAV-ΔPB1-mCherry cannot amplify (-)-sense vRNA (Figure 3-2A), validating ΔPB1-mCherry as a tool to assess the immune response to primary IAV transcription.

We hypothesized that, due to the different RNA species generated, ΔHA and ΔPB1 viruses would induce distinct immune responses. Importantly, ΔHA-mCherry and ΔPB1-mCherry virus stocks contain equal amounts of defective interfering (DI) genomes (Figure 3-2B), which have been shown to induce RIG-I activation independent of viral protein synthesis (155). Additionally, ΔHA and ΔPB1 viruses package equivalent PB1 protein (Figure 3-2C). Therefore, any differences in immune activation are due to differences in the *de novo* RNA generated by the two viruses rather than differences in incoming defective genomes or polymerase complexes.

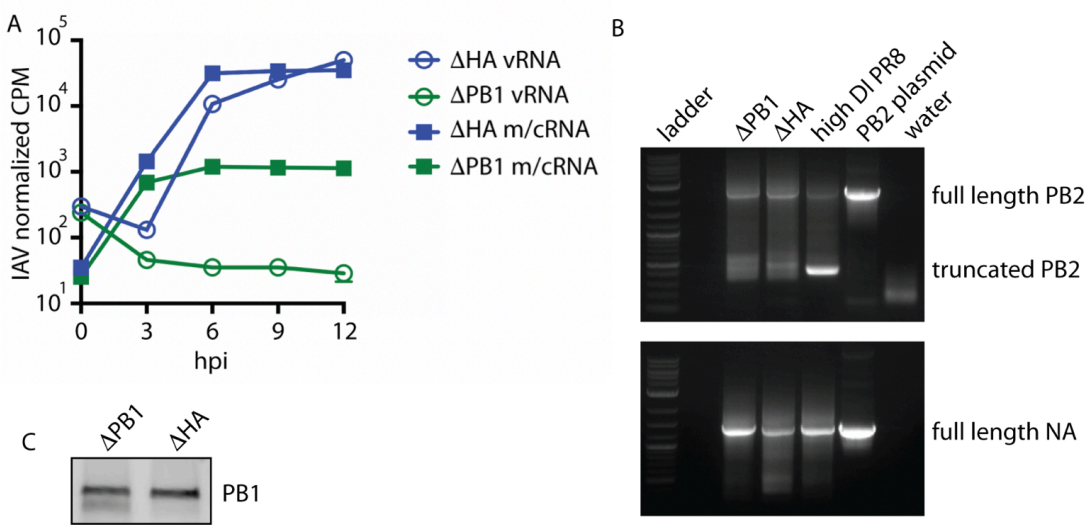


**Figure 3-2.** Genetic restriction of IAV to primary transcription. (A) A549 cells were infected with ΔHA-mCherry or ΔPB1-mCherry at MOI=1 and harvested at the indicated timepoints for RNA-seq. Positive sense (m/cRNA) and negative sense (vRNA) RNA was quantified. Data representative of two independent experiments with n=3 replicate samples per group. (B) vRNA was extracted from the indicated virus stock and PB2 (top) and NA (bottom) were amplified. Representative of two independent experiments. (C) $1.24x10^5$ PFU of ΔPB1-Cre and ΔHA-Cre virus were analyzed for PB1 protein. Representative of three independent experiments.

### *Primary transcription is detected by RIG-I in vitro*

RIG-I and not MDA5 has been reported to recognize IAV infection in primary mouse fibroblasts (147) but the processes of the viral infection and replication cycle that contribute to this recognition are not known. To understand how ΔPB1-mCherry is being detected by infected cells, we infected RIG-I$^{-/-}$, MDA5$^{-/-}$, MAVS$^{-/-}$, and non-targeted control (NTC) A549 cells (164) with ΔPB1-mCherry or ΔHA-mCherry and harvested cells for mRNA-seq analysis at 12 hpi. Importantly, naïve knockout cells do not display significant differences in overall gene expression compared to naïve NTC cells (Figure 3-3). Compared to naïve cells, both viruses robustly induce antiviral gene expression in NTC cells (Figure 3-4A).

This induction is ablated in RIG-I$^{-/-}$ and MAVS$^{-/-}$ cells. There are no genes significantly upregulated (FDR≤0.05, logFC≥2 over naïve, logCPM≥1) in ΔPB1-infected RIGI$^{-/-}$ cells (Table 3-3). In contrast, infected MDA5$^{-/-}$ cells upregulated ISGs nearly to the same extent as NTC cells (Figure 3-4A). In both NTC and MDA5$^{-/-}$ cells, ΔHA infection robustly upregulates *IFNB* and *IFNL3* (Figure 3-4B). Albeit to a much lower degree, ΔPB1 infection also significantly upregulates these IFNs (logFC≥2 over naïve, FDR≤0.05). These data indicate that RIG-I is required for detecting both primary transcription and amplified replication and that primary transcription is sufficient to induce IFN.

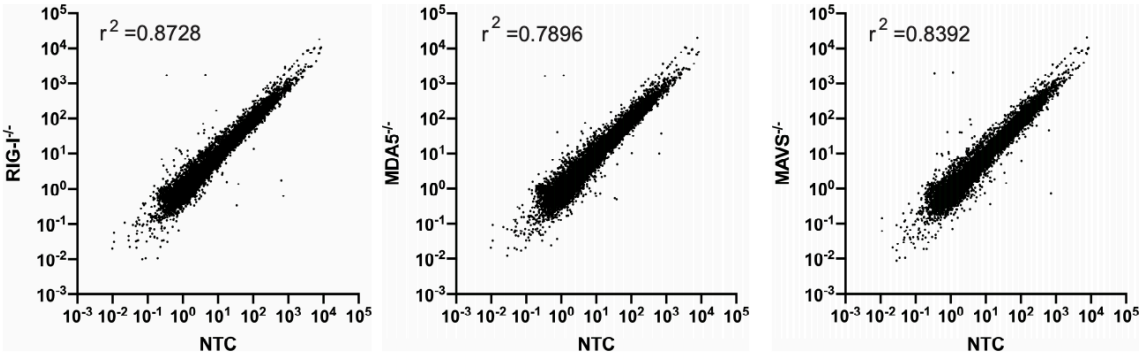


**Figure 3-3.** Basal gene expression between knockout cell lines. Individual gene expression values (CPM) for naïve NTC A549 cells were plotted against naïve RIG-I$^{-/-}$ (left), MDA5$^{-/-}$ (middle), and MAVS$^{-/-}$ (right) A549 cells. R-squared values were calculated using linear regression analysis.

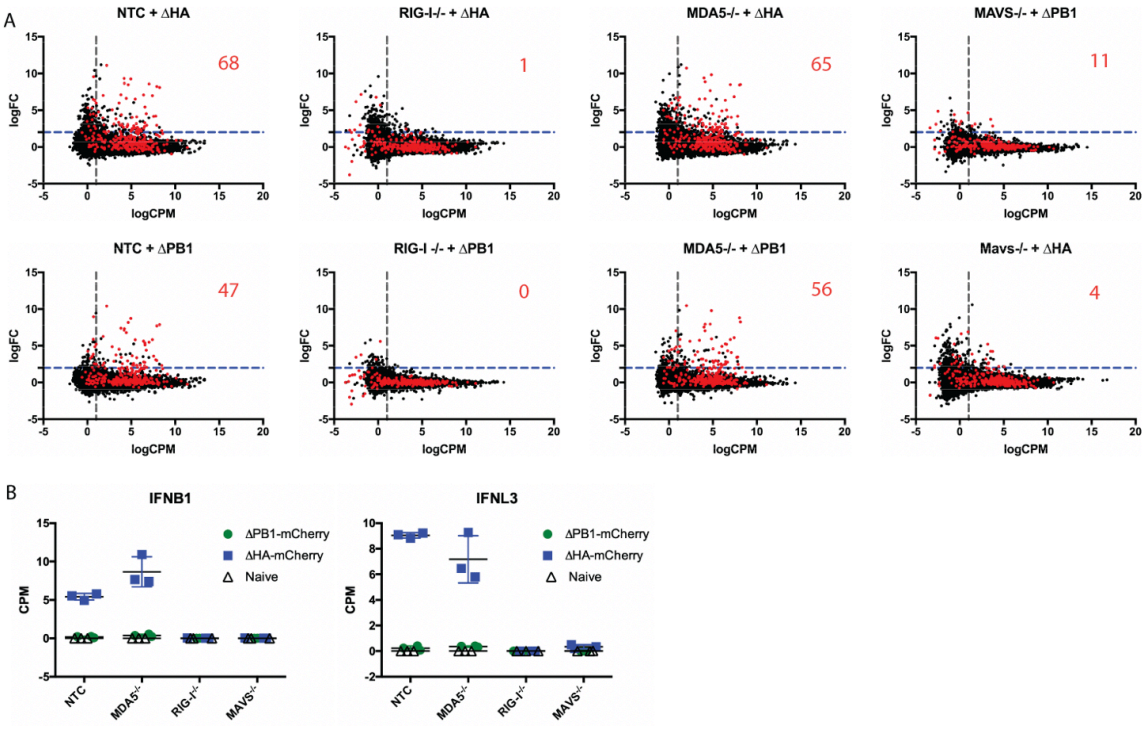


**Figure 3-4.** Primary transcription is detected by RIG-I *in vitro*. Indicated A549 cells were infected with ΔHA-mCherry or ΔPB1-mCherry at MOI=1 and RNA extracted at 12 hpi for mRNA-seq analysis. (A) Total (black) and ISGs (red) differentially expressed genes are shown. The number of genes significantly upregulated (logFC≥2, FDR≤0.05, log CPM≥1) over naïve is shown in upper right of plot. (B) Read CPM for *IFNB1* and *IFNL3* in naïve and ΔHA-mCherry or ΔPB1-mCherry infected A549 cells. Data representative of one experiment with n=3 replicate samples per group.

**Table 3-3.** Stage-specific, RLR-dependent ISG expression in vitro.

| A549 NTC | | | | A549 RIG-I-/- | | | | A549 MDA5-/- | | | | A549 MAVS-/- | | | |
|---|---|---|---|---|---|---|---|---|---|---|---|---|---|---|---|
| ΔHA-mCherry | | ΔPB1-mCherry | | ΔHA-mCherry | | ΔPB1-mCherry | | ΔHA-mCherry | | ΔPB1-mCherry | | ΔHA-mCherry | | ΔPB1-mCherry | |
| APOL1 | MIR22HG | APOL6 | IRF7 | AC007952.4 | HSPA6 | | | AC005682.1 | ISG20 | AP003119.3 | MX1 | AC005682.1 | IFIT2 | IFIT1 | MX1 |
| APOL2 | MX1 | BATF2 | ISG15 | ATF3 | MIR22HG | | | AC007952.4 | KLF4 | APOL1 | MX2 | AC007952.4 | IFIT3 | | |
| APOL6 | MX2 | C19orf66 | ISG20 | BEST1 | MXD1 | | | ADM | LINC00641 | APOL6 | MYD88 | ATF3 | LINC00641 | | |
| ATF3 | MXD1 | CCL5 | MX1 | DDIT3 | NEB | | | APOL1 | MAFF | BATF2 | NLRC5 | BEST1 | MIR22HG | | |
| BATF2 | MYD88 | CMPK2 | MX2 | DNAJB9 | NR4A3 | | | APOL2 | MIR22HG | C19orf66 | OAS1 | CCL2 | MSX1 | | |
| BEST1 | NEB | DDX58 | OAS1 | DUSP6 | NUP210L | | | APOL6 | MSX1 | CCL5 | OAS2 | DDIT3 | MX1 | | |
| C19orf66 | NLRC5 | DDX60 | OAS2 | FBXW10 | RND1 | | | ATF3 | MX1 | CMPK2 | OAS3 | DNAJB9 | MXD1 | | |
| CCL2 | NUP210L | DTX3L | OAS3 | FOS | SPRY4 | | | BATF2 | MX2 | DDX58 | OASL | DUSP6 | NEB | | |
| CCL5 | OAS1 | GBP1 | OASL | GDF15 | TNFRSF10D | | | BEST1 | MXD1 | DDX60 | PARP10 | EGR1 | NUP210L | | |
| CD274 | OAS2 | GBP3 | PARP10 | HBEGF | VTRNA1-3 | | | C19orf66 | MYD88 | DTX3L | PARP12 | FBXW10 | OASL | | |
| CMPK2 | OAS3 | HELZ2 | PARP12 | HERPUD1 | | | | CCL2 | NEB | FAM46A | PARP14 | FOS | PMAIP1 | | |
| DDIT3 | OASL | HERC5 | PARP14 | | | | | CCL5 | NLRC5 | GBP1 | PARP9 | GADD45A | RND1 | | |
| DDX58 | PARP10 | HERC6 | PARP9 | | | | | CD274 | NR4A3 | HELZ2 | PLEKHA4 | GDF15 | SPRY4 | | |
| DDX60 | PARP12 | IFI16 | PLEKHA4 | | | | | CITED2 | NT5C3A | HERC5 | PLSCR1 | HBEGF | TNFAIP3 | | |
| DNAJB9 | PARP14 | IFI27 | PLSCR1 | | | | | CMPK2 | NT5C3AP1 | HERC6 | PML | HERPUD1 | TNFRSF10D | | |
| DTX3L | PARP9 | IFI35 | RASGRP3 | | | | | DDIT3 | NUP210L | IFI16 | RASGRP3 | HSPA6 | VTRNA1-3 | | |
| DUSP6 | PLEKHA4 | IFI44 | RSAD2 | | | | | DDX58 | OAS1 | IFI27 | RSAD2 | IFIT1 | | | |
| EGR1 | PLSCR1 | IFI44L | SAMD9 | | | | | DDX60 | OAS2 | IFI35 | SAMD9 | | | | |
| FAM46A | PMAIP1 | IFI6 | SAMD9L | | | | | DNAJB9 | OASL | IFI44 | SAMD9L | | | | |
| FOS | PML | IFIH1 | SP110 | | | | | DTX3L | PARP10 | IFI44L | SP110 | | | | |
| FOSB | PPM1K | IFIT1 | STAT2 | | | | | DUSP6 | PARP12 | IFI6 | STAT1 | | | | |
| FST | PPP1R15A | IFIT2 | TRANK1 | | | | | EGR1 | PARP14 | IFIH1 | STAT2 | | | | |
| GBP1 | PSMB9 | IFIT3 | TRIM21 | | | | | FAM46A | PARP9 | IFIT1 | TAP1 | | | | |
| GBP3 | PYGM | IFIT5 | TRIM22 | | | | | FBXW10 | PLEKHA4 | IFIT2 | THEMIS2 | | | | |
| GDF15 | RASGRP3 | IFITM3 | USP18 | | | | | FOS | PLSCR1 | IFIT3 | TRANK1 | | | | |
| HBEGF | RND1 | | | | | | | GADD45A | PMAIP1 | IFIT5 | TRIM14 | | | | |
| HELZ2 | RSAD2 | | | | | | | GBP1 | PML | IFITM3 | TRIM21 | | | | |
| HERC5 | SAMD9 | | | | | | | GBP3 | PPM1K | IRF7 | TRIM22 | | | | |
| HERC6 | SAMD9L | | | | | | | GDF15 | PPP1R15A | ISG15 | UBE2L6 | | | | |
| HERPUD1 | SAMHD1 | | | | | | | HBEGF | PTGS2 | ISG20 | USP18 | | | | |
| HSPA6 | SERTAD1 | | | | | | | HELZ2 | RASGRP3 | | | | | | |
| IFI16 | SLC10A1 | | | | | | | HERC5 | RND1 | | | | | | |
| IFI27 | SLC16A12 | | | | | | | HERC6 | RSAD2 | | | | | | |
| IFI35 | SLFN5 | | | | | | | HERPUD1 | SAMD9 | | | | | | |
| IFI44 | SP100 | | | | | | | HSPA6 | SAMD9L | | | | | | |
| IFI44L | SP110 | | | | | | | IFI16 | SLFN5 | | | | | | |
| IFI6 | SPRY4 | | | | | | | IFI35 | SP110 | | | | | | |
| IFIH1 | STAT2 | | | | | | | IFI44 | SPRY4 | | | | | | |
| IFIT1 | TAP1 | | | | | | | IFI44L | STAT2 | | | | | | |
| IFIT2 | THEMIS2 | | | | | | | IFI6 | TAP1 | | | | | | |
| IFIT3 | TNFAIP3 | | | | | | | IFIH1 | THEMIS2 | | | | | | |
| IFIT5 | TNFRSF10D | | | | | | | IFIT1 | TNFAIP3 | | | | | | |
| IFITM3 | TRANK1 | | | | | | | IFIT2 | TNFRSF10D | | | | | | |
| IFNL1 | TRIM21 | | | | | | | IFIT3 | TRANK1 | | | | | | |
| IRF1 | TRIM22 | | | | | | | IFIT5 | TRIM21 | | | | | | |
| IRF7 | TRIM38 | | | | | | | IFITM3 | TRIM22 | | | | | | |
| ISG15 | TRIM69 | | | | | | | IFNB1 | TRIM38 | | | | | | |
| ISG20 | UBE2L6 | | | | | | | IFNL1 | TRIM69 | | | | | | |
| KCNB1 | USP18 | | | | | | | IL6 | UBE2L6 | | | | | | |
| KLF4 | VTRNA1-3 | | | | | | | IRF1 | USP18 | | | | | | |
| MAFF | | | | | | | | IRF7 | VTRNA1-3 | | | | | | |
| | | | | | | | | ISG15 | ZNFX1 | | | | | | |

### *Detection of cells supporting only primary transcription in vivo*

While we were able to detect virus mRNA by RNA-seq, we were unable to detect mCherry fluorescence in A549 cells infected with ΔPB1-mCherry (Figure 3-5A). The mCherry gene segment is appropriately packaged, as co-infection with wt IAV to trans-complement PB1 results in mCherry fluorescence. Due to the limited ability to detect ΔPB1-mCherry *in vitro*, we developed additional scIAVs for *in vivo* analysis. These viruses express Cre recombinase (Cre) in place of either HA or PB1 (ΔHA-Cre and ΔPB1-Cre, respectively). Cre-inducible reporter mice have previously been used to identify cells infected with IAV expressing Cre (41, 145, 146). This system allows for the tracking of infected cells via a Cre-inducible host-endogenous fluorophore, tdTomato. Therefore, detection of infected cells is

not dependent on high levels of active virus replication. tdTomato$^+$ lung epithelial cells can be detected at 24 hpi with either ΔHA-Cre or ΔPB1-Cre (Figure 3-5B). However, the geometric mean fluorescence intensity (gMFI) of tdTomato is higher in ΔPB1-Cre infected mice (Figure 3-5C). As tdTomato is a host-endogenous fluorophore, this gMFI difference could reflect differences in the ability of ΔHA and ΔPB1 viruses to induce shut-off of host transcription/translation. Using cell type-specific markers, we identified infected ciliated cells (CD24$^{hi}$ podoplanin$^-$), type I alveolar cells (ATI; CD24$^-$ podoplanin$^+$), and type II alveolar cells (ATII; CD24$^-$ podoplanin$^-$ MHCII$^+$ EpCAM$^+$) (Figure 3-6A). There are overall fewer tdTomato$^+$ cells following ΔHA-Cre infection, likely due to more robust cell death from full replication compared to ΔPB1-Cre infection (Figure 3-5D). However, the proportion of each epithelial cell type within the tdTomato$^+$ population was the same in the two infections (Figure 3-5E, Figure 3-6B), suggesting these cell types are equally susceptible to infection-induced cell death. All ΔHA-Cre infected cell types show lower tdTomato gMFI compared to ΔPB1-Cre infected cells. Intriguingly, ΔHA-Cre infected ciliated cells show reduced gMFI compared to total ΔHA-Cre tdTomato$^+$ cells. Similarly, ΔPB1-Cre infected ATI and ciliated cells show reduced tdTomato gMFI compared to total tdTomato$^+$ cells (Figure 3-6C), suggesting that there are cell type-specific responses to primary scIAV transcription and replication.

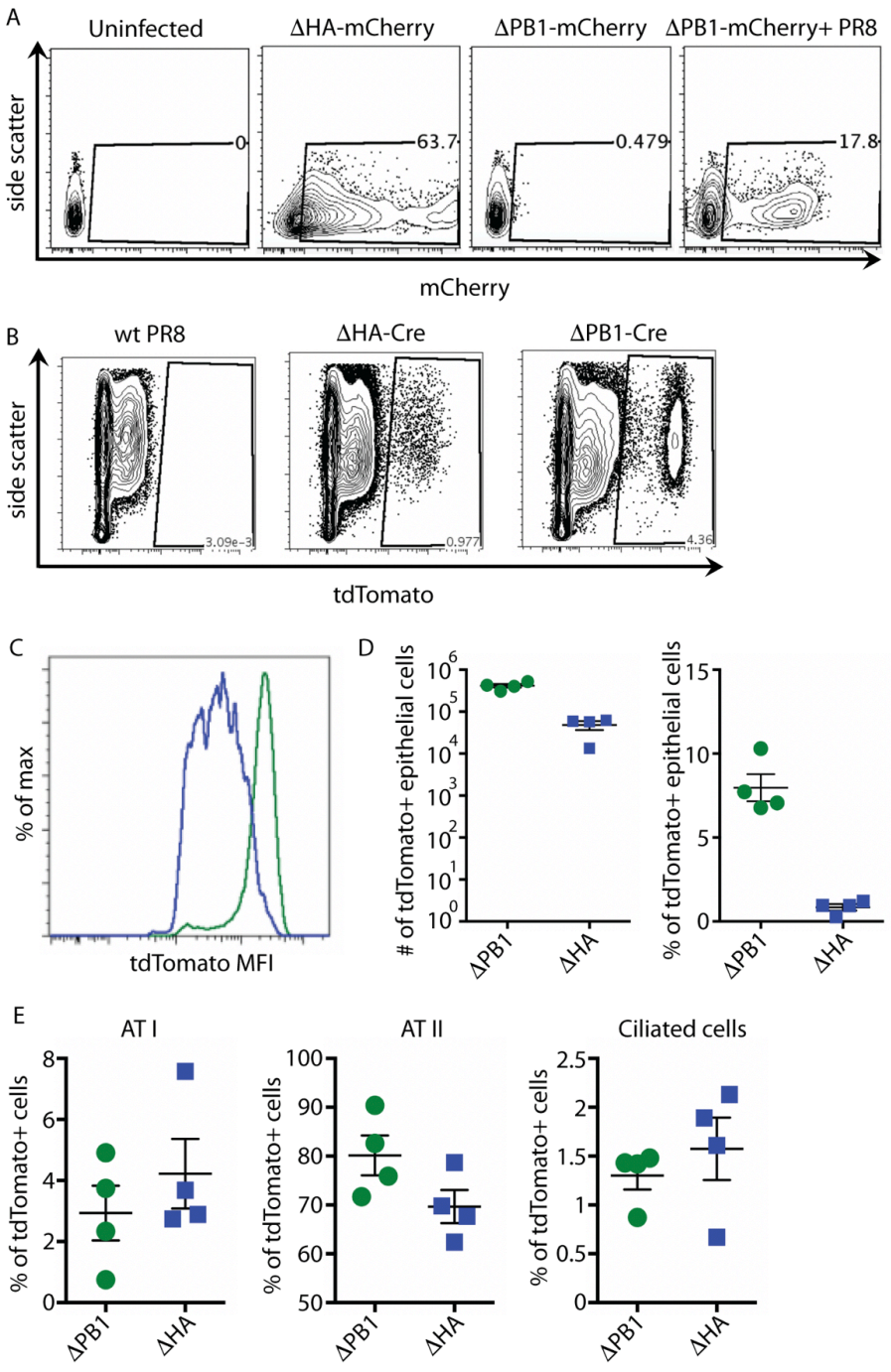


**Figure 3-5.** Detection of cells supporting only primary transcription *in vivo*. (A) A549 cells were infected with ΔHA-mCherry, ΔPB1-mCherry, or ΔPB1-mCherry and PR8 at MOI=1 and analyzed at 24 hpi by flow cytometry. Representative of 3 independent experiments with n=1 sample replicate per group. (B-E) Cre reporter mice were infected with $10^3$ PFU of PR8 or $10^5$ PFU of ΔHA-Cre, or ΔPB1-Cre and lungs analyzed by flow cytometry at 24 hpi per group. (B-C) Epithelial cells ($CD45^-CD31^-$) were analyzed for tdTomato expression. (E) The percentage of infected ($tdTomato^+$) ATI, ATII, and ATII cells was quantified. (B-E) representative of 3 independent experiments with n=3-4 mice.

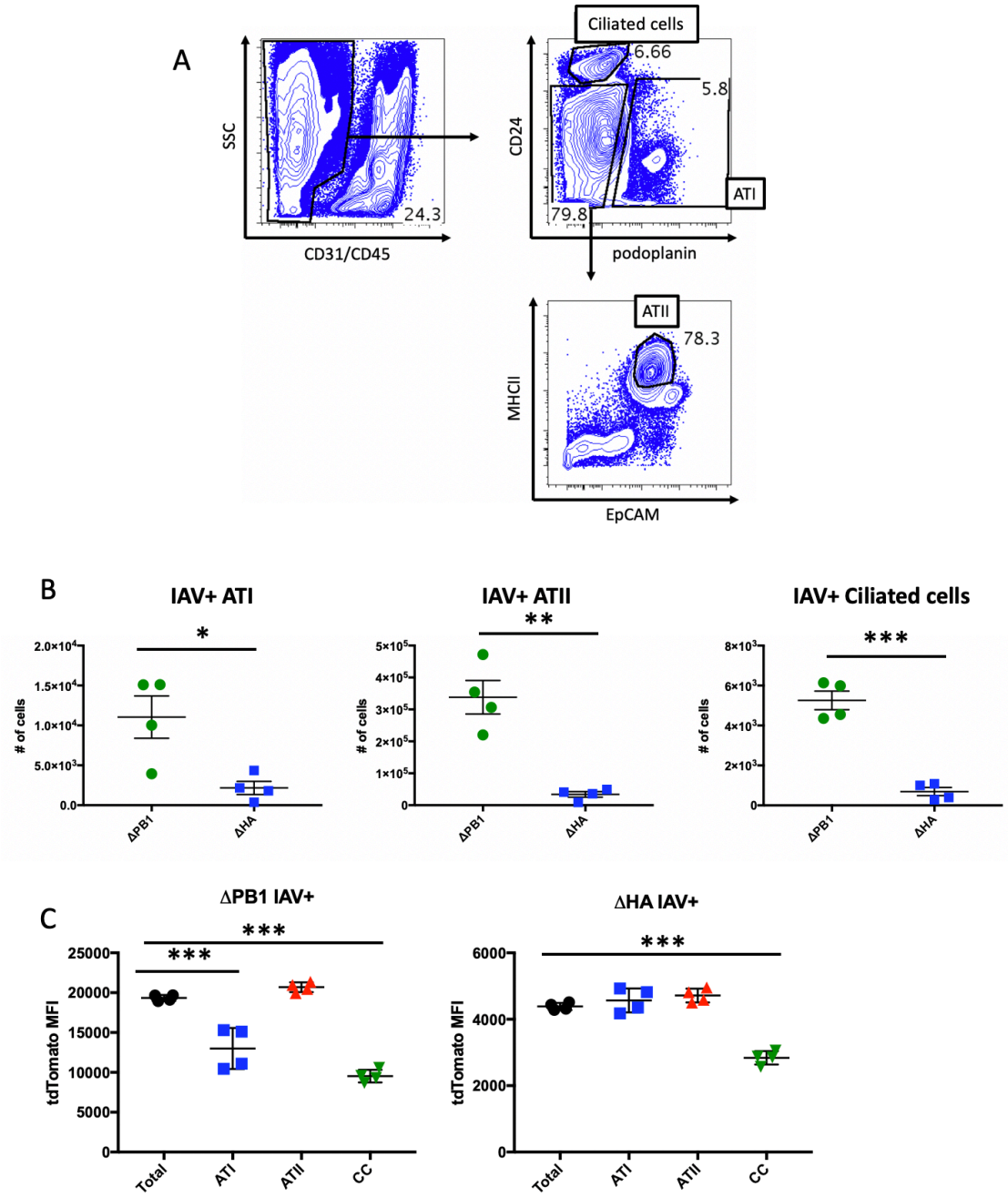


**Figure 3-6.** Detection of epithelial cell types supporting primary transcription *in vivo*. (A) representative flow plots for identifying indicated cell types. (B) Total numbers of infected ATI, ATII, and ciliated cells following ΔPB1-Cre or ΔHA-Cre infection. (C) tdTomato gMFI of individual cell types compared to total tdTomato$^{+}$ cells in ΔPB1-Cre and ΔHA-Cre infected mice. Data representative of 3 independent experiments with n=3-4 mice per group. Student's t test (B) or one-way ANOVA with Dunnett's multiple comparisons test (C) *p<0.05 **p<0.01 ***p<0.001.

***Analysis of individual epithelial cell types in vivo***

We sorted out tdTomato$^{+}$ and tdTomato$^{-}$ ATI, ATII, and ciliated cells from ΔHA-Cre and ΔPB1-Cre infected Cre-inducible reporter mice for mRNA sequencing to characterize cell type- and stage-specific responses to sclAV infection. Cells from naïve mice were used as baseline controls. We and others have previously used CD24 as a marker of ciliated cells (158, 165), and we further validated its use by quantifying co-expression of CD24 with the ciliated cell marker acetylated alpha-tubulin (aat). Importantly, the majority of CD24$^{hi}$ cells also express aat, while CD24$^{-}$ cells do not express any aat (Figure 3-8A, Figure 3-7). We also validated our gating strategy by quantifying cell type-specific gene expression; we identified cell type-specific expression of both transcription factors and cell surface proteins associated with each cell type (Figure 3-8B) (166-168). Expression of innate immune signaling genes in naïve cells could contribute to any differences in the response between cell types. We therefore quantified expression of such genes in each cell type in naïve animals. ATI cells express higher basal *Ddx58* (RIG-I) and *Ifih1* (MDA5) than ATII cells or ciliated cells; other signaling genes—*Irf3*, *Irf7*, and *Mavs*—are not different between the cell types (Figure 3-8C). Overall, these data confirm enrichment of the indicated epithelial cell types to analyze innate immune responses to sclAVs.

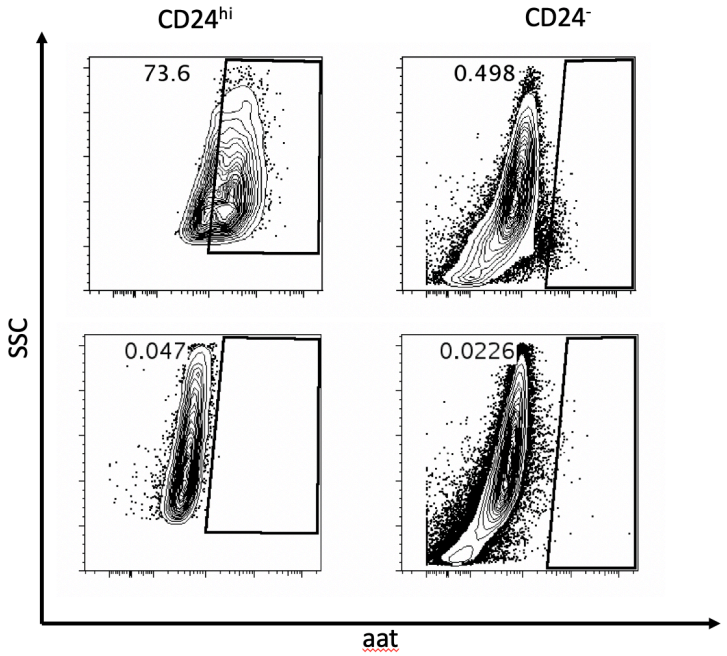


**Figure 3-7.** Verification of ciliated cell identity *in vivo*. Mice were infected with $10^5$ PFU ΔHA-mCherry and lungs harvested at 24 hpi for analysis by flow cytometry. Representative flow plots from infected (top) and fluorescence minus one control (bottom) mice are shown. Representative of one experiment with n=1-3 mice per group.

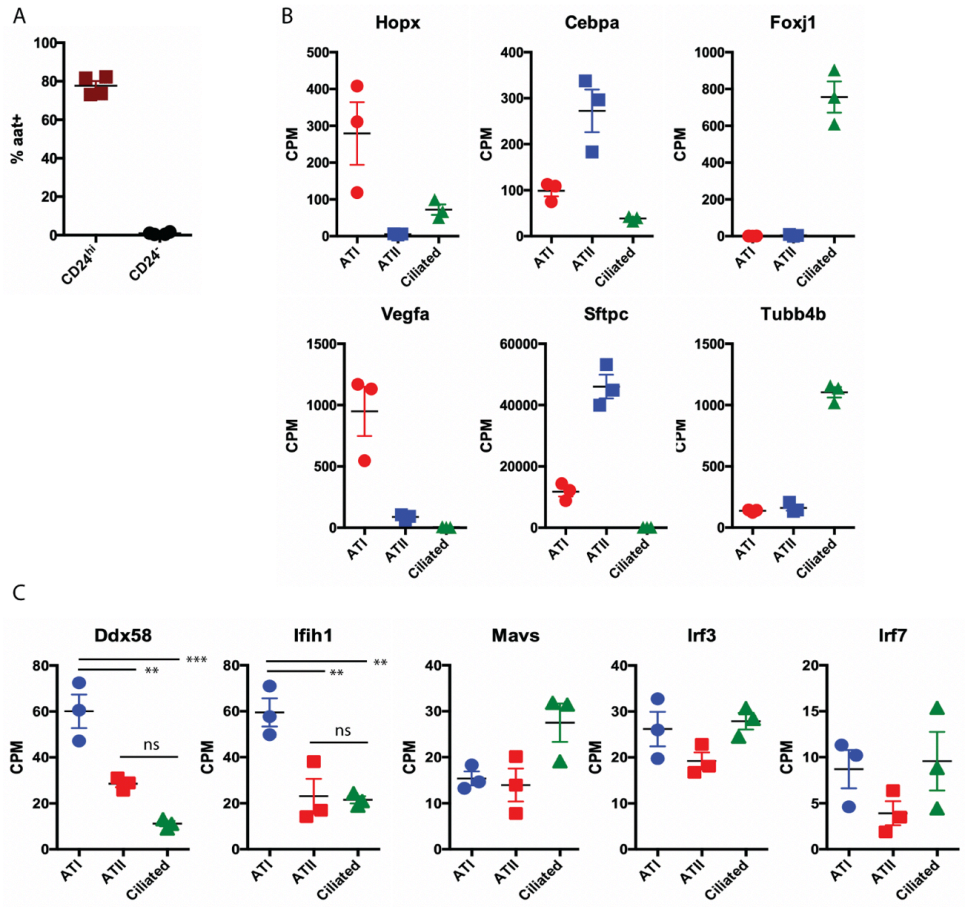


**Figure 3-8**. Analysis of individual epithelial cell types *in vivo.* (A) B6 mice were infected with $10^5$ PFU ΔHA-mCherry and lungs harvested at 24 hpi for analysis by flow cytometry. The percentage of $CD24^{hi}$ and $CD24^{-}$ cells that are $aat^{+}$ was quantified. Data representative of one independent experiment with n=3 mice. (B-C) Lungs from naïve mice were harvested and ATI, ATII, and ciliated cells were FACS sorted for mRNA-seq analysis. Levels of the indicated cell type-specific (B) and innate immune signaling (C) genes were quantified. Data representative of one independent experiment with n=3 mice. One-way ANOVA with Tukey's multiple comparisons test *** $p<0.001$, ** $p<0.01$, ns= not significant.

### *Cell type-specific responses to stages of virus replication in vivo.*

To assess cell type-specific responses to infection, we first looked at global changes in host transcripts. ATI cells respond only to direct infection, with similar responses to primary transcription and amplified replication (Figure 3-9A, left). In contrast, ATII cells have a tiered response to direct infection, and uninfected ATII

cells from ΔHA-Cre infected mice are able to respond to global inflammation (Figure 3-9A, middle). Ciliated cells only respond to direct infection, and this response is tiered to different stages of virus replication (Figure 3-9A, right). Quantification of IAV gene expression—excluding HA and PB1 reads—in each cell type revealed no differences between ΔHA-Cre-infected cells, while ΔPB1-Cre-infected ciliated cells have higher IAV reads than ΔPB1 infected ATI or ATII cells (Figure 3-9B). ATI, ATII, and ciliated cells all upregulate *Ifnb* in response to ΔHA-Cre infection (Figure 3-10). In contrast to the *in vitro* data (Figure 3-4), ΔPB1-Cre is unable to induce detectable *Ifnb* in the analyzed cell types *in vivo*, which may be due to lower relative MOI. Importantly, these cell types also do not upregulate the IFN-dependent ISG *Mx1* in response to ΔPB1-Cre infection, indicating that IFN is likely not secreted by any cell type. Both infected and uninfected cells upregulate *Mx1* in response to ΔHA-Cre, suggesting that amplified virus replication is required to induce IFN production *in vivo* and any genes upregulated in ΔPB1-Cre infected cells, including genes designated as ISGs, are likely due to direct infection.

We then analyzed the ISGs upregulated by primary transcription or amplified replication. We identified ISGs that were specific to ΔHA-Cre or ΔPB1-Cre infection, as well as genes upregulated by both infections (Figure 3-9C, Table 3-4). The previously identified putative protective ISGs (Figure 3-1E) are all upregulated exclusively by ΔHA-Cre infection. This could indicate that induction of a strongly antiviral response is dependent on *de novo* vRNA production and/or upregulation of IFN. We also identified genes that are only significantly upregulated in ΔPB1-infected cells. These genes may be upregulated in response to virus

entry, early trafficking of vRNPs, or some other early stage of virus infection. Following detection of virus RNAs, the genes upregulated in response to RLR signaling may dominate the transcriptome, which is why we do not see significant upregulation of these ΔPB1-specific genes in ΔHA infected mice.

We compared ISGs upregulated in ΔHA-Cre infected IAV$^+$ cells between cell types to identify cell type-specific responses to infection (Figure 3-9D, Table 3-5). All cell types upregulate genes involved in antigen processing and presentation (*Herc6*, *Psmb8*, *Rnf213*, *Tap1*). Ciliated cells were the only cells to upregulate several genes involved in endocytosis and vesicle transport (*Amph*, *Msr1*). ATI and ATII cells specifically upregulated RNA metabolism-associated genes (*Cnp*, *Isg20*, *Pnpt1*), which may be employed as a way to target and degrade virus RNAs. In response to ΔHA-Cre infection, all cell types were able to upregulate the putative protective ISG *Helz2* (Figure 3-1E, Table 3-1). However, only ATII cells upregulated *Adar*, *Eif2ak2*, and *Pml,* which all have known anti-IAV activity (27, 132, 169). While all cell types upregulate *Stat1* and the positive RLR regulator *Ddx60*, only ATII and ciliated cells upregulate *Ddx58* (RIG-I), *Ifih1* (MDA5), and *Stat2*. These data suggest that different cell types may employ unique strategies that are compatible with the cell function to make the cell inhospitable to virus replication.

We were also able to compare ISGs upregulated in IAV$^+$ or IAV$^-$ cells over naïve cells as a way to identify infection-specific ISGs (Figure 3-9E, Table 3-6). Many innate signaling genes are upregulated in both infected and uninfected cells from ΔHA-Cre infected mice (RLRs, *Irf7*, *Tlr3*). Among the infection-specific ISGs

upregulated during ΔHA-Cre infection are genes associated with apoptosis (*Ripk2*, *Casp1*, *Ifi27, Pmaip1*) and E3 ubiquitin ligases and proteasome genes, some of which are known to be involved in MHC-I antigen processing (*Neurl3*, *Rnf19b*, *Psmb9*). While many known ISGs with anti-IAV activity are upregulated in both $IAV^+$ and $IAV^-$ cells, *Eif2ak2* is infection-specific. Repair of virus-induced DNA damage is critical for cell survival from IAV infection (170), and several DNA damage response-associated genes (*Bub1*, *Ddit4*, *Pml*) were found to be infection-specific. Overall, the cell type infected, the stage of IAV replication, and direct infection all contribute to the antiviral response of a cell *in vivo*.

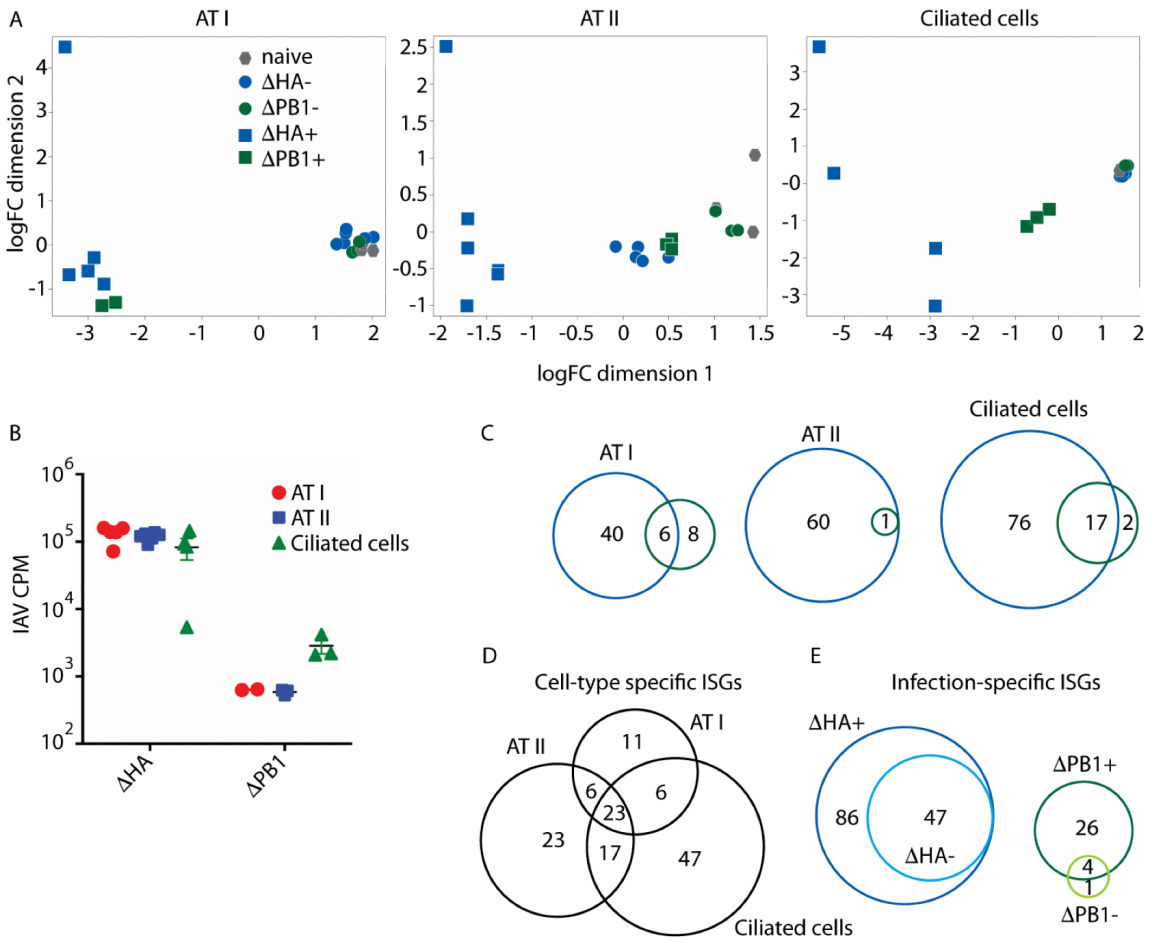


**Figure 3-9.** Cell type-specific responses to stages of virus replication *in vivo.* Cre reporter mice were infected with $10^5$ pfu ΔHA-Cre or ΔPB1-Cre and tdTomato$^+$ and tdTomato$^-$ ATI, ATII, and ciliated cells were sorted at 24 hpi for mRNA-seq analysis. (A) MDS plots of the indicated cell type. (B) IAV CPM in tdTomato$^+$ cells infected with the indicated virus. (C) Unique and overlapping ISGs significantly upregulated (logFC≥1.5, FDR ≤0.05, CPM≥10 in at least one population) in ΔHA- or ΔPB1-infected tdTomato$^+$ cells compared to naïve indicated cell type. (D) Unique and overlapping ISGs significantly upregulated in ΔHA-infected tdTomato+ cells. (E) Infection-specific ISGs were identified by comparing genes in tdTomato$^+$ (ΔHA/ΔPB1$^+$) and tdTomato$^-$ (ΔHA/PB1$^-$) mice. Data representative of one independent experiment with n=2-6 mice per group.

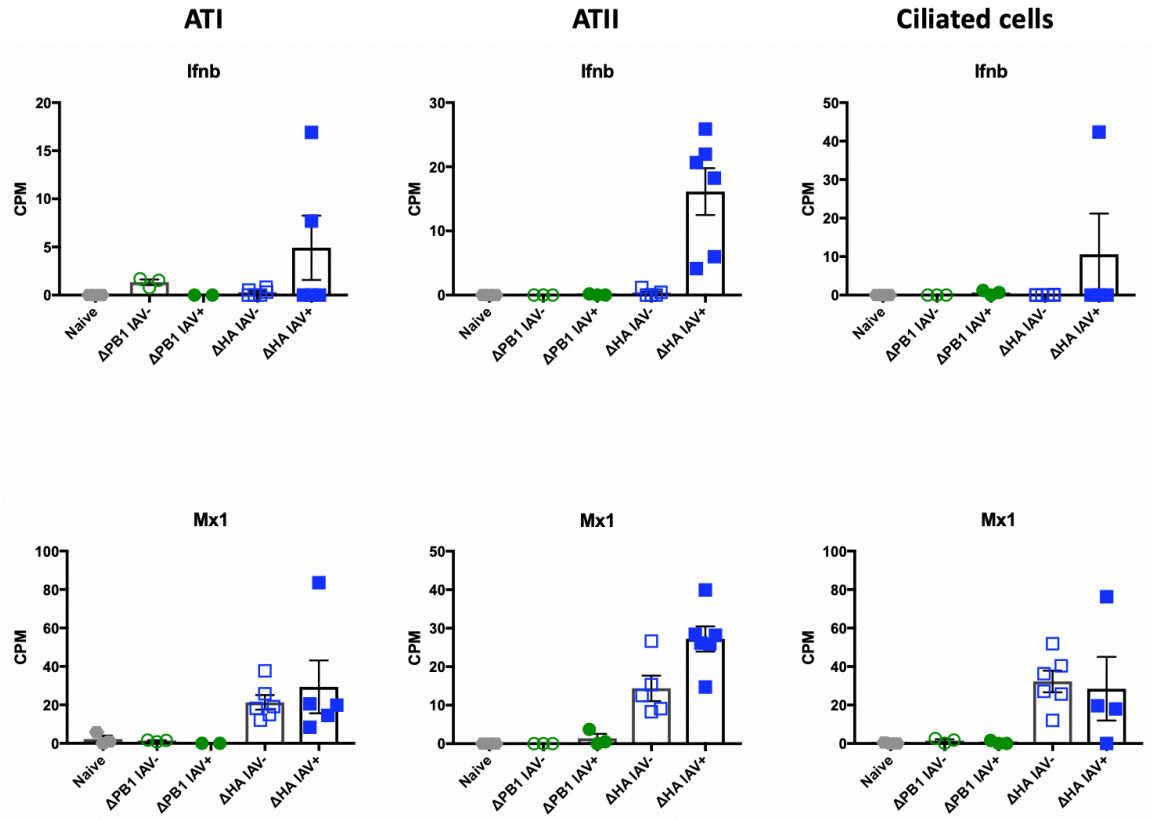


**Figure 3-10.** Amplified scIAV replication is required for IFN signaling. Expression of *Ifnb* (top) and *Mx1* (bottom) in ATI, ATII, and ciliated cells in the indicated condition. Data representative of one independent experiment with n=2-6 mice per group.

**Table 3-4.** Overlap in ISGs expressed in individual cell types between ΔHA-Cre and ΔPB1-Cre infection.

| ATI cells | | | | ATII cells | | | | Ciliated cells | | | |
|---|---|---|---|---|---|---|---|---|---|---|---|
| ΔHA-Cre | | ΔPB1-Cre | | ΔHA-Cre | | ΔPB1-Cre | | ΔHA-Cre | | ΔPB1-Cre | |
| Atf3 | Maff | Arg2 | Nrn1 | Abtb2 | Mafb | Steap4 | | Abca9 | Junb | Abca9 | Ifit1bl1 |
| Ceacam1 | Marcksl1 | Ceacam1 | Pi4k2b | Adar | Maff | | | Adm | Lamp3 | Atp10d | Ifit2 |
| Cebpd | Mov10 | Fut4 | Psmb8 | Atf3 | Mx1 | | | Ahnak2 | Lgals9 | Ccna1 | Ifit3 |
| Cnp | Mx1 | Gk | Psmb9 | B4galt5 | Mx2 | | | Amph | Lmo2 | Ceacam1 | Ifitm3 |
| Cxcl10 | Mx2 | Lamp3 | Rab27a | Bst2 | Neurl3 | | | Apol6 | Lrg1 | Cebpd | Irf7 |
| Ddit4 | Nfil3 | Lrg1 | Sqle | Ccl5 | Nt5c3 | | | Arg2 | Map3k14 | Ddx60 | Lamp3 |
| Ddx60 | Oas3 | Mthfd2l | Steap4 | Cd274 | Parp12 | | | Atf3 | Marcksl1 | Fam46c | Lgals9 |
| Dhx58 | Psmb8 | | | Cdkn1a | Pfkfb3 | | | Atp10d | Mastl | Gpx2 | Slfn5 |
| Fut4 | Rgs1 | | | Ceacam1 | Pml | | | Batf2 | Mb21d1 | Herc6 | Steap4 |
| Gch1 | Rnf213 | | | Csrnp1 | Pnpt1 | | | Bcl3 | Msr1 | Hk2 | |
| Gem | Rsad2 | | | Cxcl10 | Psmb8 | | | Bst2 | Mx1 | | |
| Gk | Rtp4 | | | Ddx58 | Ripk2 | | | Bub1 | Mx2 | | |
| Gpx2 | Stat2 | | | Ddx60 | Rnf19b | | | Casp1 | Neurl3 | | |
| Helz2 | Steap4 | | | Dhx58 | Rnf213 | | | Cd38 | Nod2 | | |
| Herc6 | Tap1 | | | Dtx3l | Rsad2 | | | Ceacam1 | Oas2 | | |
| Ifi44 | Tlr3 | | | Eif2ak2 | Rtp4 | | | Cebpd | Oas3 | | |
| Ifit1 | Tnfaip3 | | | Epsti1 | Serpine1 | | | Cxcl10 | Pim3 | | |
| Irf7 | Tnfsf10 | | | Gbp2 | Slc1a1 | | | Cxcl11 | Pmaip1 | | |
| Isg15 | Trim14 | | | Gbp3 | Sp110 | | | Cyp1b1 | Psmb8 | | |
| Isg20 | Usp18 | | | Gbp5 | Spats2l | | | Ddx58 | Psmb9 | | |
| Lap3 | Vmp1 | | | Gch1 | Stat1 | | | Ddx60 | Rgs1 | | |
| Lgals9 | Xaf1 | | | Helz2 | Stat2 | | | Dtx3l | Rnf213 | | |
| Lrg1 | Zbp1 | | | Herc6 | Steap4 | | | Dusp5 | Rsad2 | | |
| | | | | Ifi27l2a | Tap1 | | | Epsti1 | Samhd1 | | |
| | | | | Ifi35 | Tlr3 | | | Fam46c | Sat1 | | |
| | | | | Ifi44 | Tnfaip3 | | | Flt1 | Serpinb9 | | |
| | | | | Ifih1 | Tnfsf10 | | | Gbp2 | Serpine1 | | |
| | | | | Ifit1 | Trafd1 | | | Gbp3 | Slc15a3 | | |
| | | | | Ifit2 | Trim21 | | | Gbp5 | Slc16a1 | | |
| | | | | Ifit3 | Uba7 | | | Gem | Slc25a30 | | |
| | | | | Ifitm3 | Ube2l6 | | | Gja5 | Slfn5 | | |
| | | | | Irf7 | Usp18 | | | Helz2 | Stat1 | | |
| | | | | Irf9 | Xaf1 | | | Herc6 | Stat2 | | |
| | | | | Isg15 | Zbp1 | | | Hk2 | Steap4 | | |
| | | | | Lgals9 | | | | Hsh2d | Tap1 | | |
| | | | | | | | | Ifi27 | Thbd | | |
| | | | | | | | | Ifi44 | Tlr3 | | |
| | | | | | | | | Ifih1 | Tlr7 | | |
| | | | | | | | | Ifit1 | Tnfaip3 | | |
| | | | | | | | | Ifit1bl1 | Tnfaip6 | | |
| | | | | | | | | Ifit2 | Tnfsf10 | | |
| | | | | | | | | Ifit3 | Trafd1 | | |
| | | | | | | | | Ifitm3 | Trim21 | | |
| | | | | | | | | Il15 | Ube2l6 | | |
| | | | | | | | | Il1rn | Vegfc | | |
| | | | | | | | | Irf7 | Xaf1 | | |
| | | | | | | | | Isg15 | | | |

**Table 3-5.** Overlap in ISGs expressed between cell types during ΔHA-Cre infection.

| ATI cells | | ATII cells | | Ciliated cells | |
|---|---|---|---|---|---|
| Atf3 | Maff | Abtb2 | Mafb | Abca9 | Junb |
| Ceacam1 | Marcksl1 | Adar | Maff | Adm | Lamp3 |
| Cebpd | Mov10 | Atf3 | Mx1 | Ahnak2 | Lgals9 |
| Cnp | Mx1 | B4galt5 | Mx2 | Amph | Lmo2 |
| Cxcl10 | Mx2 | Bst2 | Neurl3 | Apol6 | Lrg1 |
| Ddit4 | Nfil3 | Ccl5 | Nt5c3 | Arg2 | Map3k14 |
| Ddx60 | Oas3 | Cd274 | Parp12 | Atf3 | Marcksl1 |
| Dhx58 | Psmb8 | Cdkn1a | Pfkfb3 | Atp10d | Mastl |
| Fut4 | Rgs1 | Ceacam1 | Pml | Batf2 | Mb21d1 |
| Gch1 | Rnf213 | Csrnp1 | Pnpt1 | Bcl3 | Msr1 |
| Gem | Rsad2 | Cxcl10 | Psmb8 | Bst2 | Mx1 |
| Gk | Rtp4 | Ddx58 | Ripk2 | Bub1 | Mx2 |
| Gpx2 | Stat2 | Ddx60 | Rnf19b | Casp1 | Neurl3 |
| Helz2 | Steap4 | Dhx58 | Rnf213 | Cd38 | Nod2 |
| Herc6 | Tap1 | Dtx3l | Rsad2 | Ceacam1 | Oas2 |
| Ifi44 | Tlr3 | Eif2ak2 | Rtp4 | Cebpd | Oas3 |
| Ifit1 | Tnfaip3 | Epsti1 | Serpine1 | Cxcl10 | Pim3 |
| Irf7 | Tnfsf10 | Gbp2 | Slc1a1 | Cxcl11 | Pmaip1 |
| Isg15 | Trim14 | Gbp3 | Sp110 | Cyp1b1 | Psmb8 |
| Isg20 | Usp18 | Gbp5 | Spats2l | Ddx58 | Psmb9 |
| Lap3 | Vmp1 | Gch1 | Stat1 | Ddx60 | Rgs1 |
| Lgals9 | Xaf1 | Helz2 | Stat2 | Dtx3l | Rnf213 |
| Lrg1 | Zbp1 | Herc6 | Steap4 | Dusp5 | Rsad2 |
| | | Ifi27l2a | Tap1 | Epsti1 | Samhd1 |
| | | Ifi35 | Tlr3 | Fam46c | Sat1 |
| | | Ifi44 | Tnfaip3 | Flt1 | Serpinb9 |
| | | Ifih1 | Tnfsf10 | Gbp2 | Serpine1 |
| | | Ifit1 | Trafd1 | Gbp3 | Slc15a3 |
| | | Ifit2 | Trim21 | Gbp5 | Slc16a1 |
| | | Ifit3 | Uba7 | Gem | Slc25a30 |
| | | Ifitm3 | Ube2l6 | Gja5 | Slfn5 |
| | | Irf7 | Usp18 | Helz2 | Stat1 |
| | | Irf9 | Xaf1 | Herc6 | Stat2 |
| | | Isg15 | Zbp1 | Hk2 | Steap4 |
| | | Lgals9 | | Hsh2d | Tap1 |
| | | | | Ifi27 | Thbd |
| | | | | Ifi44 | Tlr3 |
| | | | | Ifih1 | Tlr7 |
| | | | | Ifit1 | Tnfaip3 |
| | | | | Ifit1bl1 | Tnfaip6 |
| | | | | Ifit2 | Tnfsf10 |
| | | | | Ifit3 | Trafd1 |
| | | | | Ifitm3 | Trim21 |
| | | | | Il15 | Ube2l6 |
| | | | | Il1rn | Vegfc |
| | | | | Irf7 | Xaf1 |
| | | | | Isg15 | |

**Table 3-6.** Identification of infection-specific ISGs during ΔHA-Cre and ΔPB1-Cre infection.

| ΔHA-Cre | | | | ΔPB1-Cre | | | |
|---|---|---|---|---|---|---|---|
| IAV+ | | IAV- | | IAV+ | | IAV- | |
| Abca9 | Lamp3 | Adar | Lgals9 | Arg2 | Ifit3 | Ddx60 | Ifitm3 |
| Abtb2 | Lap3 | Bst2 | Mx1 | Abca9 | Ifitm3 | Ifit1 | Irf7 |
| Adar | Lgals9 | Cxcl10 | Mx2 | Atp10d | Irf7 | Ifit3 | |
| Adm | Lmo2 | Ddx58 | Oas2 | Ccna1 | Lamp3 | | |
| Ahnak2 | Lrg1 | Ddx60 | Oas3 | Ceacam1 | Lgals9 | | |
| Amph | Mafb | Dhx58 | Parp12 | Cebpd | Lrg1 | | |
| Apol6 | Maff | Dtx3l | Psmb8 | Ddx60 | Mthfd2l | | |
| Arg2 | Map3k14 | Epsti1 | Rnf213 | Fam46c | Nrn1 | | |
| Atf3 | Marcksl1 | Gbp2 | Rsad2 | Fut4 | Pi4k2b | | |
| Atp10d | Mastl | Gbp3 | Rtp4 | Gk | Psmb8 | | |
| B4galt5 | Mb21d1 | Gbp5 | Sp110 | Gpx2 | Psmb9 | | |
| Batf2 | Mov10 | Helz2 | Stat1 | Herc6 | Rab27a | | |
| Bcl3 | Msr1 | Herc6 | Stat2 | Hk2 | Slfn5 | | |
| Bst2 | Mx1 | Ifi27l2a | Steap4 | Ifit1bl1 | Sqle | | |
| Bub1 | Mx2 | Ifi35 | Tap1 | Ifit2 | Steap4 | | |
| Casp1 | Neurl3 | Ifi44 | Tlr3 | | | | |
| Ccl5 | Nfil3 | Ifih1 | Tnfsf10 | | | | |
| Cd274 | Nod2 | Ifit1 | Trafd1 | | | | |
| Cd38 | Nt5c3 | Ifit1bl1 | Uba7 | | | | |
| Cdkn1a | Oas2 | Ifit2 | Ube2l6 | | | | |
| Ceacam1 | Oas3 | Ifit3 | Usp18 | | | | |
| Cebpd | Parp12 | Ifitm3 | Xaf1 | | | | |
| Cnp | Pfkfb3 | Irf7 | Zbp1 | | | | |
| Csrnp1 | Pim3 | Isg15 | | | | | |
| Cxcl10 | Pmaip1 | | | | | | |
| Cxcl11 | Pml | | | | | | |
| Cyp1b1 | Pnpt1 | | | | | | |
| Ddit4 | Psmb8 | | | | | | |
| Ddx58 | Psmb9 | | | | | | |
| Ddx60 | Rgs1 | | | | | | |
| Dhx58 | Ripk2 | | | | | | |
| Dtx3l | Rnf19b | | | | | | |
| Dusp5 | Rnf213 | | | | | | |
| Eif2ak2 | Rsad2 | | | | | | |
| Epsti1 | Rtp4 | | | | | | |
| Fam46c | Samhd1 | | | | | | |
| Flt1 | Sat1 | | | | | | |
| Fut4 | Serpinb9 | | | | | | |
| Gbp2 | Serpine1 | | | | | | |
| Gbp3 | Slc15a3 | | | | | | |
| Gbp5 | Slc16a1 | | | | | | |
| Gch1 | Slc1a1 | | | | | | |
| Gem | Slc25a30 | | | | | | |
| Gja5 | Slfn5 | | | | | | |
| Gk | Sp110 | | | | | | |
| Gpx2 | Spats2l | | | | | | |
| Helz2 | Stat1 | | | | | | |
| Herc6 | Stat2 | | | | | | |
| Hk2 | Steap4 | | | | | | |
| Hsh2d | Tap1 | | | | | | |
| Ifi27 | Thbd | | | | | | |
| Ifi27l2a | Tlr3 | | | | | | |
| Ifi35 | Tlr7 | | | | | | |
| Ifi44 | Tnfaip3 | | | | | | |
| Ifih1 | Tnfaip6 | | | | | | |
| Ifit1 | Tnfsf10 | | | | | | |
| Ifit1bl1 | Trafd1 | | | | | | |
| Ifit2 | Trim14 | | | | | | |
| Ifit3 | Trim21 | | | | | | |
| Ifitm3 | Uba7 | | | | | | |
| Il15 | Ube2l6 | | | | | | |
| Il1rn | Usp18 | | | | | | |
| Irf7 | Vegfc | | | | | | |
| Irf9 | Vmp1 | | | | | | |
| Isg15 | Xaf1 | | | | | | |
| Isg20 | Zbp1 | | | | | | |
| Junb | | | | | | | |

## DISCUSSION

The early innate response in infected cells is critical for controlling IAV pathogenesis *in vivo*. Following import into the nucleus, the IAV RdRp first transcribes vRNA to generate mRNA and protein. After *de novo* polymerase complexes are generated, the vRNA is replicated. These two distinct stages of early virus replication are of critical importance in innate immune signaling, as *de novo* vRNA is necessary for induction of IFN-β during IAV infection. IFN-β production within the first hour of IAV infection has been documented in both human and mouse cells (171). IFN-independent, IRF-dependent upregulation of some ISGs has been described (31-33). In these studies, detection of viral RNA products is still required for virus-induced gene expression. We are unable to detect IFN expression following ΔPB1 infection *in vivo*, and the observed induction of antiviral genes could therefore be driven directly through RLR signaling. Membrane perturbations—such as those that occur during virus binding and entry into the host cell—have been shown to be sufficient to induce IRF3-mediated gene activation *in vitro* (35), and this response is independent of RLR signaling (34). The upregulation of ISGs we see during ΔPB1 infection could therefore be due to virus entry rather than production of new virus RNA species, and these responses would be revealed in RLR signaling deficient cells. As RIG-I knockout and MAVS knockout cells do not significantly upregulate any genes following ΔPB1-mCherry infection, virus entry induces little response *in vitro*. However, the ΔPB1-specific genes upregulated *in vivo* may be in response to entry. An additional facet of the early innate immune response to viruses is the upregulation of endogenous

transposable elements (172). This upregulation occurs prior to IFN induction. As primary transcription is sufficient for induction of antiviral genes, transposable elements are likely also upregulated and contributing to the cellular response.

Various techniques have been employed to assess distinct stages of IAV infection within a cell. These studies use inhibitors to prevent protein synthesis or transcription, which effectively halt virus replication but also target cellular processes (155-157). This limits the ability to analyze the immune response, as expression of host genes is compromised. Specific inhibition of virus replication could be achieved by using drugs that target the IAV polymerase specifically, either by targeted drug design or by engineering IAVs to be susceptible to drug control, as described through the use of the small molecule assisted shutoff tag. Addition of this tag to an IAV polymerase gene resulted in an IAV whose replication was susceptible to hepatitis C virus protease inhibitors (173), allowing for specific inhibition of IAV replication. In addition to inhibition of replication, recent studies using single-cell RNA sequencing technologies have uncovered cellular responses to IAVs lacking one or more gene segments, including viruses lacking polymerase segments. Similar to our results using ΔPB1 scIAVs, cells infected with viruses lacking vRNP genes produce less virus mRNA and induce little to no IFN (62). However, a virus lacking both PB1 and NS1 potently induced IFN (63). While our data suggest that primary transcription can induce antiviral gene expression in an IFN-independent manner, in the absence of immune antagonism, primary IAV transcription may be sufficient to drive IFN expression.

We and others have identified cell type-specific responses to IAV infection *in vivo* (158, 165). Unlike previous studies, we are able to compare three different epithelial cell types, the stage of replication (primary virus transcription vs amplified replication), and assess the response of bystander cells. Some of these cell type differences may be explained by an incompatibility with certain ISGs and the function of a given cell type (*e.g.* expression of *Eif2ak2* may be incompatible with critical ciliated cell function). The only ISG upregulated by all cell types in during both full replication and primary transcription is *Steap4*. STEAP4—also known as STAMP2—is a metalloreductase that has antiviral activity during hepatitis B virus (HBV) infection. STEAP4 prevents HBV-induced metabolic dysregulation and can antagonize HBV gene expression, thereby protecting cells from HBV (174). Expression of *Steap4* in scIAV-infected cells could serve a similar function.

Basal levels of signaling genes may contribute to the observed differential antiviral responses between cell types. However, this does not fully explain expression differences, as ATI cells express higher levels of *Ddx58* and *Ifih1* (Figure 3-8C) but ciliated cells upregulate the most ISGs, even in uninfected cells. In addition to upregulating more ISGs than other epithelial cell types, the highest upregulated ISG in ΔPB1-Cre-infected ciliated cells is *Ifitm3*. IFITM3 is known to inhibit entry/uncoating of IAV (25, 26); the potent upregulation of *Ifitm3* during early stages of infection and/or the rapid upregulation of ISGs could explain our previously described protection of ciliated cells during virus spread (158). The epigenetic landscape of different cell types prior to and during early infection could

also contribute to differences in gene expression, as epigenetic differences affect functional outcomes during virus infections (175).

RIG-I is known to detect short (10-300bp) cytosolic RNAs with 5' triphosphate ends (176). While aberrant (-)-sense IAV RNA products—DI genomes and mini viral RNAs—are detected by RIG-I, the contribution of (+)-sense IAV RNAs to innate immune detection is unclear. Triphosphate-independent recognition of lariat structures derived from vRNA and cRNA has been described, and both potently upregulate IFN-I (177). ΔPB1 viruses are able to generate (+)-sense RNA, therefore cRNA-derived structures could be driving the response to ΔPB1 infection.

Overall, we have described the use of a genetically restricted scIAV to assess cell type- and virus replication stage-specific host responses to infection. We determined that both primary virus transcription and amplified replication are detected through RIG-I. Additionally, we found that the magnitude of early replication, the stage of replication, and the cell type infected all contribute to the antiviral response *in vivo*. Altogether, these data offer insight into the mechanisms of innate immune activation during IAV infection.

**FOOTNOTES**

[1]This work is currently under review at PLoS Pathogens.

[2]Additional contributions: ΔPB1 viruses and ΔHA-Cre viruses were generated by S.L. Aron. Flow cytometry experiments were completed by E.J. Fay and S.L. Aron and analyzed by E.J. Fay. RNA-seq experiments were completed by E.J. Fay and S.L. Aron and analyzed by E.J. Fay, M.G. Macchietto, M.W. Markman, and S. Shen. K. Esser-Nobis and M. Gale, Jr. generated A549 KO cells. E.J. Fay and R.A. Langlois wrote the manuscript.

[3]Abbreviations used this chapter: aat, acetylated alpha-tubulin; ATI, type I alveolar; ATII, type II alveolar; CPM, counts per million; Cre, Cre recombinase; cRNA, complementary RNA; DI, defective interfering; EpCAM, epithelial cell adhesion molecule; FACS, fluorescence-activated cell sorting; FDR, false discovery rate; GFP, green fluorescent protein; gMFI, geometric mean fluorescence intensity; GO, gene ontology; HA, hemagglutinin; HBV, hepatitis B virus; i.n., intranasal; IAV, influenza A virus; IFITM3, IFN-induced transmembrane protein 3; IFN, interferon; ISG, IFN-stimulated gene; logFC, logarithmic fold change; MAVS, mitochondrial antiviral signaling protein; MDA5, melanoma differentiation-associated protein 5; MDCK, Madin-Darby canine kidney; MDS, multidimensional scaling; MHC, major histocompatibility complex; NA, neuraminidase; NTC, non-targeting control; PB1, polymerase basic 1; PFU, plaque forming unit; PKR, protein kinase R; RdRp, RNA-dependent RNA polymerase; RIG-I, retinoic acid-inducible gene 1; RLR, RIG-I-like receptor; scIAV, single-cycle IAV; STAMP2, six transmembrane protein of prostate 2; STEAP4, six transmembrane epithelial antigen of the prostate 4; vRNA, viral RNA; vRNP, viral ribonucleoprotein

## CHAPTER 4: Innate immune barriers to intra- and inter-species transmission of viruses


### SUMMARY

Viruses emerging from zoonotic reservoirs represent a major public health concern. While identifying potential zoonoses is paramount to pandemic preparedness, there are few experimental models that are able to characterize virus and host factors necessary for cross-species transmission. Here, we leverage a model whereby pet store mice—which harbor a myriad of mouse pathogens—are co-housed with clean laboratory mice. This 'dirty' mouse model offers a platform for studying the acute transmission of viruses between hosts via natural mechanisms—through direct contact, air, and saliva and other fluids. We co-housed pet store mice with wild type laboratory mice and mice that are deficient in interferon receptors and harvested various organs for RNA sequencing analysis. This model system gives us unique access to both the reservoir and the new host, allowing us to analyze mutations and adaptations that occur in the virus population during transmission to and spread within a new host. We have also co-housed our laboratory mice with the bedding of pet store rats to analyze species-specific immune and non-immune barriers to transmission. By also analyzing the virus infections in the rats, we will be able to identify virus mutations necessary to overcome these species barriers. Overall, this mouse model allows for the analysis of barriers to transmission of natural rodent viruses.

## INTRODUCTION

Many emerging viruses are transmitted to humans from zoonotic reservoirs. These viruses represent a major public health risk, as existing immunity to human viruses offer little protection against these viruses. Classic examples of zoonoses include human immunodeficiency virus (HIV), Ebolavirus, and avian influenza viruses (178-180). The ongoing outbreak of a novel coronavirus highlights the critical need for pandemic preparedness in the face of zoonotic viruses. Understanding virus adaptations that allow for transmission within and between animal species is imperative to understand mechanisms of emergence.

Viruses are capable of rapid evolution to both adapt to new hosts and evade host immune responses. Within a single host, a virus population will exist with a wide array of variants. Very few virus particles transmit between hosts, creating a genetic bottleneck (181). The subset of variants that do transmit rapidly expands to create a new variant population in the new host. The viral diversity within a host can have a dramatic impact on the outcome of infection and the potential for spread to additional hosts.

There is little preexisting immunity to novel emerging viruses, making innate immune control of emerging viruses necessary for survival of the host and preventing spread to a new host. Innate immune responses—interferon (IFN) in particular—has placed immense evolutionary pressure on viruses, and this pressure continues on presently emerging viruses. Understanding how viruses evolve to evade innate immune pressures in a new host is a critical to understanding zoonotic transmission to humans. In the case of HIV-1, the

precursor SIV first gained the ability to spread from monkeys to chimpanzees, then from chimpanzees to humans. A major driver of zoonotic transmission to humans was the adaptation of HIV-1 to antagonize the human restriction factors APOBEC3 family proteins and Tetherin, highlighting the importance of immune evasion in permitting cross-species transmission events (178, 182). The ability to identify such adaptations in circulating virus populations in animal species may help predict viruses with potential to spread to humans, allowing us to better prepare for pandemics.

*Rodentia* is the most diversified mammalian order, comprising 40% of all mammalian species (183). Rodents harbor many pathogens because they live in dense, highly social groups. Because of the close proximity to humans, many mouse pathogens have transmitted to humans, including lymphocytic choriomeningitis virus and Leptospira species (184). Rodent-borne hantaviruses are a global public health concern, as they can cause severe disease, including hemorrhagic fever, in humans despite limited pathology in rodent hosts (185). Additional pathogens have been identified in wild-caught mice and other rodents (184, 186, 187). Rodents—along with primates and bats—have historically been dominant reservoirs for pathogens that jump to humans, and it is pertinent to understand how viruses transmit within and between rodent species.

We are using a model whereby pet store mice—which harbor a myriad of natural mouse pathogens—are co-housed with our specific pathogen free (SPF) laboratory mice. During co-housing, pathogens and other microbes transmit from the pet store mice to our laboratory mice, giving us the opportunity to assess

transmission of viruses via natural routes—through air, direct contact, feces, and saliva and other fluids (188). We have found a broad array of viruses and other pathogens in pet store mice, many of which are able to spread to co-housed mice. Several of these virus populations appear to be dynamic as they transmit to and disseminate within a new host. By using laboratory mice deficient in IFN signaling, we assessed the role of the IFN response in constraining virus populations during transmission and spread. Additionally, through the use of pet store rats, we have identified rat pathogens that are able to overcome species barriers and replicate in mice. Overall, the dirty mouse platform can be used to characterize barriers to virus transmission.

## MATERIALS AND METHODS

### *Mice, co-housing, and antibiotic treatment.*

Wild-type C57BL/6J and B6(Cg)-Ifnar1$^{tm1.2Ees}$/J (IFN$\alpha$R$^{-/-}$) mice were purchased from The Jackson Laboratory. B6.IL-28RA$^{-/-}$ (IFN$\lambda$R$^{-/-}$) and B6.IL-28RA$^{-/-}$Ifnar1$^{-/-}$ (IFN$\alpha\lambda$R$^{-/-}$) mice were a kind gift from Dr. Sergio Kotenko (Rutgers University, (21, 189)). Pet store mice were purchased from Twin Cities area pet stores. Mice were co-housed within a BSL-3 facility. Age-matched mice housed in SPF facilities served as controls. 250 µL antibiotic cocktail (1 mg/mL ampicillin, 10 mg/mL metronidazole, 5 mg/mL vancomycin, 10 mg/mL neomycin) or water was administered to the indicated mice via oral gavage as previously described (190).

### *Serology*

Pet store mice were screened using EZ-spot methods (Charles River Laboratories). Whole blood was collected at the time of sacrifice and submitted as per the Charles River Laboratories guidelines.

### *Identification of viral species by mRNA-seq*

Indicated tissues were homogenized in a GentleMacs M tube (Miltenyi Biotec) in Buffer RLT Plus (Qiagen) supplemented with 2-mercaptoethanol (10 µL/1 mL) and Reagent DX (0.5% v/v, Qiagen). RNA was extracted using the AllPrep DNA/RNA Mini kit (Qiagen). TruSeq mRNA Stranded cDNA libraries were sequenced using NovaSeq (Illumina, 50bp PE reads). 12-20 million reads/sample were obtained. Total reads were mapped to the *Mus musculus* genome (mm10) and unmapped reads were extracted using STAR aligner (191). Unmapped reads were concatenated an assembled using Trinity (192). Prospective species IDs were assigned to each assembled contig using BLASTn. The estimated counts for each species was calculated using Salmon (193). Normalized virus reads were generated using DESeq2 (194).

### *Phylogenetic analysis*

Reads mapping to the narnavirus-like RdRp were assembled and translated. Similar protein sequences were identified using NCBI BLASTp and were used to construct the phylogenetic tree. Alignments between these sequences and the novel sequence were built using Clustal Omega (195).

Maximum likelihood phylogeny was built using RAxML-NG with 1000 bootstraps (196).

### *Mutation analysis*

Total reads were mapped to the Mus musculus genome (mm10) and unmapped reads were extracted using STAR aligner, concatenated, and assembled using Trinity as described above. Assembled contigs were aligned to the indicated viral gene for per-contig variant analysis using BLASTn. Viral genomes used were murine astrovirus 2 (GenBank: MF175073.1) and murine hepatitis virus A59 (GenBank: MF618252.1).

### *Amplicon sequencing and variant analysis*

Amplicon sequencing will be performed based on previously described methods (197). Briefly, primers for the murine astrovirus RNA-dependent RNA polymerase (RdRp) and capsid genes, the MHV spike glycoprotein gene, and the kobuvirus capsid gene were designed based on sequences identified in tissue samples from pet store and co-housed mice. Previously described primers were used to amplify pan-kobuvirus 3D gene (RdRp) (198), pan-coronavirus RdRp (199), and lymphocytic choriomeningitis virus S gene (184) (see Table 4-1 for primer information). Primers were designed to amplify 200-600bp regions of the gene of interest. Virus amplicons were generated using the SuperScript IV One-Step RT-PCR System (ThermoFisher Scientific). Amplicons were isolated by gel electrophoresis and purified using the NucleoSpin Gel and PCR Clean-up kit

(Macherey-Nagel). Paired-end 250nt reads will be generated using the MiSeq v2 platform (Illumina). Each amplicon will be independently generated and sequenced in duplicate.

**Table 4-1.** Primers for amplicon sequencing.

| Virus | Gene | Size (bp) | Primer sequence |
|---|---|---|---|
| Astrovirus | RdRp | 620 | For: GGCACCCTATATAAAAGAGTTTGC |
| | | | Rev: GTCTCAAACTCCACAAACTTTTCAATA |
| | Capsid | 430 | For: ACGCCTGGGAAGCATGGGA |
| | | | Rev: ACGATCATCCAGACCGTGTTTC |
| Coronavirus | RdRp (universal) | 440 | For: ACTCAAHTGAATYTNAARTAYGC |
| | | | For: GGTTGGGAYTAYCCHAARTGYGA |
| | | | Rev: CCATCATCASWNARAATCATCAT |
| | Spike | 570 | For: ACACCTCTAATGCTAGCGCTC |
| | | | Rev: CATCTGCATAATACGCATAAAAAGTAC |
| Kobuvirus | RdRp (3D; universal) | 216 | For: TGGAYTACAARTGTTTTGATGC |
| | | | Rev: ATGTTGTTRATGATGGTGTTGA |
| | Capsid/nonstructural protein (VP1/2A/2B) | 488 | For: TGCCACCAATTTCACCCTGG |
| | | | Rev: GAGCGGCTTCGGTTACAGAT |
| LCMV | S | 380 | For: CGCACAGTGGATCCTAGGC |
| | | | Rev: CWAGRTCRGCYGCAARRGAC |

### *Ethics statement*

Care and use of the animals was in accordance with the Guide for the Care and Use of Laboratory Animals from the National Research Council and the USDA Animal Care Resource Guide. All experimental protocols involving the use of mice were approved by the Institutional Animal Care and Use Committee at the University of Minnesota (protocol: 1811-36488A. approved 03/25/2019; expires 03/24/2022).

## RESULTS

### *Identifying pathogens that transmit from pet store mice to co-housed laboratory mice*

Virus emergence from zoonotic reservoirs can cause devastating pandemics and remains a global threat to human populations. To understand how viruses evolve as they spread within rodent species, we have leveraged a previously described model whereby pet store mice (*Mus musculus*) are co-housed with specific pathogen free (SPF) laboratory mice (188). During co-house, pathogens will transmit from the pet store mice to the SPF mice, allowing us to assess virus populations both within the reservoir (pet store mice) and the recipient (SPF mice). Wild-type B6 (B6), IFN-$\alpha$ receptor knockout (IFN$\alpha$R$^{-/-}$), IFN-$\lambda$ receptor knockout (IFN$\lambda$R$^{-/-}$), and double receptor knockout (IFN$\alpha\lambda$R$^{-/-}$) mice were co-housed with pet store mice for up to 5 days, at which time animals were sacrificed and indicated tissues were processed for mRNA-seq analysis. This cage set-up was repeated three independent times. Additional co-house cages with only some SPF mouse strains and pet store mice from a single pet store were also analyzed; analyses will only include these cages when noted. During co-house, IFN knockout animals typically lose weight (Figure 4-1). Upon sacrifice, one pet store mouse in cage 1 was found to have an intestinal blockage, which would affect fecal-oral transmission of pathogens and may explain the lack of weight loss. Cage 3 SPF mice—particularly the IFN$\alpha\lambda$R$^{-/-}$ mouse—were moribund at day 3 post co-house and were therefore sacrificed for analysis at that time.

We co-housed SPF mice with mice from two different pet stores to increase pathogen diversity in the model. Mice from these pet stores have distinct pathogen histories as revealed by serology (Figure 4-2A). For example, only mice from pet store B have been exposed to pneumonia virus of mice. To identify viruses that are transmitting and replicating, we created cDNA libraries using polyadenylated (polyA) RNA. We developed a pipeline to extract non-mouse reads from the total RNA, assemble these into contigs, and search for sequence similarity to published data (Figure4-2B). Using this approach, we identified many pathogens in the pet store mice—including viruses—and some of these pathogens transmit to the co-housed mice (Figure 4-2C).

While a polyA-based cDNA synthesis approach was selected to specifically identify viruses transmitting and replicating in our mice, this will exclude viruses that do not polyadenylate their mRNAs. Such viruses include arenaviruses and hantaviruses. Specifically, this approach will exclude lymphocytic choriomeningitis virus (LCMV), which has been identified in pet store mice by serology and can transmit to co-housed SPF mice (188). We therefore screened our pet store mice for LCMV by PCR using primers for the LCMV S gene. We identified one pet store mouse positive for LCMV (Figure 4-2D). Additional PCR screening will determine if LCMV has transmitted to co-housed SPF mice.

While many viruses readily transmit from pet store mice to co-housed SPF mice, several viruses have been identified in pet store mice that never transmit. Feline stool-associated (FESA)-like virus reads have been identified in pet store small intestine and spleen/lymph node samples (Figure 4-2C). FESA-like virus

may be present in other animals in the pet store and have the ability to transmit to but not between mice, making mice a dead-end host for the virus. Lactate dehydrogenase-elevating virus (LDV)—which is known to transmit vertically in mice (200)—does not transmit to co-housed mice (Figure 4-3A). This verifies our model is working biologically and bioinformatically and suggests minimal cross-contamination between samples. Many viruses that do transmit to co-housed mice transmit readily to all strains of SPF mice. However, murine norovirus (MNV) transmits more robustly to IFN receptor knockout strains, particularly IFN$\alpha\lambda R^{-/-}$ mice (Figure 4-3B). Altogether, these data show the dirty mouse model can be used to characterize transmission of viruses.

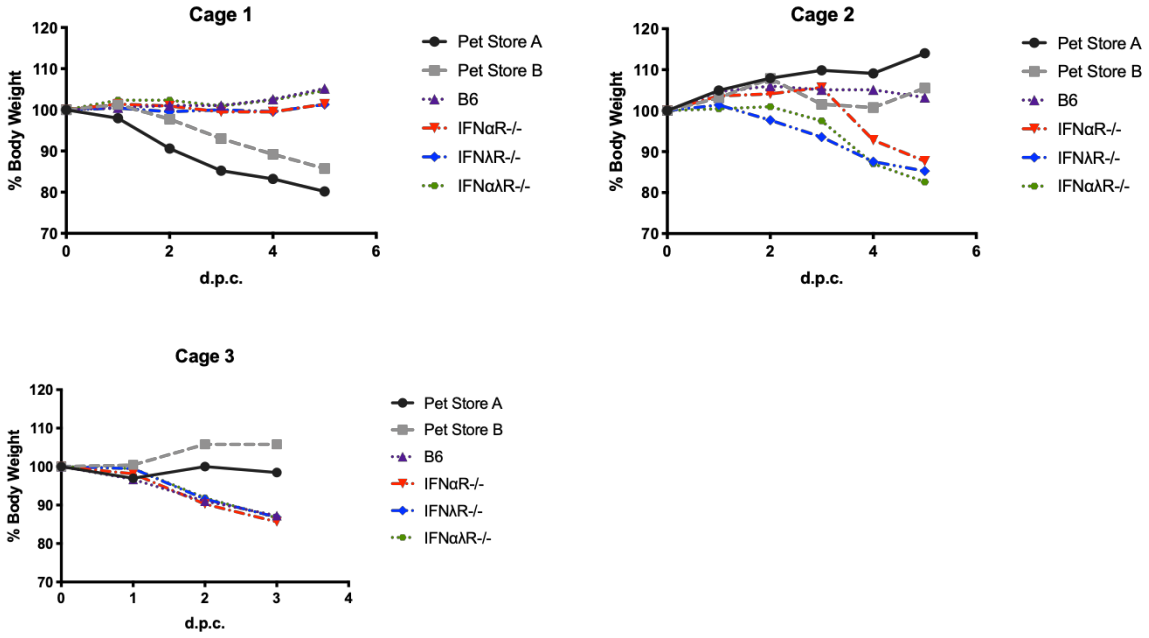


**Figure 4-1.** Co-housed SPF mice lose weight. B6, IFN$\alpha R^{-/-}$, IFN$\lambda R^{-/-}$, and IFN$\alpha\lambda R^{-/-}$ mice were co-housed with pet store mice for up to 5 days. Pet store mice were purchased on day 0. Three individual cages were set up in three consecutive weeks using new pet store mice for each cage.

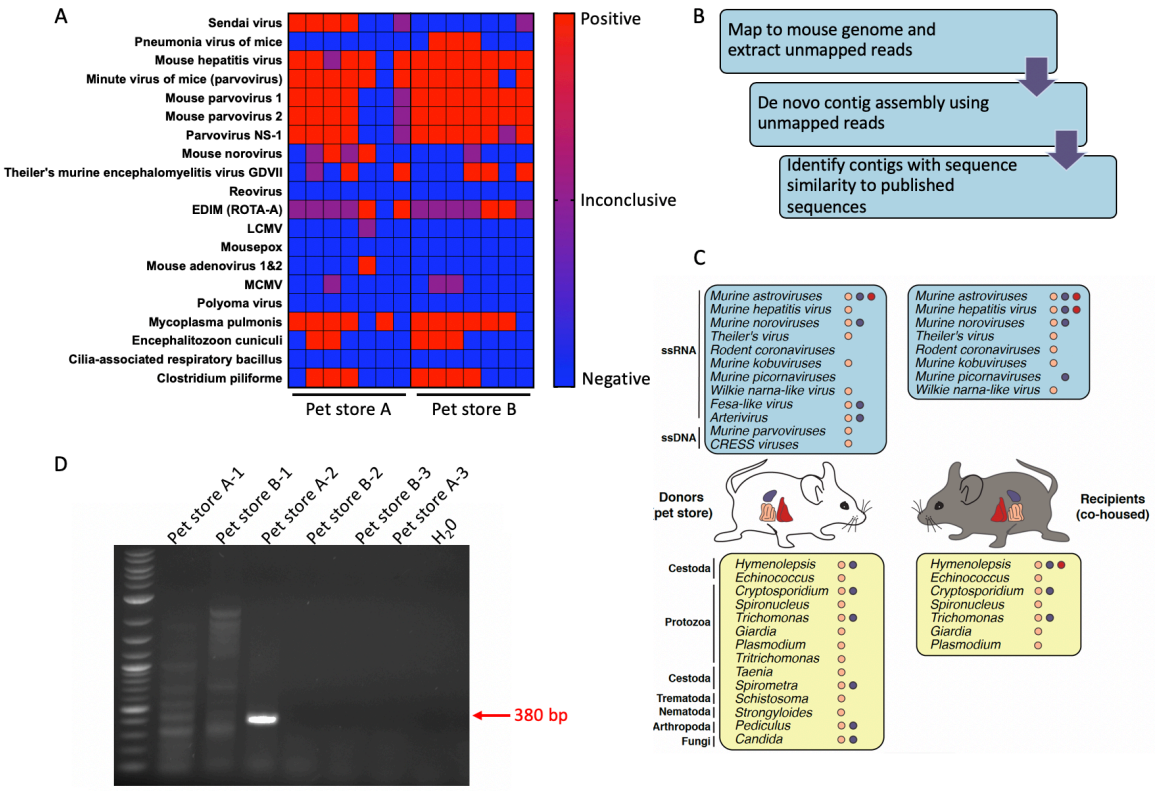


**Figure 4-2.** Identification of pathogens in pet store and co-housed SPF mice. (A) Serum from mice from pet store A and pet store B was tested for antibodies against the indicated pathogens. Columns are individual mice. (B) Pipeline for identifying pathogen reads from total polyadenylated RNA sequencing data. (C) Summary of pathogens identified in pet store mice (left) and in co-housed mice (right) that do not appear in non-co-housed SPF mice. Colored circles indicate tissue. Includes cages with only some SPF strains. (D) Small intestine RNA from pet store mice shown in figure 4-1 was screened by RT-PCR for LCMV.

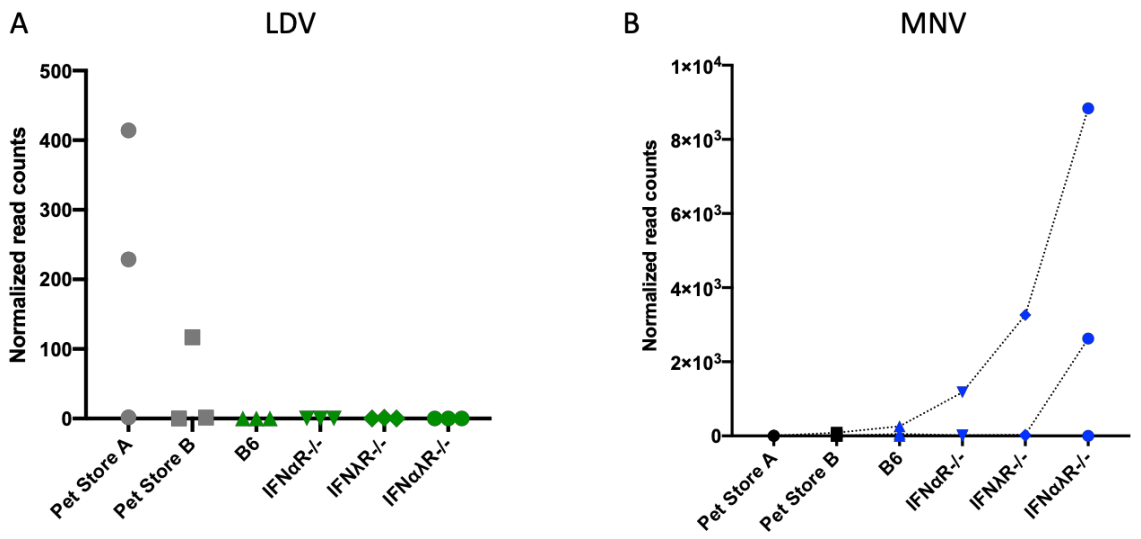


**Figure 4-3.** Viruses with unique transmission patterns. Pooled spleen/lymph node (A) or small intestine (B) RNA was sequenced as in figure 4-2. (A) Normalized reads mapping to lactate dehydrogenase-elevating virus in the indicated mouse. (B) Normalized reads mapping to murine norovirus in the indicated mouse. Dotted line connects mice from the same co-housed cage.

### *Co-transmission analysis identifies a novel alveolate virus*

In addition to identifying viruses, we identified several other parasites present in the intestines of pet store mice that transmitted to co-housed mice. We were able to assess co-transmission of pathogens (Figure 4-4A). This identified a strong correlation between *Cryptosporidium* spp. and a set of viral reads similar to Wilkie narna-like and Matryoshka RNA viruses (Figure 4-4B). Matryoshka viruses were identified in *Plasmodium* and *Leucocytozoon* species and were so named because they are viruses that infect a parasite that infects an animal, analogous to the Russian nesting dolls (201). Similarly, Wilkie narna-like virus (WNLV) was identified in mosquitos but likely infects fungi that infect mosquitos (202). Protozoan *Cryptosporidium* are obligate gastrointestinal parasites that can cause gastroenteritis in many vertebrate species including humans, particularly among

immunocompromised hosts (203, 204). The reads identified in our samples mapped to the WNLV RdRp, and phylogenetic analysis suggests a novel narnavirus (Figure 4-4C). This novel virus likely infects *Cryptosporidium* within our mice. Ongoing analyses will explore additional transmission correlations.

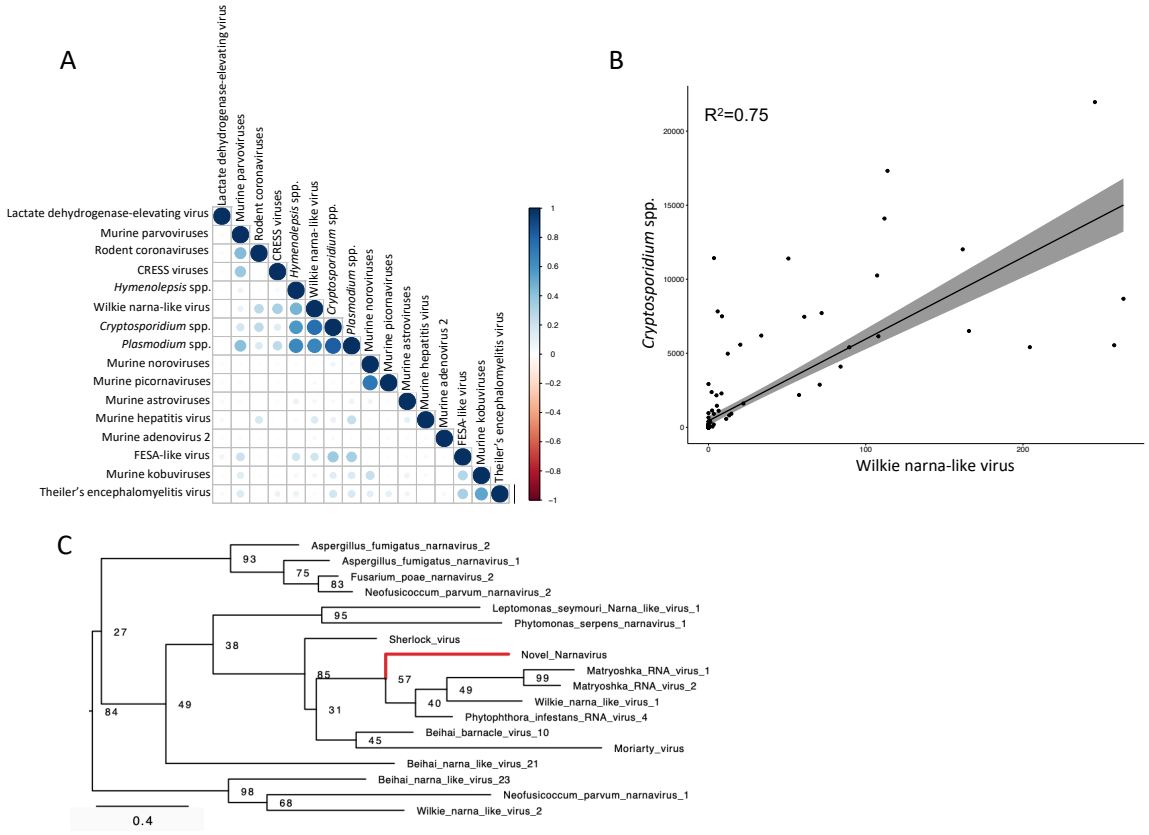


**Figure 4-4.** Co-transmission analysis identifies a novel alveolate virus. (A) Transmission correlation heat map. Includes cages with only some SPF strains. (B) Correlation as in (A) for reads mapping to Cryptosporidium species and WNLV. (C) Reads mapping to WNLV virus RdRp were assembled and translated. Similar proteins were identified using NCBI BLASTp and were used to build a maximum likelihood phylogenetic tree. The scale bar represents units of substitution per site. Bootstrap support values are shown at nodes.

### *Amplicon-based approach to quantify virus variants*

While we identified many murine viruses transmitting from pet store mice to SPF mice, we selected three viruses for variant analysis. Murine astrovirus-2 (MAst-2) was identified in all three cages and readily transmitted to co-housed mice (Figure 4-5A). In cages where it was present, murine hepatitis virus (MHV) was the most abundant virus in the mice, accounting for up to 7% of total reads in some small intestine samples (Figure 4-6A, bottom). Reads mapping to murine kobuvirus (MKobu) were much lower. However, using pan-kobuvirus primers specific for the conserved RdRP, we were able to amplify kobuvirus RNA from samples with very low MKobu read counts in the deep sequencing data (Table 4-2).

We performed preliminary variant analysis for reads mapping to MAst-2 because we achieved near-complete sequence coverage in many of our tissue samples (Figure 4-5B). We specifically analyzed contigs mapping to the virus RdRp and the capsid. We found little derivation from the published sequence for reads mapping to the RdRP, and the variant per 100 base pairs does not increase following transmission or dissemination (Figure 4-5C, left). The number of variants per 100 base pairs is much higher in reads mapping to the capsid sequence, and we overall see more contigs with greater variance following transmission and dissemination (Figure 4-5C, right). These data suggest that the capsid region of the MASt-2 genome is more plastic than the RdRP, and that there may be changes in the virus population during transmission and dissemination. While we obtained lower coverage of the MHV genome in some samples (Figure 4-6B), we were able

to perform variant analysis on the MHV RdRp and the surface spike glycoprotein. Similar to MAst-2, contigs mapping to the spike gene contain more variants per 100 base pairs than contigs mapping to the RdRp (Figure 4-6C).

Using mRNA-seq, we were able to identify reads mapping to known viruses. However, we did not achieve sufficient depth to quantify virus variants and bottlenecks during transmission and dissemination. Additionally, variability in gene sequences between samples could be due to sequencing error rather than biological variance, and technical replicates are needed to verify results. We therefore designed primers to amplify 200-600 bp regions of the RdRp and the spike glycoprotein (MHV) or capsid (MAst-2 and MKobu) gene for each virus. Amplicons will be generated in duplicate and deep sequenced with a minimum of 400 reads per site, as described previously (197). The consensus sequence of the amplified region in the pet store small intestine (SI), co-housed SI, and co-housed liver will be determined and compared between animals within a single cage. Additionally, variant analysis will be performed to identify bottlenecks and/or adaptive changes that occurred during transmission (pet store SI to co-housed SI) and dissemination (co-housed SI to co-house liver). Variants will be called at a 3% frequency minimum across replicates. Analyses will be performed using the iVar software package (197).

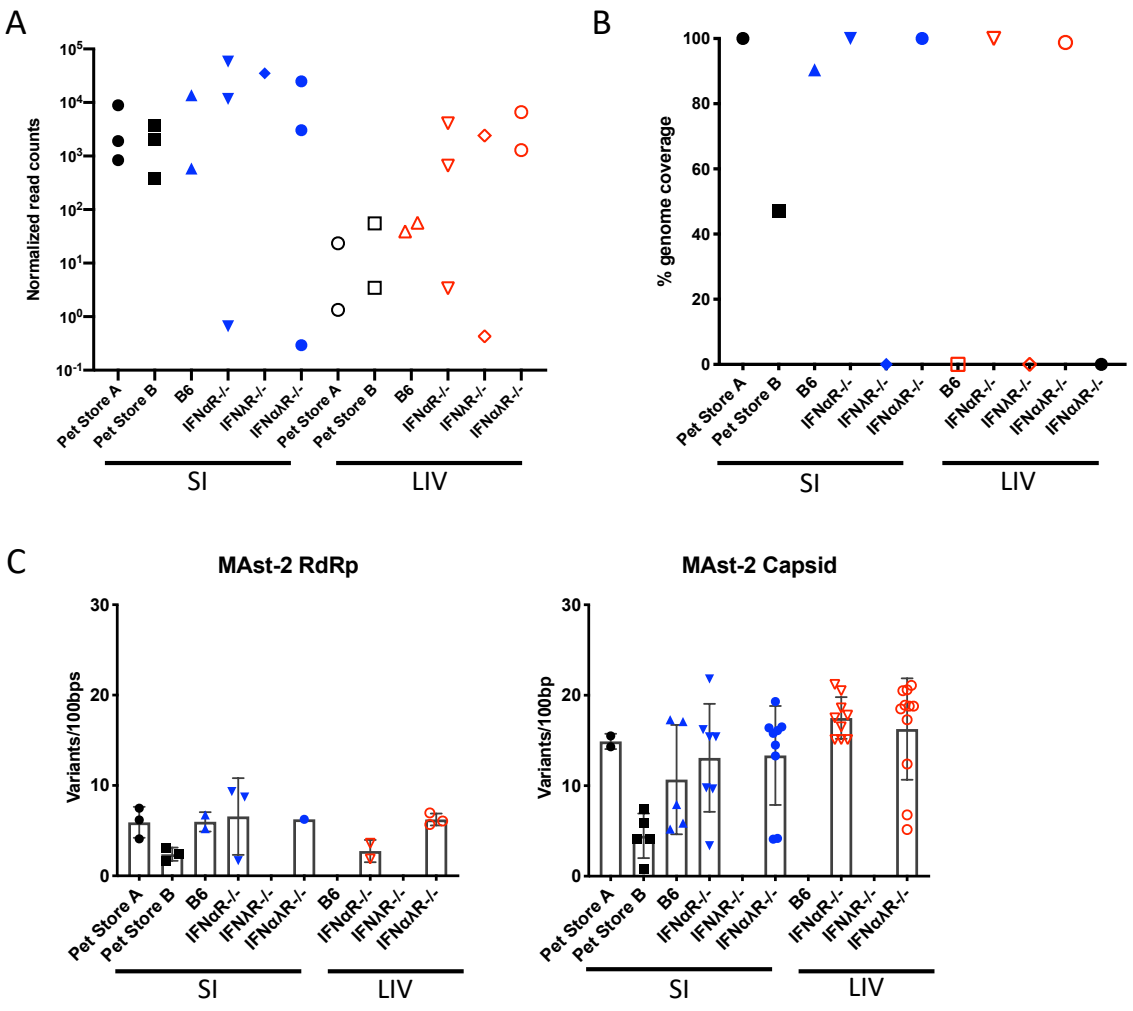


**Figure 4-5.** Murine astrovirus-2 readily transmits to and disseminates in co-housed mice. (A) Normalized reads mapping to the MAst-2 genome in the indicated tissue in the indicated mouse. (B) Coverage of MAst-2 genome in a single cage. (C) Reads mapping to the MAst-2 RdRp (left; contig length 255-1551 nt) or capsid (right; contig length 202-2500 nt) in the indicated tissues of mice in a single cage were analyzed for similarity to the published sequence.

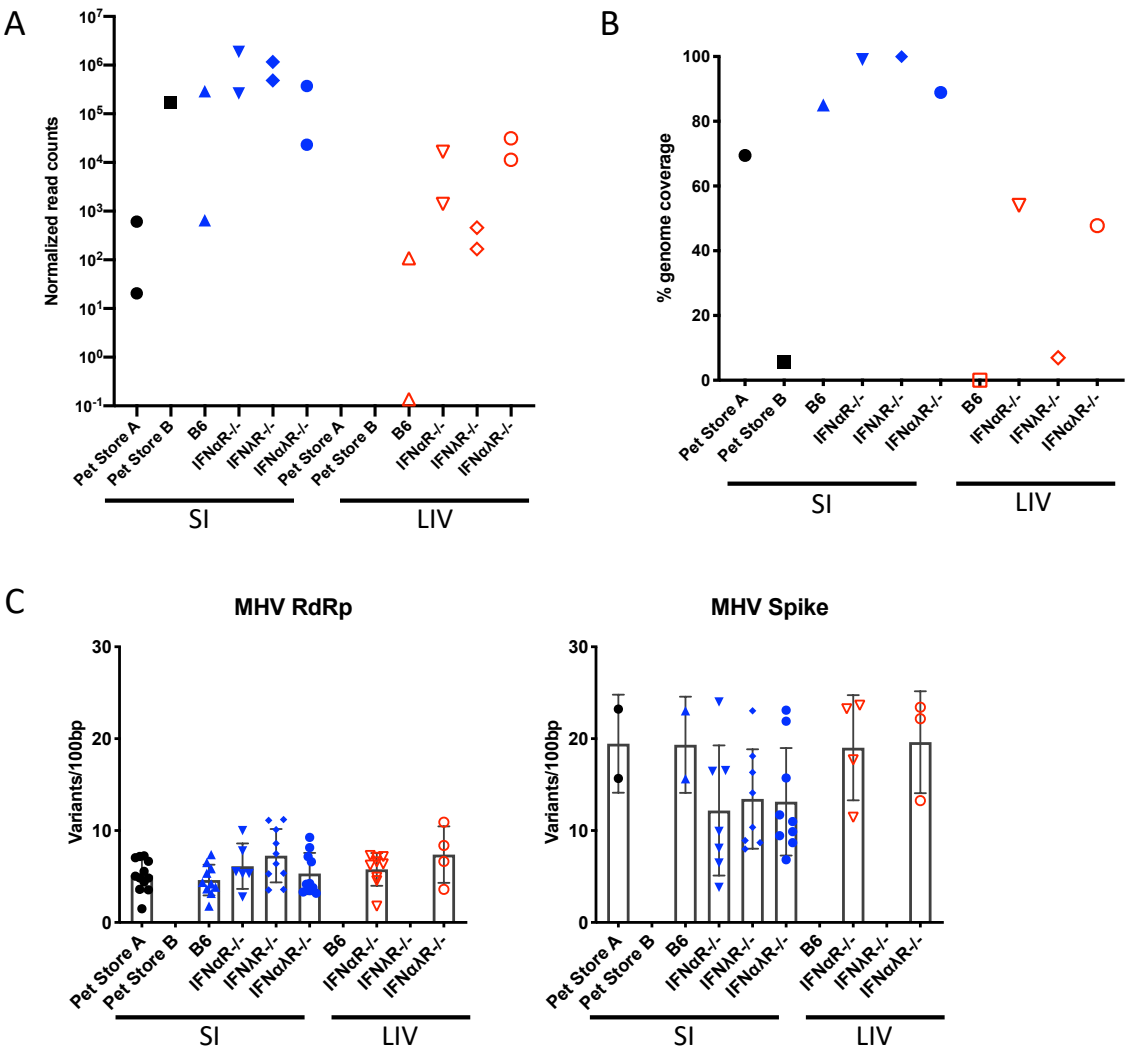


**Figure 4-6.** Murine hepatitis virus readily transmits to and disseminates in co-housed mice. (A) Normalized reads mapping to the MHV genome in the indicated tissue in the indicated mouse. (B) Coverage of MHV genome in a single cage. (C) Reads mapping to the MHV RdRp (left; contig length 204-18,142 nt) or spike glycoprotein (right; contig length 253-2353 nt) in the indicated tissues of mice in a single cage were analyzed for similarity to the published sequence.

**Table 4-2.** Kobuvirus identified by RT-PCR. + or – denotes positive or negative screen (see Table 4-1 for primer information). +/- denotes inconclusive screening results.

| Mouse | Tissue | 3D (RdRp) amplicon | MKobu mRNA-seq reads |
|---|---|---|---|
| B6-cohoused | SI | + | 0 |
| IFNAR KO-cohoused | SI | + | 222 |
| IFNLR KO-cohoused | SI | + | 1115 |
| IFNLAR KO-cohoused | SI | + | 280 |
| Pet A | SI | + | 22 |
| Pet B | SI | + | 9 |
| B6-cohoused | SI | + | 63 |
| IFNAR KO-cohoused | SI | +/- | 11 |
| IFNLR KO-cohoused | SI | + | 5 |
| IFNLAR KO-cohoused | SI | + | 75 |
| Pet A | SI | - | 15 |
| Pet B | SI | + | 3 |
| B6-cohoused | SI | - | 0 |
| IFNAR KO-cohoused | SI | - | 5 |
| IFNLR KO-cohoused | SI | - | 28 |
| IFNLAR KO-cohoused | SI | - | 8 |
| Pet B | SI | + | 63 |
| Pet A | SI | - | 21 |

### *Identifying species barriers to transmission using rat fomites*

In order to infect and replicate within a new species, a virus needs to both evade the new host immune system and use key host proteins for replication, such as entry and protein synthesis machinery. To extend the use of our model system to include identification of these immune and non-immune species barriers to cross-species transmission, we obtained two rats (*Rattus norvegicus*) from different pet stores and co-housed them together. We transferred bedding—including fecal matter—daily from rat cages to cages of our SPF B6 and IFN$\alpha\lambda$R$^{-/-}$ mice for 7 days (Figure 4-7A-B). Additionally, we homogenized fresh fecal pellets from each rat in PBS and delivered 200µL to each mouse via oral gavage daily. After 7 days, we sacrificed both the rats and the mice for deep sequencing of the SI and liver. We also transferred bedding and delivered oral gavage to a cage of

SPF IFNαλR$^{-/-}$ mice for 5 days, then transferred the mice to a new cage and added SPF B6 mice (Figure 4-7C-D). After an additional 7 days, we sacrificed mice for deep sequencing the SI and liver. In this model, any pathogen from the rats first needs to overcome non-immune species barriers to replicate in the IFNαλR$^{-/-}$ mice and would then need to adapt immune evasion strategies to replicate in the B6 mice. Sequencing and analysis are ongoing, however SPF mice lost weight during bedding transfer (Figure 4-7B/D). Overall, this model will allow us to identify patterns of virus adaptations that allow for cross-species transmission.

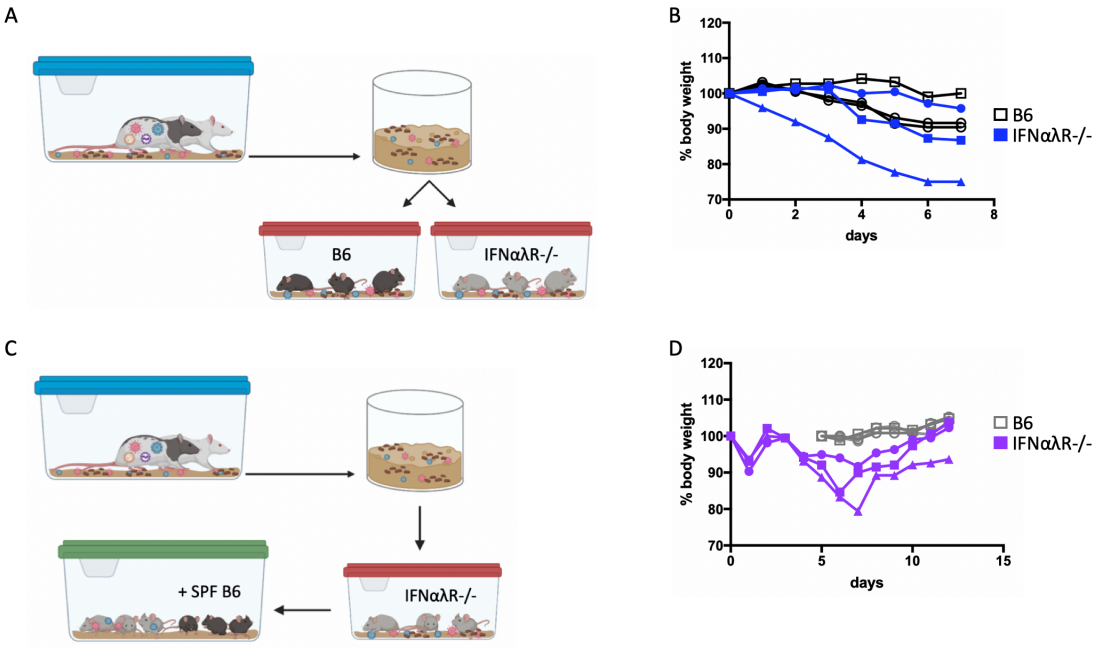


**Figure 4-7.** Pet store rats to characterize cross-species transmission of pathogens. (A) Bedding from the pet store rat cage was transferred to cages of SPF B6 or IFNαλR$^{-/-}$ mice daily for 7 days. After 7 days, rats and mice were sacrificed for virome analysis. (B) Weight loss of mice in (A). (C) Bedding from the pet store rat cage was transferred to a cage of IFNαλR$^{-/-}$ mice daily for 5 days. After 5 days, the IFNαλR$^{-/-}$ mice were moved to a fresh cage with SPF B6 mice. After an additional 7 days, mice were sacrificed for virome analysis. (D) weight loss of mice in (C).

## ONGOING ANALYSES AND FUTURE DIRECTIONS

In addition to amplicon sequencing and analysis of cross-species transmission using pet store rats, we are also performing 16s sequencing on small and large intestine contents for all experiments. These data will add depth to our co-transmission analysis. Bacteria are known to stabilize some picornaviruses, and the intestinal microbiota enhances infection of an array of enteric viruses (205-207). To further examine the relationship between bacterial and viral transmission, we co-housed SPF B6 and IFN$\alpha$R$^{-/-}$ mice with pet store mice that have been given antibiotics via oral gavage (Figure 4-8A). After 5 days, we sacrificed mice for virome sequencing. While we saw more robust MAst-2 transmission to IFN$\alpha$R$^{-/-}$ mice from antibiotic-treated pet store mice (Figure 4-8B), we are currently validating depletion of intestinal bacteria in our pet store mice. We will perform additional replicates and include all strains of SPF mice to validate these results. In addition to analyzing bacterial reads in intestinal contents, we will also sequence the total RNA in the intestinal contents. This will identify viruses and other pathogens that transmit to co-housed mice but are unable to infect/replicate in the new host. This will be especially critical for cross-species experiments, as it could reveal pathogens that are unable to overcome species barriers to infection.

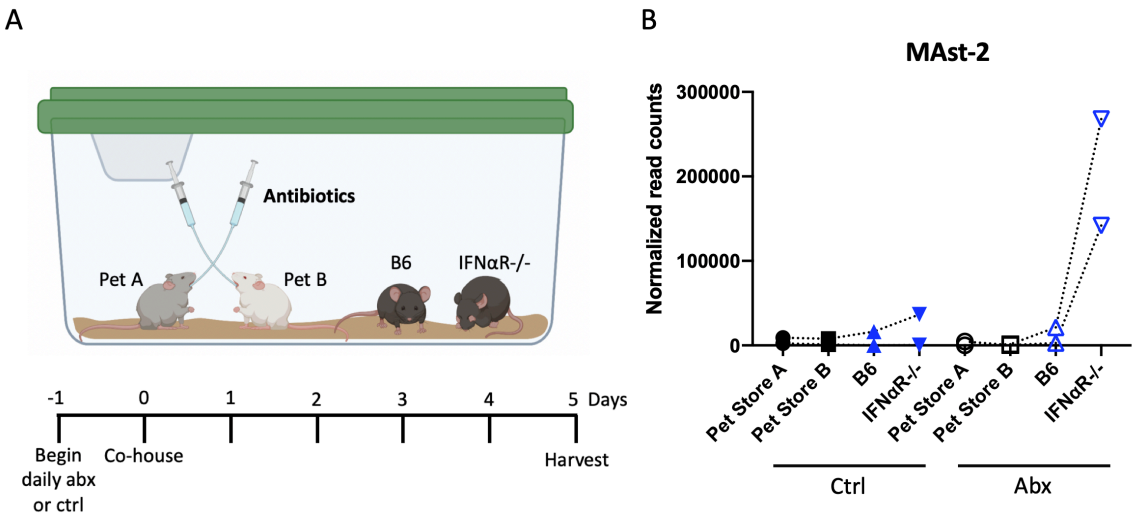


**Figure 4-8.** Antibiotic treatment to analyze the role of intestinal bacteria in virus transmission. (A) Model and timeline for antibiotic treatment. (B) Normalized reads mapping to MAst-2 in the small intestine of indicated mice from cages with control (left) or antibiotic treated (right) pet store mice. Dotted lines connect mice from individual cages.

## DISCUSSION

Zoonotic pathogens are a serious public health concern. Understanding the adaptive changes that allow for species jump into humans is paramount to predicting and responding to emerging viruses. A key step to identifying viruses that have the potential to transmit to humans is comprehensive virome profiling of species that live in close contact with humans, including rodent species. Another approach to analyze pathogen transmission is to through 'rewilded' laboratory mice, or mice released into semi-secure outdoor environments (208, 209). While pathogens do transmit to the mice, there have not been robust virus infections in this model. Additionally, in these models, only the current host of the virus is known; it is not known where these pathogens originated or what changes occurred to allow them to replicate in mice. In our experimental system, we

uniquely have access to both the original reservoir and the new host. Through available knockout mice, we are also able to analyze the critical role of innate immune proteins in transmission and spread in a new host. This model can be extended to characterize the role of additional proteins such as pattern recognition receptors that detect virus infections and key signaling proteins that amplify the response. Additionally, we can use different hosts as sources for pathogens, including using other species of rodents. The species used in the model system described here—*Mus musculus* and *Rattus norvegicus*—are estimated to have diverged 10-12 million years ago (mya) (210, 211). We may see differences in pathogen transmission when the host is more (*e.g.* deer mice, *Peromyscus maniculatus*, ~25 mya (210)) or less (*e.g. Mus* subgenus *Nannomys*, ~7 mya (212)) diverged. Wild-caught mice show similar immune activation compared to pet store mice (188), but potentially have been exposed to unique pathogens. Co-housing laboratory mice with wild mice would therefore expand our system to include additional murine pathogens.

While our model is currently limited to rodent pathogens, the virus families we identified have human species that are significant public health concerns. Human astroviruses have only recently been appreciated as a leading cause of viral gastroenteritis worldwide. Astrovirus strains have been identified in many species, and there is evidence of interspecies transmission (213). MHV is the longstanding model of coronavirus infections and has produced much of our knowledge of basic coronavirus biology (214). Aichi virus—human kobuvirus—infections cause gastroenteritis, nausea, and fever, and 80-95% of adults

worldwide have antibodies against Aichi virus (198). Severe disease and death can occur in young children, particularly in developing countries (215). Many picornaviruses are well-studied, however the unique capsid structure of kobuviruses could result in distinct mechanisms of virus entry and genome release (216, 217). Kobuviruses have been identified in many animal species, and cross-species transmission likely exists (198, 215). There is no animal model, and isolation and characterization of a murine kobuvirus will offer important insight into kobuvirus pathogenesis.

Here, we describe the dirty mouse model as a platform for analyzing transmission of pathogens within and between species. We have identified pathogens that readily transmit from pet store mice to co-housed laboratory mice. Through amplicon sequencing, we will identify changes in populations of virus species that occur during transmission and dissemination and the role of IFN during these processes. Additionally, using pet store rats, we will identify and characterize cross-species transmission events. This model can be expanded to analyze the role of additional host factors in transmission. Overall, this experimental system will provide insight into mechanisms of zoonosis and pathogen emergence.

## FOOTNOTES

[1]Additional contributions: E.J. Fay performed mouse and rat experiments. K.M. Balla performed virome analyses. E.J. Fay performed mutation analysis. E.J. Fay, D. Putri, and A. Tucker generated amplicons. M. Pierson and D. Masopust support and maintain the dirty mouse facility. E.J. Fay, K.M. Balla, N.C. Elde, and R.A. Langlois conceived and designed experiments and analyses.

[2]Abbreviations used this chapter: abx, antibiotics; APOBEC3, apolipoprotein B mRNA editing enzyme, catalytic polypeptide-like 3H; FESA, feline stool-associated; HIV, human immunodeficiency virus; IFN, interferon; IFN$\alpha$R, IFN-$\alpha$ receptor; IFN$\lambda$R, IFN-$\lambda$ receptor; LCMV, lymphocytic choriomeningitis virus; LDV, lactate dehydrogenase elevating virus; LIV, liver; MAst-2, murine astrovirus 2; MHV, murine hepatitis virus; MKobu, murine kobuvirus; MNV, murine norovirus; RdRp, RNA-dependent RNA polymerase; SI, small intestine; SIV, simian immunodeficiency virus; SPF, specific pathogen-free; WNLV, Wilkie narna-like virus

# CHAPTER 5: Innate immunity, emerging viruses, and pandemic preparedness.

## CONCLUSIONS

Predicting which viruses have pandemic potential in humans is extremely difficult. It requires both extensive screening of animal populations to track viromes and an in-depth understanding of virus and host factors that allow a virus to replicate in a given host. My thesis work has—to some degree—addressed both of these concerns. In Chapters 2 and 3, I described studies that have elucidated mechanisms of resistance or susceptibility to influenza infection using single-cycle influenza A viruses (scIAVs). This work revealed distinct antiviral signatures associated with the magnitude of scIAV replication, the stage of replication, and the cell type infected in a mouse model. In Chapter 4, I introduced a new model for assessing intra- and inter-species barriers to virus transmission. This model provides a platform for identifying and characterizing innate immune barriers to virus transmission. Here, I discuss the broad implications of my thesis work.

### *Replication and response heterogeneity during early IAV infection*

Replication heterogeneity observed during early IAV infection is likely due to both virus and host factors and is both a cause and effect of the antiviral response heterogeneity. The ability to identify cells that are resistant to IAV infection could reveal novel IAV restriction factors. *Helz2* was consistently upregulated in cells with low IAV infection (Figure 3-1E) but has no defined antiviral activity against IAV. Additionally, we found that cells with high levels of IAV

replication upregulate inflammatory cytokines and upregulate apoptosis-associate genes as early as 12 hpi (Figures 2-5G and 3-1E). These data suggest that only a subset of infected cells contribute to severe immunopathology. Further defining virus and host factors that contribute to this phenotype could reveal novel therapeutic targets to treat severe IAV infections.

With the advancement of deep sequencing technologies—particularly the development of single-cell sequencing—many groups have identified heterogeneity in the antiviral response within an infected cell population. This is at least partially a result of heterogeneity in a virus population; for example, during IAV infection, cells infected with viruses lacking the immune antagonist gene NS1 were the primary inducers of interferon (IFN) (63). Similarly, both magnitude of IAV replication and the abundance of defective viral genomes contribute to the immune response *in vitro* (161). Virus differences do not always account for immune differences, as was found during West Nile virus infection (64). Using a combination of chromatin immunoprecipitation with sequencing (ChIP-seq), bulk RNA-seq, and single cell RNA-seq (scRNA-seq), it was found that innate immune genes such as cytokines and chemokines that display high cell-to-cell variability in their expression are also genes that are highly divergent across species (218). In contrast, regulatory genes are both more conserved evolutionarily and less variable between responding cells in a population. These data suggest that immune response heterogeneity will always be observed between cells during infection, independent of viral factors.

***Cell type-specific innate immune responses to IAV***

The epithelial cell types analyzed in Chapters 2 and 3 all have critical functions in the lung: type I alveolar (ATI) cells are the site of gas exchange (167), type II alveolar (ATII) cells secrete surfactant to maintain pulmonary compliance (167), and ciliated cells produce mucus and help expel pathogens from the lung (219). The differential immune responses we uncovered between these cell types are likely both a cause and effect of their functions. Basal differences in the cell biology likely contribute to differential ability to respond, and the responses may have evolved to maintain the important functions of each cell type during IAV infection.

We uncovered basal differential expression of immune signaling genes between ATI, ATII, and ciliated cells (Figure 3-8C). However, this only partially explains differences in the response to scIAVs. The efficiency of entry and early trafficking to the nucleus could affect the early replication and resulting response. This could be why ciliated cells display higher levels of IAV mRNA following ΔPB1 infection (Figure 3-9B) and more robust IFN-stimulated gene (ISG) activation following infection with either scIAV (Figure 3-9C). IAV relies on the microtubule network for intracellular trafficking, and IAV entry requires reorganization of the cytoskeletal network (220). Ciliary beating—the mechanism by which ciliated cells expel pathogens—requires careful organization of microtubule architecture (221). This results in a unique cytoskeletal network compared to other epithelial cell types, and this difference may drive in early differences in scIAV entry, trafficking, and replication in ciliated cells.

The rapid induction of ISGs in ciliated cells could also explain their unique protection against 'secondary' infection (*i.e.* virus spread; Figure 2-7), particularly because of the upregulation of *Ifitm3*. IFITM3 inhibits early stages of IAV infection, including entry and uncoating (25, 26). Ciliated cells may be poised to respond to IFN stimulation and rapidly upregulate potent antiviral genes as a way to preserve mucociliary clearance during infection. Epigenetic modifications are known to modulate the immune response to virus infections (175). Differences in the epigenetic landscape of naïve epithelial cell types could lead to differential accessibility for virus-activated transcription factors and ultimately differences in gene expression during early infection.

Some cell type-specific ISGs upregulated during ΔHA-Cre infection regulate or perform metabolic functions (*e.g.* ATI: *Ddit4*, *Fut4*; ATII: *B4gal5*, *Pfkfb3*; ciliated cells: *Cyp1b1*, *Hk2*; Table 3-5). Signaling through IFN receptors can activate kinases other than classical JAKs, including PI3K (222). A major target of PI3K is mTOR, a master regulator of cell metabolism, growth, and survival (223). PI3K activation has been described during IAV infection, both as a result of binding/entry and via IAV NS1 (224). Activation of PI3K during IAV infection could have many functional outcomes due to the varied outputs of PI3K activity between cell types, either due to expression or activation differences for PI3K and its signaling partners. Differences in naïve cell metabolic states could result in IFN-dependent, JAK-independent differential gene expression.

Some components of the IFN response can be toxic to cells. OAS family proteins—which sense and initiate degradation of dsRNA through RNase L—can

sense and induce destruction of cellular RNAs (93, 225). PKR activity inhibits protein synthesis and can induce cell death during virus infection (226, 227). For this reason, IFN signaling and antiviral gene activity are tightly regulated. While the evolutionary loss of some innate immune genes has been described between species, there could also be evolutionary mechanisms to prevent expression of certain genes in a cell type-specific manner within an organism. PKR, OAS2, and OAS3 are all upregulated by ΔHA-Cre in a cell type-specific manner (ATII only, ciliated cells only, and ATI and ciliated cells, respectively, Table 3-5). Different cell types may be more susceptible to the deleterious effects of these or other antiviral proteins, leading to mechanisms of repression. Stem cells do not respond to IFN, and this is at least partially due to inaccessible ISREs (72, 74, 228). Similar restrictions could limit antiviral gene expression in a cell type-specific manner.

***Virus adaptations during transmission and dissemination***

While huge numbers of virions can be produced within an infected host, relatively few transmit/disseminate to a new site of infection (181). This creates a genetic bottleneck where the genetic diversity within the original reservoir is reduced to few variants in the new host. Such bottlenecks could be viewed as evolutionarily disadvantageous, as random transmission would bypass natural selection. However, some variants may be poised for more efficient dissemination/transmission, and this would remove deleterious mutations from the population in the new site of infection. The presence of certain traits within a virus population, such as the ability to induce IFN production, can have a profound

impact on the rest of the virus population and could ultimately affect spread (229). The experimental system described in Chapter 4 could help identify variant patterns associated with transmission and dissemination, as well as the susceptibility of such variants to IFN.

For viruses that can replicate in more than one tissue, adaptations may be necessary for dissemination. Measles virus first replicates in lymphatic tissues then spreads to epithelial tissues; this dissemination is associated with adaptations in the virus phosphoprotein and changes in virus gene expression levels, primarily expression of an IFN antagonist protein (230). For many viruses broadened tissue tropism is associated with more severe disease, including during IAV infections (231, 232). Characterizing virus adaptations that allow for dissemination within a host can help identify factors associated with severe pathogenesis. Additionally, the efficacy of antiviral drugs may vary depending on tissue tropism; identifying tissue-specific virus adaptations could identify novel therapeutic targets for severe virus infections.

Many predictions of viruses with pandemic potential rely on computational analyses applied to empirical data. Such analyses must take into account both virus and host traits that could impact spread. While many factors contribute to IAV zoonosis, there are several host factors that establish species specificity of IAV, including surface sialic acids and the nuclear protein ANP32A (233). Similarly, there are known variants in IAV genes that allow for spread between avian and mammalian hosts (233). These patterns of adaptations that contribute to zoonosis likely exist for other viruses and could be identified through comprehensive

profiling of viromes within different species. It is important to not just predict which viruses can jump to humans, but also which viruses could cause severe pathology in humans. Using data on known human viruses, virus family and primary tissue tropism are the strongest predictors of virulence (234). Furthermore, higher disease mortality is associated with greater evolutionary distance between hosts (235). The expansion of the model described in Chapter 4 to include additional hosts could reveal additional factors that contribute to pathogenesis. Additional factors, such as global distribution and virus richness within a species, can also impact zoonotic potential (236). There are many complex interacting factors that permit or prohibit zoonosis, and a deeper understanding of any of these mechanisms will aid in pandemic predictions and preparedness. Ultimately, understanding both the virus and host factors that contribute to cross-species transmission will improve our ability to identify viruses in zoonotic reservoirs that could spread to humans.

**FOOTNOTES**

[1]Abbreviations used this chapter: ANP32A, acidic nuclear phosphoprotein 32 family member A; ATI, type I alveolar; ATII, type II alveolar; IAV, influenza A virus; IFITM3, IFN-induced transmembrane protein 3; IFN, interferon; ISG, IFN-stimulated gene; ISRE, IFN-stimulated response element; JAK, Janus kinase; mTOR, mammalian target of rapamycin; NS1, nonstructural 1; OAS, oligoadenylate synthetase; PB1, polymerase basic 1; PI3K, phosphoinositide 3-kinase; PKR, protein kinase R; scIAV, single-cycle IAV

## REFERENCES


1. Simmonds P, Adams MJ, Benkő M, Breitbart M, Brister JR, Carstens EB, Davison AJ, Delwart E, Gorbalenya AE, Harrach B, Hull R, King AMQ, Koonin EV, Krupovic M, Kuhn JH, Lefkowitz EJ, Nibert ML, Orton R, Roossinck MJ, Sabanadzovic S, Sullivan MB, Suttle CA, Tesh RB, Vlugt RAvd, Varsani A, Zerbini FM. 2017. Virus taxonomy in the age of metagenomics. Nature Reviews Microbiology 15:161-168.
2. Carroll D, Daszak P, Wolfe ND, Gao GF, Morel CM, Morzaria S, Pablos-Méndez A, Tomori O, Mazet JAK. 2018. The Global Virome Project. Science 359:872-168.
3. Taubenberger JK, Kash JC, Morens DM. 2019. The 1918 influenza pandemic: 100 years of questions answered and unanswered. Science Translational Medicine 11:eaau5485.
4. Rehwinkel J, Gack MU. 2020. RIG-I-like receptors: their regulation and roles in RNA sensing. Nature Reviews Immunology:1-15.
5. Ma Z, Ni G, Damania B. 2018. Innate Sensing of DNA Virus Genomes. Annual Review of Virology 5:341-362.
6. Streicher F, Jouvenet N. 2019. Stimulation of Innate Immunity by Host and Viral RNAs. Trends in Immunology 40:1134-1148.
7. Baum A, Sachidanandam R, García-Sastre A. 2010. Preference of RIG-I for short viral RNA molecules in infected cells revealed by next-generation sequencing. Proc Natl Acad Sci USA 107:16303-16308.
8. Tapia K, Kim W, Sun Y, Mercado-López X, Dunay E, Wise M, Adu M, López C. 2013. Defective Viral Genomes Arising In Vivo Provide Critical Danger Signals for the Triggering of Lung Antiviral Immunity. PLoS Pathogens 9:e1003703.
9. Mura M, Combredet C, Najburg V, David RYS, Tangy F, Komarova AV. 2017. Nonencapsidated 5′ Copy-Back Defective Interfering Genomes Produced by Recombinant Measles Viruses Are Recognized by RIG-I and LGP2 but Not MDA5. J Virol 91:e00643-17.
10. Hoffmann HH, Schneider WM, Rice CM. 2015. Interferons and viruses: an evolutionary arms race of molecular interactions. Trends in Immunology 36:124-38.
11. Platanitis E, Demiroz D, Schneller A, Fischer K, Capelle C, Hartl M, Gossenreiter T, Müller M, Novatchkova M, Decker T. 2019. A molecular switch from STAT2-IRF9 to ISGF3 underlies interferon-induced gene transcription. Nature Communications 10:1-17.
12. Yamagami M, Otsuka M, Kishikawa T, Sekiba K, Seimiya T, Tanaka E, Suzuki T, Ishibashi R, Ohno M, Koike K. 2018. ISGF3 with reduced phosphorylation is associated with constitutive expression of interferon-induced genes in aging cells. npj Aging and Mechanisms of Disease 4:1-10.
13. Lazear H, Nice T, Diamond M. 2015. Interferon-λ: Immune function at barrier surfaces and beyond. Immunity 23:15-28.
14. Kotenko SV, Durbin JE. 2017. Contribution of type III interferons to antiviral immunity: location, location, location. J Biol Chem 292:7295-7303.

15. Marcello T, Grakoui A, Barba-Spaeth G, Machlin E, Kotenko S, MacDonald M, Rice C. 2006. Interferons alpha and lambda inhibit hepatitis C virus replication with distinct signal transduction and gene regulation kinetics. Gastroenterology 131:1887-1898.
16. Forero A, Ozarkar S, Li H, Lee C, Hemann E, Nadjsombati M, Hendricks M, So L, Green R, Roy C, Sarkar S, von Moltke J, Anderson S, Gale MJ, Savan R. 2020. Differential Activation of the Transcription Factor IRF1 Underlies the Distinct Immune Responses Elicited by Type I and Type III Interferons. Immunity 51:451-464.
17. Österlund PI, Pietilä TE, Veckman V, Kotenko SV, Julkunen I. 2007. IFN Regulatory Factor Family Members Differentially Regulate the Expression of Type III IFN (IFN-λ) Genes. J Immunol 179:3434-3442.
18. Jewell NA, Cline T, Mertz SE, Smirnov SV, Flaño E, Schindler C, Grieves JL, Durbin RK, Kotenko SV, Durbin JE. 2010. Lambda Interferon Is the Predominant Interferon Induced by Influenza A Virus Infection In Vivo. J Virol 84:11515-11522.
19. Nice TJ, Baldridge MT, McCune BT, Norman JM, Lazear HM, Artyomov M, Diamond MS, Virgin HW. 2015. Interferon-λ cures persistent murine norovirus infection in the absence of adaptive immunity. Science 347:269-273.
20. Davidson S, McCabe TM, Crotta S, Gad HH, Hessel EM, Beinke S, Hartmann R, Wack A. 2016. IFNλ is a potent anti-influenza therapeutic without the inflammatory side effects of IFNα treatment. EMBO Molecular Medicine 8:1099-1112.
21. Galani IE, Triantafyllia V, Eleminiadou EE, Koltsida O, Stavropoulos A, Manioudaki M, Thanos D, Doyle SE, Kotenko SV, Thanopoulou K, Andreakos E. 2017. Interferon-λ Mediates Non-redundant Front-Line Antiviral Protection against Influenza Virus Infection without Compromising Host Fitness. Immunity 46:875-890.e6.
22. Shaw AE, Hughes J, Gu Q, Behdenna A, Singer JB, Dennis T, Orton RJ, Varela M, Gifford RJ, Wilson SJ, Palmarini M. 2017. Fundamental properties of the mammalian innate immune system revealed by multispecies comparison of type I interferon responses. PLoS Biology 15:e2004086.
23. Schoggins JW, Wilson SJ, Panis M, Murphy MY, Jones CT, Bieniasz P, Rice CM. 2011. A diverse range of gene products are effectors of the type I interferon antiviral response. Nature 472:481-485.
24. Schoggins JW, MacDuff DA, Imanaka N, Gainey MD, Shrestha B, Eitson JL, Mar KB, Richardson RB, Ratushny AV, Litvak V, Dabelic R, Manicassamy B, Aitchison JD, Aderem A, Elliott RM, Garcia-Sastre A, Racaniello V, Snijder EJ, Yokoyama WM, Diamond MS, Virgin HW, Rice CM. 2014. Pan-viral specificity of IFN-induced genes reveals new roles for cGAS in innate immunity. Nature 505:691-5.
25. Feeley EM, Sims JS, John SP, Chin CR, Pertel T, Chen L-M, Gaiha GD, Ryan BJ, Donis RO, Elledge SJ, Brass AL. 2011. IFITM3 Inhibits Influenza A Virus Infection by Preventing Cytosolic Entry. PLoS Pathogens 7:e1002337.

26. Desai TM, Marin M, Chin CR, Savidis G, Brass AL, Melikyan GB. 2014. IFITM3 Restricts Influenza A Virus Entry by Blocking the Formation of Fusion Pores following Virus-Endosome Hemifusion. PLoS Pathogens 10:e1004048.
27. Lu Y, Wambach M, Katze M, RM K. 1995. Binding of the influenza virus NS1 protein to double-stranded RNA inhibits the activation of the protein kinase that phosphorylates the eIF-2 translation initiation factor. Virology 214:222-228.
28. Dittmann M, Hoffmann H-H, Scull MA, Gilmore RH, Bell KL, Ciancanelli M, Wilson SJ, Crotta S, Yu Y, Flatley B, Xiao JW, Casanova J-L, Wack A, Bieniasz PD, Rice CM. 2015. A Serpin Shapes the Extracellular Environment to Prevent Influenza A Virus Maturation. Cell 160:631-643.
29. Mar KB, Rinkenberger NR, Boys IN, Eitson JL, McDougal MB, Richardson RB, Schoggins JW. 2018. LY6E mediates an evolutionarily conserved enhancement of virus infection by targeting a late entry step. Nature Communications 9:1-14.
30. Rinkenberger N, Schoggins JW. 2018. Mucolipin-2 Cation Channel Increases Trafficking Efficiency of Endocytosed Viruses. mBio 9:e02314-17.
31. Ashley C, Abendroth A, McSharry B, Slobedman B. 2019. Interferon-Independent Innate Responses to Cytomegalovirus. Frontiers in Immunology 10:2751.
32. Schmid S, Mordstein M, Kochs G, Garcia-Sastre A, Tenoever BR. 2010. Transcription factor redundancy ensures induction of the antiviral state. J Biol Chem 285:42013-22.
33. Panda D, Gjinaj E, Bachu M, Squire E, Novatt H, Ozato K, Rabin R. 2019. IRF1 Maintains Optimal Constitutive Expression of Antiviral Genes and Regulates the Early Antiviral Response. Frontiers in Immunology 10:1019.
34. Paladino P, Cummings DT, Noyce RS, Mossman KL. 2006. The IFN-Independent Response to Virus Particle Entry Provides a First Line of Antiviral Defense That Is Independent of TLRs and Retinoic Acid-Inducible Gene I. J Immunol 177:8008-8016.
35. Noyce RS, Taylor K, Ciechonska M, Collins SE, Duncan R, Mossman KL. 2011. Membrane Perturbation Elicits an IRF3-Dependent, Interferon-Independent Antiviral Response. J Virol 85:10926-31.
36. Pillai PS, Molony RD, Martinod K, Dong H, Pang IK, Tal MC, Solis AG, Bielecki P, Mohanty S, Trentalange M, Homer RJ, Flavell RA, Wagner DD, Montgomery RR, Shaw AC, Staeheli P, Iwasaki A. 2016. Mx1 reveals innate pathways to antiviral resistance and lethal influenza disease. Science 352:463-466.
37. Jiang C, Zhou Z, Quan Y, Zhang S, Wang T, Zhao X, Morrison C, Heise MT, He W, Miller MS, Lin X. 2016. CARMA3 is a host factor regulating the balance of inflammatory and antiviral responses against viral infection. Cell Reports 14:2389-2401.
38. Galluzzi L, Brenner C, Morselli E, Touat Z, Kroemer G. 2008. Viral Control of Mitochondrial Apoptosis. PLoS Pathogens 4:21000018.
39. Al-Molawi N, Beardmore VA, Carter MJ, Kass GEN, Roberts LO. 2003. Caspase-mediated cleavage of the feline calicivirus capsid protein. J Gen Virol 84:1237-1244.

40. Robinson B, Van Winkle J, McCune B, Peters A, Nice T. 2019. Caspase-mediated cleavage of murine norovirus NS1/2 potentiates apoptosis and is required for persistent infection of intestinal epithelial cells. PLoS Pathogens 15:1007940.
41. Fiege JK, Stone IA, Dumm RE, Waring BM, Fife BT, Agudo J, Brown BD, Heaton NS, Langlois RA. 2019. Long-term surviving influenza infected cells evade CD8+ T cell mediated clearance. PLoS Pathogens 15:1008077.
42. Davidson S, Crotta S, McCabe TM, Wack A. 2014. Pathogenic potential of interferon αβ in acute influenza infection. Nature Communications 5:1-15.
43. Langlois RA, Legge KL. 2007. Respiratory dendritic cells: mediators of tolerance and immunity. Immunologic Research 39:128-145.
44. McNab F, Mayer-Barber K, Sher A, Wack A, O'Garra A. 2015. Type I interferons in infectious disease. Nature Reviews Immunology 15:87-103.
45. Nagata S. 2018. Apoptosis and Clearance of Apoptotic Cells. Annual Review of Immunology 36:489-517.
46. Kandasamy M, Suryawanshi A, Tundup S, Perez JT, Schmolke M, Manicassamy S, Manicassamy B. 2016. RIG-I Signaling Is Critical for Efficient Polyfunctional T Cell Responses during Influenza Virus Infection. PLoS Pathogens 12:e1005754.
47. Ye L, Schnepf D, Becker J, Ebert K, Tanriver Y, Bernasconi V, Gad HH, Hartmann R, Lycke N, Staeheli P. 2019. Interferon-λ enhances adaptive mucosal immunity by boosting release of thymic stromal lymphopoietin. Nature Immunology 20:593-601.
48. Zheng H, Qian J, Varghese B, Baker DP, Fuchs S. 2011. Ligand-Stimulated Downregulation of the Alpha Interferon Receptor: Role of Protein Kinase D2. Molecular and Cellular Biology 31:710-720.
49. Kumar KS, Barriere H, Carbone CJ, Liu J, Swaminathan G, Xu P, Li Y, Baker DP, Peng J, Lukacs GL, Fuchs SY. 2007. Site-specific ubiquitination exposes a linear motif to promote interferon-α receptor endocytosis. Journal of Cell Biology 179:935-50.
50. Kumar KGS, Krolewski JJ, Fuchs SY. 2004. Phosphorylation and Specific Ubiquitin Acceptor Sites Are Required for Ubiquitination and Degradation of the IFNAR1 Subunit of Type I Interferon Receptor. J Biol Chem 179:935-950.
51. Kumar K, Tang W, Ravindranath A, Clark W, Croze E, Fuchs S. 2003. SCF(HOS) ubiquitin ligase mediates the ligand-induced down-regulation of the interferon-α receptor. The EMBO Journal 22:5480-5490.
52. Ivashkiv LB, Donlin LT. 2013. Regulation of type I interferon responses. Nature Reviews Immunology 14:36-49.
53. Jefferies C. 2019. Regulating IRFs in IFN Driven Disease. Frontiers in Immunology 10:325.
54. Krebs D, Hilton D. 2001. SOCS Proteins: Negative Regulators of Cytokine Signaling. Stem Cells 19:378-387.
55. Schneider WM, Chevillotte MD, Rice CM. 2014. Interferon-Stimulated Genes: A Complex Web of Host Defenses. Annual Review of Immunology 32:513-545.

56. Blumer T, Coto-Llerena M, Duong FHT, Heim MH. 2017. SOCS1 is an inducible negative regulator of interferon λ (IFN-λ)–induced gene expression in vivo. J Biol Chem 292:17928-17938.
57. Malakhova OA, Kim KII, Luo J-K, Zou W, Kumar KGS, Fuchs SY, Shuai K, Zhang D-E. 2006. UBP43 is a novel regulator of interferon signaling independent of its ISG15 isopeptidase activity. The EMBO Journal 25:2358-2367.
58. Yoneyama M, Kikuchi M, Matsumoto K, Imaizumi T, Miyagishi M, Taira K, Foy E, Loo Y-M, Gale M, Akira S, Yonehara S, Kato A, Fujita T. 2005. Shared and Unique Functions of the DExD/H-Box Helicases RIG-I, MDA5, and LGP2 in Antiviral Innate Immunity. J Immunol 175:2851-2858.
59. Satoh T, Kato H, Kumagai Y, Yoneyama M, Sato S, Matsushita K, Tsujimura T, Fujita T, Akira S, Takeuchi O. 2010. LGP2 is a positive regulator of RIG-I– and MDA5-mediated antiviral responses. Proc Natl Acad Sci U S A 107:1512-1517.
60. Malur M, Gale M, Krug RM. 2012. LGP2 Downregulates Interferon Production during Infection with Seasonal Human Influenza A Viruses That Activate Interferon Regulatory Factor 3. J Virol 86:10733-10738.
61. Saito T, Hirai R, Loo Y-M, Owen D, Johnson CL, Sinha SC, Akira S, Fujita T, Jr. MG. 2007. Regulation of innate antiviral defenses through a shared repressor domain in RIG-I and LGP2. Proc Natl Acad Sci U S A 104:582-587.
62. Russell A, Trapnell C, Bloom J. 2018. Extreme heterogeneity of influenza virus infection in single cells. elife 7:e32303.
63. Russell A, Elshina E, Kowalsky J, te Velthuis A, Bloom J. 2019. Single-Cell Virus Sequencing of Influenza Infections That Trigger Innate Immunity. J Virol 93:e00500-19.
64. O'Neal JT, Upadhyay AA, Wolabaugh A, Patel NB, Bosinger SE, Suthar MS. 2019. West Nile Virus-Inclusive Single-Cell RNA Sequencing Reveals Heterogeneity in the Type I Interferon Response within Single Cells. J Virol 93:e01778-18.
65. Wyler E, Franke V, Menegatti J, Kocks C, Boltengagen A, Praktiknjo S, Walch-Rückheim B, Bosse J, Rajewsky N, Grässer F, Akalin A, Landthaler M. 2019. Single-cell RNA-sequencing of herpes simplex virus 1-infected cells connects NRF2 activation to an antiviral program. Nature Communications 10:1-14.
66. Xin X, Wang H, Han L, Wang M, Fang H, Hao Y, Li J, Zhang H, Zheng C, Shen C. 2018. Single-Cell Analysis of the Impact of Host Cell Heterogeneity on Infection with Foot-and-Mouth Disease Virus. J Virol 92:e00179-18.
67. Uccellini MB, García-Sastre A. 2018. ISRE-Reporter Mouse Reveals High Basal and Induced Type I IFN Responses in Inflammatory Monocytes. Cell Reports 25:2784-2796.
68. Gonczol E, Andrews P, Plotkin S. 1984. Cytomegalovirus replicates in differentiated but not in undifferentiated human embryonal carcinoma cells. Science 224:159-161.

69. Weichold F, Zella D, Barabitskaja O, Maciejewski J, Dunn D, Sloand E, Young N. 1998. Neither Human Immunodeficiency Virus-1 (HIV-1) nor HIV-2 Infects Most-Primitive Human Hematopoietic Stem Cells as Assessed in Long-Term Bone Marrow Cultures. Blood 91:907-915.
70. Villa NY, Bais S, Meacham AM, Wise E, Rahman MM, Moreb JS, Rosenau EH, Wingard JR, McFadden G, Cogle CR. 2016. Ex Vivo Virotherapy With Myxoma Virus Does Not Impair Hematopoietic Stem and Progenitor Cells. Cytotherapy 18:465-480.
71. Swartzendruber D, Lehman J. 1975. Neoplastic differentiation: Interaction of simian virus 40 and polyoma virus with murine teratocarcinoma cells in vitro. Journal of Cellular Physiology 85:179-187.
72. Wu X, Thi VLD, Huang Y, Billerbeck E, Saha D, Hoffmann H-H, Wang Y, Silva LAV, Sarbanes S, Sun T, Andrus L, Yu Y, Quirk C, Li M, MacDonald MR, Schneider WM, An X, Rosenberg BR, Rice CM. 2018. Intrinsic Immunity Shapes Viral Resistance of Stem Cells. Cell 172:423-438.
73. Hong X-X, Carmichael GG. 2013. Innate Immunity in Pluripotent Human Cells: Attenuated response to interferon-beta. J Biol Chem 288:16196-16205.
74. Eggenberger J, Blanco-Melo D, Panis M, Brennand KJ, tenOever BR. 2019. Type I interferon response impairs differentiation potential of pluripotent stem cells. Proc Natl Acad Sci U S A 116:1384-1393
75. Saeed S, Quintin J, Kerstens HHD, Rao NA, Aghajanirefah A, Matarese F, Cheng S-C, Ratter J, Berentsen K, Ent MAvd, Sharifi N, Janssen-Megens EM, Huurne MT, Mandoli A, Schaik Tv, Ng A, Burden F, Downes K, Frontini M, Kumar V, Giamarellos-Bourboulis EJ, Ouwehand WH, Meer JWMvd, Joosten LAB, Wijmenga C, Martens JHA, Xavier RJ, Logie C, Netea MG, Stunnenberg HG. 2014. Epigenetic programming of monocyte-to-macrophage differentiation and trained innate immunity. Science 345:1251086.
76. Tamura T, Smith M, Kanno T, Dasenbrock H, Nishiyama A, Ozato K. 2009. Inducible Deposition of the Histone Variant H3.3 in Interferon-stimulated Genes. J Biol Chem 284:12217-12225.
77. Sarai N, Nimura K, Tamura T, Kanno T, Patel MC, Heightman TD, Ura K, Ozato K. 2013. WHSC1 links transcription elongation to HIRA-mediated histone H3.3 deposition. The EMBO Journal 32:2392-2406.
78. Kamada R, Yang W, Zhang Y, Patel MC, Yang Y, Ouda R, Dey A, Wakabayashi Y, Sakaguchi K, Fujita T, Tamura T, Zhu J, Ozato K. 2018. Interferon stimulation creates chromatin marks and establishes transcriptional memory. Proc Natl Acad Sci U S A 115:e9162-9171.
79. Watanabe T, Kawakami E, Shoemaker JE, Lopes TJS, Matsuoka Y, Tomita Y, Kozuka-Hata H, Gorai T, Kuwahara T, Takeda E, Nagata A, Takano R, Kiso M, Yamashita M, Sakai-Tagawa Y, Katsura H, Nonaka N, Fujii H, Fujii K, Sugita Y, Noda T, Goto H, Fukuyama S, Watanabe S, Neumann G, Oyama M, Kitano H, Kawaoka Y. 2014. Influenza virus-host interactome screen as a platform for antiviral drug development. Cell Host & Microbe 16:795-805.

80. Ackerman EE, Kawakami E, Katoh M, Watanabe T, Watanabe S, Tomita Y, Lopes TJ, Matsuoka Y, Kitano H, Shoemaker JE, Kawaoka Y. 2018. Network-Guided Discovery of Influenza Virus Replication Host Factors. mBio 9:e02002-18.
81. Bilz NC, Jahn K, Lorenz M, Lüdtke A, Hübschen JM, Geyer H, Mankertz A, Hübner D, Liebert UG, Claus C. 2018. Rubella Viruses Shift Cellular Bioenergetics to a More Oxidative and Glycolytic Phenotype with a Strain-Specific Requirement for Glutamine. J Virol 16:e00934.
82. Fontaine KA, Sanchez EL, Camarda R, Lagunoff M, Sandri-Goldin RM. 2015. Dengue Virus Induces and Requires Glycolysis for Optimal Replication. mBio 89:2358-2376.
83. Hale BG, Randall RE, Ortín J, Jackson D. 2008. The multifunctional NS1 protein of influenza A viruses. J Gen Virol 89:2359-2376.
84. Khaperskyy D, Schmaling S, Larkins-Ford J, McCormick C, Gaglia M. 2016. Selective Degradation of Host RNA Polymerase II Transcripts by Influenza A Virus PA-X Host Shutoff Protein. PLoS Pathogens 12:e1005427.
85. Chaimayo C, Dunagan M, Hayashi T, Santoso N, Takimoto T. 2018. Specificity and functional interplay between influenza virus PA-X and NS1 shutoff activity. PLoS Pathogens 14:e1007465.
86. Harris RS, Dudley JP. 2015. APOBECs and Virus Restriction. Virology 479-480:131-145.
87. Salamango DJ, Ikeda T, Moghadasi SA, Wang J, McCann JL, Serebrenik AA, Ebrahimi D, Jarvis MC, Brown WL, Harris RS. 2019. HIV-1 Vif Triggers Cell Cycle Arrest by Degrading Cellular PPP2R5 Phospho-regulators. Cell Reports 29:1057-1065.
88. Daugherty M, Malik H. 2012. Rules of Engagement: Molecular Insights from Host-Virus Arms Races. Annual Review of Genetics 46:677-700.
89. Enard D, Petrov DA. 2018. Evidence that RNA viruses drove of adaptive introgression between Neanderthals and modern humans. Cell 175:360-371.
90. Enard D, Cai L, Gwennap C, Petrov DA. 2016. Viruses are a dominant driver of protein adaptation in mammals. eLife 17:e12469.
91. Kristiansen H, Gad H, Eskildsen-Larsen S, Despres P, Hartmann R. 2011. The oligoadenylate synthetase family: an ancient protein family with multiple antiviral activities. Journal of Interferon & Cytokine Research 31:41-47.
92. Donovan J, Dufner M, Korennykh A. 2013. Structural basis for cytosolic double-stranded RNA surveillance by human oligoadenylate synthetase 1. Proc Natl Acad Sci U S A 110:1652-1657.
93. Carey CM, Govande AA, Cooper JM, Hartley MK, Kranzusch PJ, Elde NC. 2019. Recurrent loss-of-function mutations reveal costs to OAS1 antiviralactivity in primates. Cell Host & Microbe 25:336-343.
94. Manz B, Dornfeld D, Gotz V, Zell R, Zimmermann P, Haller O, Kochs G, Schwemmle M. 2013. Pandemic Influenza A Viruses Escape from Restriction by Human MxA through Adaptive Mutations in the Nucleoprotein. PLoS Pathogens 9:e1003279.

95. Deeg C, E H, Mutz P, Rheinemann L, Gotz V, Magar L, Schilling M, Kallfass C, Nurnberger C, Soubies S, Kochs G, Haller O, Schwemmle M, Staeheli P. 2017. In vivo evasion of MxA by avian influenza viruses requires human signature in the viral nucleoprotein. J Exp Med 214:1239-1248.
96. Phillips A, Ponomarenko A, Chen K, Ashenberg O, Miao J, McHugh S, Butty V, Whittaker C, Moore C, Bloom J, Lin Y, Shoulders M. 2018. Destabilized adaptive influenza variants critical for innate immune system escape are potentiated by host chaperones. PLoS Biology 16:e1003279.
97. Duffy S. 2018. Why are RNA virus mutation rates so damn high? PLoS Biology 16.
98. Daugherty MD, Schaller AM, Geballe AP, Malik HS. 2016. Evolution-guided functional analyses reveal diverse antiviral specificities encoded by IFIT1 genes in mammals. eLife 5:e14228.
99. Münk C, Willemsen A, Bravo IG. 2012. An ancient history of gene duplications, fusions and losses in the evolution of APOBEC3 mutators in mammals. BMC Evolutionary Biology 12:71.
100. Johnson WE, Sawyer SL. 2009. Molecular evolution of the antiretroviral TRIM5 gene. Immunogenetics 61:163-176.
101. Fiege JK, Langlois RA. 2015. Investigating influenza A virus infection: tools to track infection and limit tropism. J Virol 89:6167-70.
102. Everitt AR, Clare S, Pertel T, John SP, Wash RS, Smith SE, Chin CR, Feeley EM, Sims JS, Adams DJ, Wise HM, Kane L, Goulding D, Digard P, Anttila V, Baillie JK, Walsh TS, Hume DA, Palotie A, Xue Y, Colonna V, Tyler-Smith C, Dunning J, Gordon SB, Smyth RL, Openshaw PJ, Dougan G, Brass AL, Kellam P, Investigators G, Investigators M. 2012. IFITM3 restricts the morbidity and mortality associated with influenza. Nature 484:519-23.
103. Krug RM, Shaw M, Broni B, Shapiro G, Haller O. 1985. Inhibition of influenza viral mRNA synthesis in cells expressing the interferon-induced Mx gene product. J Virol 56:201-6.
104. Pavlovic J, Haller O, Staeheli P. 1992. Human and mouse Mx proteins inhibit different steps of the influenza virus multiplication cycle. J Virol 66:2564-9.
105. Brass AL, Huang IC, Benita Y, John SP, Krishnan MN, Feeley EM, Ryan BJ, Weyer JL, van der Weyden L, Fikrig E, Adams DJ, Xavier RJ, Farzan M, Elledge SJ. 2009. The IFITM proteins mediate cellular resistance to influenza A H1N1 virus, West Nile virus, and dengue virus. Cell 139:1243-54.
106. Grandvaux N, Servant MJ, tenOever B, Sen GC, Balachandran S, Barber GN, Lin R, Hiscott J. 2002. Transcriptional profiling of interferon regulatory factor 3 target genes: direct involvement in the regulation of interferon-stimulated genes. J Virol 76:5532-9.
107. Dixit E, Boulant S, Zhang Y, Lee AS, Odendall C, Shum B, Hacohen N, Chen ZJ, Whelan SP, Fransen M, Nibert ML, Superti-Furga G, Kagan JC. 2010. Peroxisomes are signaling platforms for antiviral innate immunity. Cell 141:668-81.

108. Shapira SD, Gat-Viks I, Shum BO, Dricot A, de Grace MM, Wu L, Gupta PB, Hao T, Silver SJ, Root DE, Hill DE, Regev A, Hacohen N. 2009. A physical and regulatory map of host-influenza interactions reveals pathways in H1N1 infection. Cell 139:1255-67.
109. König R, Stertz S, Zhou Y, Inoue A, Hoffmann HH, Bhattacharyya S, Alamares JG, Tscherne DM, Ortigoza MB, Liang Y, Gao Q, Andrews SE, Bandyopadhyay S, De Jesus P, Tu BP, Pache L, Shih C, Orth A, Bonamy G, Miraglia L, Ideker T, García-Sastre A, Young JA, Palese P, Shaw ML, Chanda SK. 2010. Human host factors required for influenza virus replication. Nature 463:813-7.
110. Heaton NS, Moshkina N, Fenouil R, Gardner TJ, Aguirre S, Shah PS, Zhao N, Manganaro L, Hultquist JF, Noel J, Sachs D, Hamilton J, Leon PE, Chawdury A, Tripathi S, Melegari C, Campisi L, Hai R, Metreveli G, Gamarnik AV, García-Sastre A, Greenbaum B, Simon V, Fernandez-Sesma A, Krogan NJ, Mulder LCF, van Bakel H, Tortorella D, Taunton J, Palese P, Marazzi I. 2016. Targeting Viral Proteostasis Limits Influenza Virus, HIV, and Dengue Virus Infection. Immunity 44:46-58.
111. Heldt FS, Kupke SY, Dorl S, Reichl U, Frensing T. 2015. Single-cell analysis and stochastic modelling unveil large cell-to-cell variability in influenza A virus infection. Nature Communications 6:8938.
112. Killip M, Jackson D, Pérez-Cidoncha M, Fodor E, Randall R. 2017. Single-cell studies of IFN-β promoter activation by wild-type and NS1-defective influenza A viruses. J Gen Virol 98:357-363.
113. Fodor E, Devenish L, Engelhardt OG, Palese P, Brownlee GG, García-Sastre A. 1999. Rescue of Influenza A Virus from Recombinant DNA. Journal of Virology 73:9679-9682.
114. Hoffmann E, Neumann G, Kawaoka Y, Hobom G, Webster RG. 2000. A DNA transfection system for generation of influenza A virus from eight plasmids. Proc Natl Acad Sci U S A 97:6108-6113.
115. Matsuda T, Cepko CL. 2007. Controlled expression of transgenes introduced by in vivo electroporation. Proc Natl Acad Sci U S A 104:1027-1032.
116. Langmead B, Salzberg S. 2012. Fast gapped-read alignment with Bowtie 2. Nature Methods 9:357-359.
117. Li H, Handsaker B, Wysoker A, Fennell T, Ruan J, Homer N, Marth G, Abecasis G, Durbin R, Subgroup GPDP. 2009. The Sequence Alignment/Map format and SAMtools. Bioinformatics 25:2078-2079.
118. Liao Y, Smyth G, Shi W. 2014. featureCounts: an efficient general purpose program for assigning sequence reads to genomic features. Bioinformatics 30:923-930.
119. Robinson JT, Thorvaldsdóttir H, Winckler W, Guttman M, Lander ES, Getz G, Mesirov JP. 2011. Integrative genomics viewer. Nature Biotechnology 29:24-26.
120. Gu Z, Eils R, Schlesner M. 2016. Complex heatmaps reveal patterns and correlations in multidimensional genomic data. Bioinformatics 32:2847-2849.
121. Robinson MD, McCarthy DJ, Smyth GK. 2010. edgeR: a Bioconductor package for differential expression analysis of digital gene expression data. Bioinformatics 26:139-140.

122. McCarthy DJ, Chen Y, Smyth GK. 2012. Differential expression analysis of multifactor RNA-Seq experiments with respect to biological variation. Nucleic Acids Research 40:4288-4297.
123. Marsh GA, Hatami R, Palese P. 2007. Specific residues of the influenza A virus hemagglutinin viral RNA are important for efficient packaging into budding virions. J Virol 81:9727-36.
124. Martinez-Sobrido L, Cadagan R, Steel J, Basler CF, Palese P, Moran TM, Garcia-Sastre A. 2010. Hemagglutinin-pseudotyped green fluorescent protein-expressing influenza viruses for the detection of influenza virus neutralizing antibodies. J Virol 84:2157-63.
125. Floyd DL, Ragains JR, Skehel JJ, Harrison SC, van Oijen AM. 2008. Single-particle kinetics of influenza virus membrane fusion. Proc Natl Acad Sci U S A 105:15382-7.
126. Smith AM, Perelson AS. 2011. Influenza A virus infection kinetics: quantitative data and models. Wiley Interdiscip Rev Syst Biol Med 3:429-45.
127. Smith AM, Adler FR, McAuley JL, Gutenkunst RN, Ribeiro RM, McCullers JA, Perelson AS. 2011. Effect of 1918 PB1-F2 expression on influenza A virus infection kinetics. PLoS Comput Biol 7:e1001081.
128. Baccam P, Beauchemin C, Macken CA, Hayden FG, Perelson AS. 2006. Kinetics of influenza A virus infection in humans. J Virol 80:7590-9.
129. Saira K, Lin X, DePasse JV, Halpin R, Twaddle A, Stockwell T, Angus B, Cozzi-Lepri A, Delfino M, Dugan V, Dwyer DE, Freiberg M, Horban A, Losso M, Lynfield R, Wentworth DN, Holmes EC, Davey R, Wentworth DE, Ghedin E, Group IFS, Group IFS. 2013. Sequence analysis of in vivo defective interfering-like RNA of influenza A H1N1 pandemic virus. J Virol 87:8064-74.
130. Brooke CB, Ince WL, Wrammert J, Ahmed R, Wilson PC, Bennink JR, Yewdell JW. 2013. Most influenza a virions fail to express at least one essential viral protein. J Virol 87:3155-62.
131. Dou D, Hernández-Neuta I, Wang H, Östbye H, Qian X, Thiele S, Resa-Infante P, Kouassi NM, Sender V, Hentrich K, Mellroth P, Henriques-Normark B, Gabriel G, Nilsson M, Daniels R. 2017. Analysis of IAV Replication and Co-infection Dynamics by a Versatile RNA Viral Genome Labeling Method. Cell Reports 20:251-263.
132. Chelbi-Alix MK, Quignon F, Pelicano L, Koken MH, de Thé H. 1998. Resistance to virus infection conferred by the interferon-induced promyelocytic leukemia protein. J Virol 72:1043-51.
133. Liu B, Li NL, Shen Y, Bao X, Fabrizio T, Elbahesh H, Webby RJ, Li K. 2016. The C-Terminal Tail of TRIM56 Dictates Antiviral Restriction of Influenza A and B Viruses by Impeding Viral RNA Synthesis. J Virol 90:4369-4382.
134. Li X, Zhao X, Fang Y, Jiang X, Duong T, Fan C, Huang CC, Kain SR. 1998. Generation of destabilized green fluorescent protein as a transcription reporter. J Biol Chem 273:34970-5.

135. Balachandran S, Roberts PC, Brown LE, Truong H, Pattnaik AK, Archer DR, Barber GN. 2000. Essential role for the dsRNA-dependent protein kinase PKR in innate immunity to viral infection. Immunity 13:129-41.
136. Battich N, Stoeger T, Pelkmans L. 2015. Control of Transcript Variability in Single Mammalian Cells. Cell 163:1596-610.
137. Pelkmans L. 2012. Cell Biology. Using cell-to-cell variability--a new era in molecular biology. Science 336:425-6.
138. Shalek AK, Satija R, Shuga J, Trombetta JJ, Gennert D, Lu D, Chen P, Gertner RS, Gaublomme JT, Yosef N, Schwartz S, Fowler B, Weaver S, Wang J, Wang X, Ding R, Raychowdhury R, Friedman N, Hacohen N, Park H, May AP, Regev A. 2014. Single-cell RNA-seq reveals dynamic paracrine control of cellular variation. Nature 510:363-9.
139. Steuerman Y, Cohen M, Peshes-Yaloz N, Valadarsky L, Cohn O, David E, Frishberg A, Mayo L, Bacharach E, Amit I, Gat-Viks I. 2018. Dissection of Influenza Infection In Vivo by Single-Cell RNA Sequencing. Cell Syst 6:679-691.e4.
140. van Boxel-Dezaire A, Rani M, GR S. 2006. Complex modulation of cell type-specific signaling in response to type I interferons. Immunity 25:361-372.
141. Pérez-Cidoncha M, Killip MJ, Oliveros JC, Asensio VJ, Fernández Y, Bengoechea JA, Randall RE, Ortín J. 2014. An Unbiased Genetic Screen Reveals the Polygenic Nature of the Influenza Virus Anti-Interferon Response. J Virol 88:4632-4646.
142. Du Y, Xin L, Shi Y, Zhang T-H, Wu NC, Dai L, Gong D, Brar G, Shu S, Luo J, Reiley W, Tseng Y-W, Bai H, Wu T-T, Wang J, Shu Y, Sun R. 2018. Genome-wide identification of interferon-sensitive mutations enables influenza vaccine design. Science 359:290-296.
143. Benitez A, Panis M, Xue J, Varble A, Shim J, Frick A, López C, Sachs D, tenOever B. 2015. In vivo RNAi screening identifies MDA5 as a significant contributor to the cellular defense against influenza A virus. Cell Reports 11:1714-1726.
144. Langlois RA, Varble A, Chua MA, García-Sastre A, tenOever BR. 2012. Hematopoietic-specific targeting of influenza A virus reveals replication requirements for induction of antiviral immune responses. Proc Natl Acad Sci U S A 109:12117-22.
145. Heaton N, Langlois R, Sachs D, Lim J, Palese P, tenOever B. 2014. Long-term survival of influenza virus infected club cells drives immunopathology. J Exp Med 211:1707-14.
146. Hamilton JR, Sachs D, Lim JK, Langlois RA, Palese P, Heaton NS. 2016. Club cells surviving influenza A virus infection induce temporary nonspecific antiviral immunity. Proc Natl Acad Sci U S A 113:3861-6.
147. Loo Y-M, Fornek J, Crochet N, Bajwa G, Perwitasari O, Martinez-Sobrido L, Akira S, Gill MA, García-Sastre A, Katze MG, Jr. MG. 2008. Distinct RIG-I and MDA5 Signaling by RNA Viruses in Innate Immunity. J Virol 82:335-345.
148. te Velthuis A, Fodor E. 2016. Influenza virus RNA polymerase: insights into the mechanisms of viral RNA synthesis. Nature Reviews Microbiology 14:479-493.

149. York A, Hengrung N, Vreede F, Huiskonen J, Fodor E. 2013. Isolation and characterization of the positive-sense replicative intermediate of a negative-strand RNA virus. Proc Natl Acad Sci U S A 110:E4238-45.
150. Rehwinkel J, Tan C, Goubau D, Schulz O, Pichlmair A, Bier K, Robb N, Vreede F, Barclay W, Fodor E, Reis e Sousa C. 2010. RIG-I detects viral genomic RNA during negative-strand RNA virus infection. Cell 140:397-408.
151. Kouba T, Drncová P, Cusack S. 2019. Structural snapshots of actively transcribing influenza polymerase. Nature Structural & Molecular Biology 26:460-470.
152. Vreede F, Jung T, Brownlee G. 2004. Model Suggesting that Replication of Influenza Virus Is Regulated by Stabilization of Replicative Intermediates. J Virol 78:9568-9572.
153. Österlund P, Strengell M, Sarin L, Poranen M, Fagerlund R, Melén K, Julkunen I. 2012. Incoming Influenza A Virus Evades Early Host Recognition, while Influenza B Virus Induces Interferon Expression Directly upon Entry. J Virol 86:11183-11193.
154. Te Velthuis A, Long J, Bauer D, Fan R, Yen H, Sharps J, Siegers J, Killip M, French H, Oliva-Martín M, Randall R, de Wit E, van Riel D, Poon L, Fodor E. 2018. Mini viral RNAs act as innate immune agonists during influenza virus infection. Nature Microbiology 3:1234-1242.
155. Liu G, Lu Y, Liu Q, Zhou Y. 2019. Inhibition of Ongoing Influenza A Virus Replication Reveals Different Mechanisms of RIG-I Activation. J Virol 93:e02066-18.
156. Killip M, Smith M, Jackson D, Randall R. 2014. Activation of the Interferon Induction Cascade by Influenza A Viruses Requires Viral RNA Synthesis and Nuclear Export. J Virol 88:3942-3952.
157. Amorim M, Read E, Dalton R, Medcalf L, Digard P. 2007. Nuclear Export of Influenza A Virus mRNAs Requires Ongoing RNA Polymerase II Activity. Traffic 8:1-11.
158. Sjaastad LE, Fay EJ, Fiege JK, Macchietto MG, Stone IA, Markman MW, Shen S, Langlois RA. 2018. Distinct antiviral signatures revealed by the magnitude and round of influenza virus replication in vivo. Proc Natl Acad Sci U S A 115:9610-9615.
159. Hemann EA, Sjaastad LE, Langlois RA, Legge KL, Schultz-Cherry S. 2016. Plasmacytoid Dendritic Cells Require Direct Infection To Sustain the Pulmonary Influenza A Virus-Specific CD8 T Cell Response. J Virol 90:2830-2837.
160. Ramos I, Smith G, Ruf-Zamojski F, Martínez-Romero C, Fribourg M, Carbajal EA, Hartmann BM, Nair VD, Marjanovic N, Monteagudo PL, DeJesus VA, Mutetwa T, Zamojski M, Tan GS, Jayaprakash C, Zaslavsky E, Albrecht RA, Sealfon SC, García-Sastre A, Fernandez-Sesma A, Williams BRG. 2019. Innate Immune Response to Influenza Virus at Single-Cell Resolution in Human Epithelial Cells Revealed Paracrine Induction of Interferon Lambda 1. J Virol 93:e00559-19.
161. Wang C, Forst CV, Chou T-w, Geber A, Wang M, Hamou W, Smith M, Sebra R, Zhang B, Zhou B, Ghedin E, Denison MR. 2020. Cell-to-Cell Variation in Defective Virus Expression and Effects on Host Responses during Influenza Virus Infection. mBio 11:e02880-19.

162. Kallfass C, Lienenklaus S, Weiss S, Staeheli P. 2013. Visualizing the Beta Interferon Response in Mice during Infection with Influenza A Viruses Expressing or Lacking Nonstructural Protein 1. J Virol 87:6925-6930.
163. Stifter S, Bhattacharyya N, Sawyer A, Cootes T, Stambas J, Doyle S, Feigenbaum L, Paul W, Britton W, Sher A, Feng C. 2019. Visualizing the selectivity and dynamics of interferon signaling in vivo. Cell Reports 29:3539-3550.
164. Esser-Nobis K, Aarreberg LD, Roby JA, Fairgrieve MR, Green R, Michael Gale J. 2019. Comparative Analysis of African and Asian Lineage-Derived Zika Virus Strains Reveals Differences in Activation of and Sensitivity to Antiviral Innate Immunity. J Virol 93:e00640-19.
165. Ma JZ, Ng WC, Zappia L, Gearing LJ, Olshansky M, Pham K, Cheong K, Hsu A, Turner SJ, Wijburg O, Londrigan SL, Brooks AG, Reading PC. 2019. Unique Transcriptional Architecture in Airway Epithelial Cells and Macrophages Shapes Distinct Responses following Influenza Virus Infection Ex Vivo. J Virol 93:e01986-18.
166. Montoro DT, Haber AL, Biton M, Vinarsky V, Lin B, Birket SE, Yuan F, Chen S, Leung HM, Villoria J, Rogel N, Burgin G, Tsankov AM, Waghray A, Slyper M, Waldman J, Nguyen L, Dionne D, Rozenblatt-Rosen O, Tata PR, Mou H, Shivaraju M, Bihler H, Mense M, Tearney GJ, Rowe SM, Engelhardt JF, Regev A, Rajagopal J. 2018. A revised airway epithelial hierarchy includes CFTR-expressing ionocytes. Nature 560:319-324.
167. Wang Y, Tang Z, Huang H, Li J, Wang Z, Yu Y, Zhang C, Li J, Dai H, Wang F, Cai T, Tang N. 2018. Pulmonary alveolar type I cell population consists of two distinct subtypes that differ in cell fate. Proc Natl Acad Sci U S A 115:2407-2412.
168. Treutlein B, Brownfield DG, Wu AR, Neff NF, Mantalas GL, Espinoza FH, Desai TJ, Krasnow MA, Quake SR. 2014. Reconstructing lineage hierarchies of the distal lung epithelium using single-cell RNA-seq. Nature 509:371-375.
169. Suspène R, Petit V, Puyraimond-Zemmour D, Aynaud M-M, Henry M, Guétard D, Rusniok C, Wain-Hobson S, Vartanian J-P. 2011. Double-Stranded RNA Adenosine Deaminase ADAR-1-Induced Hypermutated Genomes among Inactivated Seasonal Influenza and Live Attenuated Measles Virus Vaccines. J Virol 85:2458-62.
170. Chambers BS, Heaton BE, Rausch K, Dumm RE, Hamilton JR, Cherry S, Heaton NS. 2019. DNA mismatch repair is required for the host innate response and controls cellular fate after influenza virus infection. Nature Microbiology 4:1964-1977.
171. Mäkelä SM, Österlund P, Westenius V, Latvala S, Diamond MS, Gale M, Julkunen I. 2015. RIG-I Signaling Is Essential for Influenza B Virus-Induced Rapid Interferon Gene Expression. J Virol 89:12014-12025.
172. Macchietto MG, Langlois RA, Shen SS. 2020. Virus-induced transposable element expression up-regulation in human and mouse host cells. Life Science Alliance 3:e201900536.
173. Fay EJ, Aron SL, Stone IA, Waring BM, Plemper RK, Langlois RA. 2019. Engineered Small-Molecule Control of Influenza A Virus Replication. J Virol 93:e01677-18.

174. Kim HY, Cho HK, Yoo SK, Cheong J. 2012. Hepatic STAMP2 decreases hepatitis B virus X protein-associated metabolic deregulation. Experimental & Molecular Medicine 44:622-632.
175. Menachery VD, Schäfer A, Burnum-Johnson KE, Mitchell HD, Eisfeld AJ, Walters KB, Nicora CD, Purvine SO, Casey CP, Monroe ME, Weitz KK, Stratton KG, Webb-Robertson B-JM, Gralinski LE, Metz TO, Smith RD, Waters KM, Sims AC, Kawaoka Y, Baric RS. 2018. MERS-CoV and H5N1 influenza virus antagonize antigen presentation by altering the epigenetic landscape. Proc Natl Acad Sci U S A 115:1012-1021.
176. Chow K, Gale MJ, Loo Y. 2018. RIG-I and Other RNA Sensors in Antiviral Immunity. Annual Review of Immunology 36:667-694.
177. Davis WG, Bowzard JB, Sharma SD, Wiens ME, Ranjan P, Gangappa S, Stuchlik O, Pohl J, Donis RO, Katz JM, Cameron CE, Fujita T, Sambhara S. 2012. The 3' Untranslated Regions of Influenza Genomic Sequences Are 5'PPP-Independent Ligands for RIG-I. PLoS One 7:e32661.
178. Sauter D, Kirchhoff F. 2019. Key Viral Adaptations Preceding the AIDS Pandemic. Cell Host & Microbe 25:27-38.
179. Holmes EC, Dudas G, Rambaut A, Andersen KG. 2016. The evolution of Ebola virus: Insights from the 2013–2016 epidemic. Nature 538:193-200.
180. Krammer F. 2015. Emerging influenza viruses and the prospect of a universal influenza virus vaccine - Krammer - 2015 - Biotechnology Journal - Wiley Online Library. Biotechnology Journal 10:690-701.
181. Zwart M, Elena S. 2015. Matters of Size: Genetic Bottlenecks in Virus Infection and Their Potential Impact on Evolution. Annual Review of Virology 2:161-179.
182. Warren C, Sawyer S. 2019. How host genetics dictates successful viral zoonosis. PLoS Biology 17.
183. Fabre P-H, Hautier L, Dimitrov D, Douzery EJP. 2012. A glimpse on the pattern of rodent diversification: a phylogenetic approach. BMC Evolutionary Biology 12:1-19.
184. Williams SH, Che X, Garcia JA, Klena JD, Lee B, Muller D, Ulrich W, Corrigan RM, Nichol S, Jain K, Lipkin WI, Denison MR. 2018. Viral Diversity of House Mice in New York City. mBio 9:e01354-17.
185. Schountz T, Prescott J. 2014. Hantavirus Immunology of Rodent Reservoirs: Current Status and Future Directions. Viruses 6:1317-1335.
186. Firth C, Bhat M, Firth MA, Williams SH, Frye MJ, Simmonds P, Conte JM, Ng J, Garcia J, Bhuva NP, Lee B, Che X, Quan P-L, Lipkin WI. 2014. Detection of Zoonotic Pathogens and Characterization of Novel Viruses Carried by Commensal Rattus norvegicus in New York City. mBio 5:e01354-17.
187. Tsoleridis T, Chappell JG, Monchatre-Leroy E, Umhang G, Shi M, Bennett M, Tarlinton RE, McClure CP, Holmes EC, Ball JK. 2019. Discovery and Prevalence of Divergent RNA Viruses in European Field Voles and Rabbits. Viruses 12:47.

188. Beura LK, Hamilton SE, Bi K, Schenkel JM, Odumade OA, Casey KA, Thompson EA, Fraser KA, Rosato PC, Filali-Mouhim A, Sekaly RP, Jenkins MK, Vezys V, Haining WN, Jameson SC, Masopust D. 2016. Normalizing the environment recapitulates adult human immune traits in laboratory mice. Nature 532:512-6.
189. Ank N, Iversen MB, Bartholdy C, Staeheli P, Hartmann R, Jensen UB, Dagnaes-Hansen F, Thomsen AR, Chen Z, Haugen H, Klucher K, Paludan SR. 2008. An Important Role for Type III Interferon (IFN-λ/IL-28) in TLR-Induced Antiviral Activity. J Immunol 180:2474-2485.
190. Reese AT, Cho EH, Klitzman B, Nichols SP, Wisniewski NA, Villa MM, Durand HK, Jiang S, Midani FS, Nimmagadda SN, O'Connell TM, Wright JP, Deshusses MA, David LA. 2018. Antibiotic-induced changes in the microbiota disrupt redox dynamics in the gut. eLife 19:e35987.
191. Dobin A, Davis CA, Schlesinger F, Drenkow J, Zaleski C, Jha S, Batut P, Chaisson M, Gingeras TR. 2013. STAR: ultrafast universal RNA-seq aligner. Bioinformatics 29:15-21.
192. Grabherr MG, Haas BJ, Yassour M, Levin JZ, Thompson DA, Amit I, Adiconis X, Fan L, Raychowdhury R, Zeng Q, Chen Z, Mauceli E, Hacohen N, Gnirke A, Rhind N, di Palma F, Birren BW, Nusbaum C, Lindblad-Toh K, Friedman N, Regev A. 2011. Full-length transcriptome assembly from RNA-Seq data without a reference genome. Nature Biotechnology 29:644-52.
193. Patro R, Duggal G, Love MI, Irizarry RA, Kingsford C. 2017. Salmon provides fast and bias-aware quantification of transcript expression. Nat Methods 14:417-419.
194. Love MI, Huber W, Anders S. 2014. Moderated estimation of fold change and dispersion for RNA-seq data with DESeq2. Genome Biology 15:1-21.
195. Sievers F, Higgins D. 2017. Clustal Omega for making accurate alignments of many protein sequences - Sievers - 2018 - Protein Science - Wiley Online Library. Protein Science 27:135-145.
196. Kozlov AM, Darriba D, Flouri T, Morel B, Stamatakis A. 2019. RAxML-NG: a fast, scalable and user-friendly tool for maximum likelihood phylogenetic inference. Bioinformatics 35:4453-4455.
197. Grubaugh ND, Gangavarapu K, Quick J, Matteson NL, De Jesus JG, Main BJ, Tan AL, Paul LM, Brackney DE, Grewal S, Gurfield N, Van Rompay KKA, Isern S, Michael SF, Coffey LL, Loman NJ, Andersen KG. 2019. An amplicon-based sequencing framework for accurately measuring intrahost virus diversity using PrimalSeq and iVar. Genome Biol 20:8.
198. Khamrin P, Maneekarn N, Okitsu S, Ushijima H. 2014. Epidemiology of human and animal kobuviruses. Virusdisease 25:195-200.
199. Wang W, Lin XD, Guo WP, Zhou RH, Wang MR, Wang CQ, Ge S, Mei SH, Li MH, Shi M, Holmes EC, Zhang YZ. 2015. Discovery, diversity and evolution of novel coronaviruses sampled from rodents in China. Virology 474:19-27.

200. Zitterkopf N, Haven T, Huela M, Bradley D, Cafruny W. 2002. Transplacental Lactate Dehydrogenase-elevating Virus (LDV) Transmission: Immune Inhibition of Umbilical Cord Infection, and Correlation of Fetal Virus Susceptibility with Development of F4/80 Antigen Expression. Placenta 23:438-446.
201. Charon J, Grigg M, Eden J, Piera K, Rana H, William T, Rose K, Davenport M, Antsey N, Holmes E. 2019. Novel RNA viruses associated with Plasmodium vivax in human malaria and Leucocytozoon parasites in avian disease. PLoS Pathogens 15:e1008216.
202. Shi M, Neville P, Nicholson J, Eden J-S, Imrie A, Holmes EC. 2017. High-Resolution Metatranscriptomics Reveals the Ecological Dynamics of Mosquito-Associated RNA Viruses in Western Australia. J Virol 91:e00680-17.
203. Bouzid M, Hunter P, Chalmers R, Tyler K. 2013. Cryptosporidium Pathogenicity and Virulence. Clinical Microbiology Reviews 26:115-134.
204. Chalmers R, Davies A, Tyler K. 2019. Cryptosporidium Microbiology 165.
205. Aguilera ER, Nguyen Y, Sasaki J, Pfeiffer JK. 2019. Bacterial Stabilization of a Panel of Picornaviruses. mSphere 4:e00183-19.
206. Kuss SK, Best GT, Etheredge CA, Pruijssers AJ, Frierson JM, Hooper LV, Dermody TS, Pfeiffer JK. 2011. Intestinal Microbiota Promote Enteric Virus Replication and Systemic Pathogenesis. Science 334:248-252.
207. Baldridge MT, Nice TJ, McCune BT, Yokoyama CC, Kambal A, Wheadon M, Diamond MS, Ivanova Y, Artyomov M, Virgin HW. 2015. Commensal microbes and interferon-λ determine persistence of enteric murine norovirus infection. Science 347:266-269.
208. Leung J, Budischak S, Chung The H, Hansen C, Bowcutt R, Neill R, Shellman M, Loke P, Graham A. 2018. Rapid environmental effects on gut nematode susceptibility in rewilded mice. PLoS Biology 16:e2004108.
209. Yeung F, Chen Y, Lin J, Leung J, McCauley C, Devlin J, Hansen C, Cronkite A, Stephens Z, Drake-Dunn C, Fulmer Y, Shopsin B, Ruggles K, Round J, Loke P, Graham A, Cadwell K. 2020. Altered Immunity of Laboratory Mice in the Natural Environment Is Associated with Fungal Colonization. Cell Host & Microbe: 27:1014.
210. Ramsdell CM, Lewandowski AA, Glenn JLW, Vrana PB, O'Neill RJ, Dewey MJ. 2008. Comparative genome mapping of the deer mouse (Peromyscus maniculatus) reveals greater similarity to rat (Rattus norvegicus) than to the lab mouse (Mus musculus). BMC Evolutionary Biology 8:1-14.
211. Kimura Y, Hawkins MTR, McDonough MM, Jacobs LL, Flynn LJ. 2015. Corrected placement of Mus - Rattus fossil calibration forces precision in the molecular tree of rodents. Scientific Reports 5:1-9.
212. Veyrunes F, Britton-Davidian J, Robinson T, Calvet E, Denys C, Chevret P. 2005. Molecular phylogeny of the African pygmy mice, subgenus Nannomys (Rodentia, Murinae, Mus): Implications for chromosomal evolution. Molecular Phylogenetics and Evolution 36:358-369.

213. Wohlgemuth N, Honce R, Schultz-Cherry S. 2019. Astrovirus evolution and emergence. Infection, Genetics and Evolution 69:30-37.
214. Weiss S, Leibowitz J. 2011. Coronavirus Pathogenesis. Advances in Virus Research 81:85-164.
215. Reuter G, Boros A, Pankovics P. 2011. Kobuviruses – a comprehensive review. Reviews in Medical Virology 21:32-21.
216. Sabin C, Füzik T, Škubník K, Pálková L, Lindberg AM, Plevka P. 2016. Structure of Aichi Virus 1 and Its Empty Particle: Clues to Kobuvirus Genome Release Mechanism. J Virol 90:10800-10.
217. Zhu L, Wang X, Ren J, Kotecha A, Walter TS, Yuan S, Yamashita T, Tuthill TJ, Fry EE, Rao Z, Stuart DI. 2016. Structure of human Aichi virus and implications for receptor binding. Nature Microbiology 1:1-6.
218. Hagai T, Chen X, Miragaia RJ, Rostom R, Gomes T, Kunowska N, Henriksson J, Park J-E, Proserpio V, Donati G, Bossini-Castillo L, Braga FAV, Naamati G, Fletcher J, Stephenson E, Vegh P, Trynka G, Kondova I, Dennis M, Haniffa M, Nourmohammad A, Lässig M, Teichmann SA. 2018. Gene expression variability across cells and species shapes innate immunity. Nature 563:197-202.
219. Tilley AE, Walters MS, Shaykhiev R, Crystal RG. 2015. Cilia Dysfunction in Lung Disease. Annual Review of Physiology 77:379-406.
220. Simpson C, Yamauchi Y. 2020. Microtubules in Influenza Virus Entry and Egress. Viruses 12:117.
221. Namba T, Ishihara S. 2020. Cytoskeleton polarity is essential in determining orientational order in basal bodies of multi-ciliated cells. PLoS Computational Biology 16:e1007649.
222. Kaur S, Uddin S, Platanias DLC. 2005. The PI3' Kinase Pathway in Interferon Signaling. Journal of Interferon & Cytokine Research 25:780-787.
223. M L, DM S. 2012. mTOR Signaling in Growth Control and Disease. Cell 149:274-293.
224. Ayllon J, García-Sastre A, Hale BG. 2012. Influenza A viruses and PI3K. Virulence 3:411-414.
225. Dan M, Zheng D, Field LL, Bonnevie-Nielsen V. 2012. Induction and activation of antiviral enzyme 2',5'-oligoadenylate synthetase by in vitro transcribed insulin mRNA and other cellular RNAs. Molecular Biology Reports 39:7813-7822.
226. Zhang P, Samuel CE. 2007. Protein Kinase PKR Plays a Stimulus- and Virus-Dependent Role in Apoptotic Death and Virus Multiplication in Human Cells. J Virol 81:8192-8200.
227. Toth AM, Devaux P, Cattaneo R, Samuel CE. 2009. Protein Kinase PKR Mediates the Apoptosis Induction and Growth Restriction Phenotypes of C Protein-Deficient Measles Virus. J Virol 83:961-968.
228. Li D, Liu J, Yang X, Zhou C, Guo J, Wu C, Qin Y, Guo L, He J, Yu S, Liu H, Want X, Wu F, Kuang J, Hutchins A, Chen J, Pei D. 2017. Chromatin Accessibility Dynamics during iPSC Reprogramming. Cell Stem Cell 21:819-833.

229. Domingo-Calap P, Segredo-Otero E, Durán-Moreno M, Sanjuán R. 2019. Social evolution of innate immunity evasion in a virus. Nature Microbiology 4:1006-1013.
230. Donohue R, Pfaller C, Cattaneo R. 2019. Cyclical adaptation of measles virus quasispecies to epithelial and lymphocytic cells: To V, or not to V. PLoS Pathogens 15:e1007605.
231. Horman W, Nguyen T, Kedzierska K, Bean A, Layton D. 2018. The Drivers of Pathology in Zoonotic Avian Influenza: The Interplay Between Host and Pathogen. Frontiers in Immunology 9:1812.
232. Kenney AD, McMichael TM, Imas A, Chesarino NM, Zhang L, Dorn LE, Wu Q, Alfaour O, Amari F, Chen M, Zani A, Chemudupati M, Accornero F, Coppola V, Rajaram MVS, Yount JS. 2019. IFITM3 protects the heart during influenza virus infection. Proc Natl Acad Sci U S A 116:18607-18612.
233. Long JS, Mistry B, Haslam SM, Barclay WS. 2018. Host and viral determinants of influenza A virus species specificity. Nature Reviews Microbiology 17:67-81.
234. Brierley L, Pedersen AB, Woolhouse MEJ. 2019. Tissue tropism and transmission ecology predict virulence of human RNA viruses. PLoS Biology 17:e3000206.
235. Farrell MJ, Davies TJ. 2019. Disease mortality in domesticated animals is predicted by host evolutionary relationships. Proc Natl Acad Sci U S A 116:7911-7915.
236. Olival KJ, Hosseini PR, Zambrana-Torrelio C, Ross N, Bogich TL, Daszak P. 2017. Host and viral traits predict zoonotic spillover from mammals. Nature 546:646-650.